UNIVERSITAT DE BARCELONA

Electrochemical immunosensors for pesticide residue detection in food matrices

Klaudia Lilla Kopper

Universitat de Barcelona, Facultat de Farmacia i Ciencies de l'Alimentació

Consejo Superior de Investigaciones Científicas

Instituto de Química Avançada de Catalunya

Nanobiotechnology for Diagnostics group

Centro de Investigación Biomédica en Red de Bioingeniería, Biomateriales y Nanomedicina

UNIVERSITAT DE BARCELONA

FACULTAT DE FARMÀCIA I CIÈNCIES DE L'ALIMENTACIÓ

ELECTROCHEMICAL IMMUNOSENSORS FOR PESTICIDE RESIDUE DETECTION IN FOOD MATRICES

Klaudia Lilla Kopper 2021

UNIVERSITAT DE BARCELONA

FACULTAT DE FARMÀCIA I CIÈNCIES DE L'ALIMENTACIÓ

PROGRAMA DE DOCTORAT DE BIOTECNOLOGIA

ELECTROCHEMICAL IMMUNOSENSORS FOR PESTICIDE RESIDUE DETECTION IN FOOD MATRICES

Memòria presentada per Klaudia Lilla Kopper per optar al títol de doctor per la Universitat de Barcelona.

Directors:

Prof. M.-Pilar Marco Colás
Professora d'Investigació
Dept. de Nanotecnologia Química y Biomolecular
Nb4D group, IQAC-CSIC

Dr. Roger Galve Bosch
Investigador
Dept. de Nanotecnologia Química y Biomolecular
Nb4D group, IQAC-CSIC

Doctorand:

Klaudia Lilla Kopper

Tutor:

Dr. Josefa Badia Palacin

Professora titular
Departament de Bioquímica i Fisiologia
Universitat de Barcelona

Klaudia Lilla Kopper 2021

ACKNOWLEDGEMENTS

I still can't quite believe that after the last four long and hard but also incredibly rewarding and eventful years I am closing this chapter of my life and writing these lines. I have learned an incredible amount during these years and have grown not only as a scientist but as a person as well. I would hereby like to thank everyone who has accompanied me on this journey and in some way, shape or form has contributed to my successes and has also helped me through the more challenging times.

First of all, I want to express my endless gratitude to the entire Nb4D research group who have not only taught me an extreme amount in the lab but have also welcomed me with open arms and let me be a part of their family, making me feel at home away from home.

- I especially want to thank you, Pilar for having me in your group and for giving me the opportunity to carry out my PhD in the framework of the European FoodSmartphone project, which truly has changed my life by giving me a countless number of amazing opportunities.
- Thank you, Roger for being my supervisor, for teaching and believing in me but also for pushing me to be better by making me step out of my comfort zone.
- Thank you, Pablo for being my supervisor during my Erasmus traineeship and teaching me about electrochemical immunosensors and for giving great advice whenever I had a problem with my experiments.
- Lluisa and Montse, thank you for always being so kind and caring with me, for listening to my problems and trying to help in every situation.
- Núria and the indispensable team of CabS, thank you for introducing me to the wonderful world of antibodies and for keeping me in such good company in the Sensors lab.
- Carla and Juan, thank you for being so open and friendly, it has been a pleasure spending time with you during our coffee and lunch breaks but also outside the lab.
- Dear David, thank you for teaching me a little bit of organic chemistry, but most importantly thank you for your uplifting and motivating personality, for the amazing coffee talks, for making me a travel enthusiast and for giving the best tips and tricks, I will forever be grateful for Karimunjawa.

- Querido Julian, thank you for being the best travel companion on all our FoodSmartphone trips, for our unforgettable conversations and for your constant encouragement and support, you truly have become like a brother to me and made the last two years of my PhD very special.
- Astrid, thank you for being the kindest person I have ever met, for helping me with anything and everything, for opening up to me, for baking with me and of course for the incredible nights of boardgames.
- I also want to thank previous members of the group, who have been an important part of this journey. Ana, thank you for teaching me how to do an ELISA, for being the best mentor anyone could ever ask for and for making me feel part of the group right from the start by always including me in every activity.
- Enric, it has been a pleasure sharing the ups and downs of the PhD with you, thank you for all our conversations and of course for teaching me some Spanish.
- Luciano, thank you for being the best lab neighbour, for helping and giving amazing advice to every problem and of course for discovering Costa Brava with me.
- Melek, thank you for your openness and kindness towards me, I am very grateful for all the moments we have shared in but mostly outside of the lab in the past years.
- Ina, it has been a pleasure getting to know you and spending so much time with you during your time at the Nb4D, I hope that we will have the chance to do more fun things together.
- Izaskun, Ginevra, Pablico, Ana González and Claudy, even though we haven't shared that much time in the lab together, you have all been an important part of my journey in some way and I really appreciate all of you.

I would also like to thank the entire consortium of the FoodSmartphone project, all the other ESRs but especially Michel, our amazing project coordinator, who went above and beyond to make sure that everyone had the best PhD experience.

I also want to thank everyone at CSEM for being so kind to me during my secondment there and of course Davide for teaching me everything about electrochemistry and screen printing.

And of course, none of this would have been possible without the love and support of my family and friends from home. Anya, Apa, Menyus, Viki és Attila, köszönöm a folytonos támogatást, igazán szerencsésnek mondhatom magam, hogy ilyen csodás és szerető családom van, akik mindent megtettek értem még ilyen távolról is. Andris és Gergő, nektek pedig köszönöm, hogy még a legnehezebb időszakaimban is sikerült mosolyt csalnotok az arcomra. Kedves barátnőimnek, Julcsinak, Orsinak, Dórinak, Krisztinek, Katának, Fruzsinak és Esztinek pedig köszönöm, hogy folyamatosan bíztattatok, hogy meglátogattatok és hogy a távolság ellenére is ilyen jól megmaradt a barátságunk.

Végül, de nem utolsó sorban pedig Balázs, Neked szeretném megköszönni, hogy legnagyobb támaszom voltál az elmúlt évek alatt és még a legnehezebb pillanatokban is kitartottál, pedig tudom nem volt mindig könnyű. Ez a diploma legalább annyira a tied is, mint az enyém, mert együtt küzdöttük le az akadályokat, amik elvezettek idáig.

TABLE OF CONTENTS

1 CONTEXT SCENARIO, OBJECTIVES AND STRUCTURE

1.1 CONTEXT SCENARIO

The present doctoral thesis has been developed in the framework of the following research project:

FoodSmartphone – Smartphone analyzers for on-site testing of food quality and safety. (Grant Agreement: 720325 – FoodSmartphone – H2020-MSCA-ITN). The FoodSmartphone consortium consists of 7 Training Sites (3 universities, 3 research centres, 1 innovation SME) and 2 Partner Organisations (1 global food industry and 1 diagnostics SME). The main objective of this European project was the development of smartphone-based (bio)analytical sensing and diagnostics tools for simplified and rapid on-site pre-screening of food quality and safety parameters for pesticides, allergens, mycotoxins, food spoilage organisms and marine toxins. Furthermore, the project also focused on the development of user-friendly and rapid integrated sample preparation and smartphone-compatible Apps, to ultimately ensure adequate field implementation for both professionals and future Citizen Science.

1.2 OBJECTIVES OF THE THESIS

Taking into account the scenario explained above, the main objective of this thesis was the development of user-friendly smartphone-connected electrochemical immunosensors for pesticide detection in different food matrices. The target pesticides were selected from the groups of herbicides (atrazine, paraquat) and insecticides (bromopropylate, chlorpyrifos) based on their significant impact in the field of food safety. The proposed scientific strategy consisted of the following steps:

1. Evaluation of the performance of the immunoreagents necessary for the detection of the selected target pesticides (atrazine, chlorpyrifos, bromopropylate and paraquat) by ELISA. (Most of the immunoreagents were previously developed by the Nb4D research group.)
2. Production, modification and characterization of carbon-based screen printed electrodes.

3. Development and analytical characterization of electrochemical immunosensors for the detection of the target pesticides in different food matrices such as cereals, fruit juices and jams.
4. Study of a multiplexed smartphone connected immunosensor as a potential on-site diagnostic tool.

1.3 THESIS STRUCTURE

In order to achieve the main goal of this thesis (described in chapters 4-7), the development of electrochemical immunosensors for the detection of different pesticides in food matrices, it was divided into the following sections:

1. Introduction and state of the art of smartphone-connected electrochemical biosensors (Chapter 2 and 3)
2. Production, modification and characterization of carbon-based screen printed electrodes (Chapter 4)
3. Development and evaluation of an electrochemical immunosensor for the detection of atrazine in orange juice samples (Chapter 5)
4. Development and evaluation of an electrochemical immunosensor for the detection of chlorpyrifos in flour samples (Chapter 6)
5. Development and evaluation of electrochemical immunosensors for the detection of bromopropylate and paraquat (Chapter 7)
6. Proof-of-concept of a multiplexed electrochemical immunosensor for pesticide detection (Chapter 8)

One annex has been added to this thesis (Chapter 9), describing the development of a multiplexed electrochemical immunosensor for the detection of contaminants in seawater. It was developed in the framework of the European SEA-on-a-CHIP project in which I have participated as an Erasmus+ student at the very beginning of my PhD.

The detailed structure of this thesis is represented in Figure 1.1.

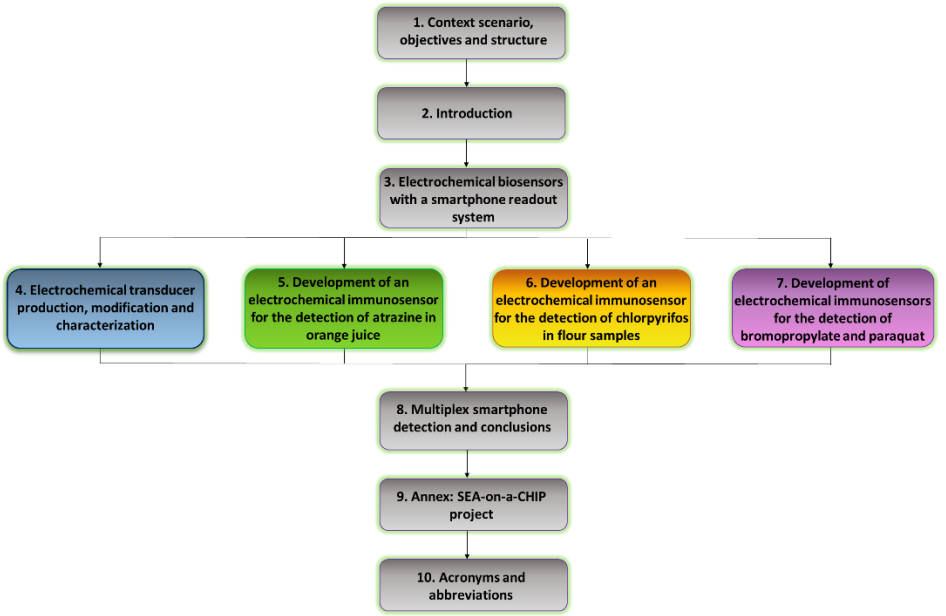

Figure 1.1. *The structure of this thesis related to the different chapters.*

2 INTRODUCTION

2.1 PESTICIDES

Pesticides are synthetic chemical substances used in agriculture for the treatment of crops. In the modern era, pesticides have been extensively applied to enhance overall agricultural productivity [1]. Their main role is to control or repel any pest (i.e. weeds, fungi, insects etc.) that could be found in food, destroy properties or spread diseases. Thus, their use is inadmissible in the food production industry, they are necessary to protect and increase the yields of crops, which is particularly important in countries that suffer from food shortages. Herbicides and insecticides are mainly used in the pre-harvest stages, rodenticides are employed in the post-harvest storage stages whereas fungicides can be applied at any stage of the process depending on the crop [2].

One of the main drawbacks of pesticides however (especially in the case of the older, cheaper pesticides) is the fact that their residues may remain in soil and water for years after their use, leading to significant environmental damages [3,4]. Even though many of these chemicals have already been banned from agricultural use in developed countries, they are unfortunately still being used in many developing countries. Besides being found in soil and water, these residues can also enter into the food chain and pose a severe threat to the health of humans and animals [5].

Pesticides can have both acute and chronic health effects, depending on the quantity and ways in which a person is exposed. The adverse effects of pesticide residues mainly depend on the nature of the pesticide, as well as the amount and duration of exposure. Symptoms of acute poisoning include irritation, nausea, vomiting, diarrhea, abdominal pain, dizziness, headaches and numbness. In severe cases, people may even have difficulties in breathing, blurred vision and convulsion. Prolonged excessive intakes of pesticide residues have been shown to cause chronic complications such as diaebetes, asthma, cancer, damage to the nervous system or other organs such as liver and kidneys, as well as affecting fetal development [6-8]. Despite the large number of new pesticide classes introduced into agricultural practice over the last 50 years, most deaths and severe poisonings are still caused by a small number of older compounds. Organophosphorus, carbamate insecticides and the herbicide paraquat are the most important ones. The potential for occupational exposure is high, particularly in lower- and middle-income countries. However, exposures that

occur by inhalation or dermal exposure are usually smaller than those occurring by ingestion [9]. Human exposure to these chemicals could be avoided or controlled by i) their use in a more controlled manner, ii) employment of natural pesticides, iii) use of other agricultural practices (e.g., crop rotation and maintaining crop diversity), and iv) avoiding the uptake of contaminated food/water. Furthermore, the uptake of these harmful chemicals can be avoided by detecting their presence in a precise and timely manner.

2.2 FOOD SAFETY MONITORING

Even though nowadays the monitoring of food contaminants is conducted in an intensive manner, food scandals are still a reoccurring topic in the news. Numerous techniques have been developed over the past decades for the determination of pesticide residues in environmental and food samples. Due to the wide variety of formulated pesticides, previously the analysis was carried out mainly using different traditional analytical methods such as gas chromatography (GC) or high performance liquid chromatography (HPLC) coupled to mass spectrometry (MS). However, the highly industrialized food production and the current globalization of the food market makes it difficult to monitor food contaminants from farm-to-fork, thus there is a great need for improved and innovative detection methods. These methods not only need to be reliable and precise but also significantly cheaper, faster and potentially portable. The use of screening methods for food safety analysis has significantly increased in the last few years, such as immunoassays and electrochemical/optical sensors (including immunosensors) due to their capabilities of allowing “multiplexed” on-site analytical measurements. However, it is important to mention that there is still a need to validate the performance of these screening methods by confirmatory analytical methods [10].

During recent years biosensors began to stand out in the analysis of food contaminants due to their simplicity, rapidness, reduced solvent consumption, cost-effectiveness and the possibility of on-site detection. Sensor-based methods usually achieve the desired selectivity and specificity by the employment of biomolecules such as antibodies, aptamers or enzymes, which

interact with the target analyte. This interaction is typically monitored by optical or electrochemical detection systems. The confirmatory analysis used for the validation of these screening methods is generally based on chromatographic separation and mass spectrometric detection of the analytes.

The use of electrochemical immunosensors for the detection of food contaminants brings a great advantage to the currently available analytical methods in the food safety industry. Since nowadays potentiostats are becoming smaller and also relatively cheaper, even the development of multiplexed electrochemical sensors for on-site analysis is becoming a possibility. The emerging use of smartphones in the field of food testing is also worth mentioning. The idea behind the use of smartphones as analytical detection tools is the development of end-user friendly detection tools, which means that even people with no expertise would be able to use these devices to test their food.

2.2.1 END-USER REQUIREMENTS, EU LEGISLATION

Due to the fact that pesticides are intrinsically toxic and deliberately spread in the environment, their production, distribution, and use requires strict regulation and control. Furthermore, the regular monitoring of residues in food and environment is also required. In order to protect food consumers from the adverse effects of pesticides, the European Commission (EC) has developed internationally-accepted maximum residue limits (MRL) for numerous analytes in a great number of matrices [10]. The EC Regulation 396/2005 has set MRLs for more than 1100 pesticides in 315 raw plant- and animal-based food and feed, providing an online database where the user can easily search for information and also export the data. In the case of pesticides for which no MRL has been set, the default value of 0.010 mg kg^{-1} limit is to be applied. Even though the EU legal framework is well established and one of the strictest globally, there are still many challenges towards achieving safe and sustainable food production. In this regard the European Food Safety Authority (EFSA) is continuously providing scientific information and opinions in order to help shape the upcoming legislations of the EC. In the case of pesticides the EFSA releases a yearly report on controversial issues and the prediction of dietary pesticide intakes for example.

2.3 BIBLIOGRAPHY

[1] A.S. Davis, J.D. Hill, C.A. Chase, A.M. Johanns, M. Liebman. (2012). Increasing Cropping System Diversity Balances Productivity, Profitability and Environmental Health, 7 1–8. https://doi.org/10.1371/journal.pone.0047149.

[2] M. LeDoux. (2011). Analytical methods applied to the determination of pesticide residues in foods of animal origin. A review of the past two decades, J. Chromatogr. A. 1218 1021–1036. https://doi.org/10.1016/j.chroma.2010.12.097.

[3] F.P. Carvalho. (2006). Agriculture, pesticides, food security and food safety, 9 685–692. https://doi.org/10.1016/j.envsci.2006.08.002.

[4] M.J. Cerejeira, P. Viana, S. Batista, T. Pereira, E. Silva, M.J. Val, A. Silva, M. Ferreira, A.M. (2003). Silva-fernandes, Pesticides in Portuguese surface and ground waters, 37 1055–1063.

[5] Salas, B.V., Duran, E.I.G., Wiener, M.S. (2000). Impact of pesticides use on human health in Mexico: A review. Rev. Environ. Health 15, 399–412. https://doi.org/10.1515/reveh.2000.15.4.399

[6] A. Evenset, I.G. Hallanger, M. Tessmann, N. Warner, A. Ruus, K. Borgå, G.W. Gabrielsen, G. Christensen, P.E. Renaud. (2016). Science of the Total Environment Seasonal variation in accumulation of persistent organic pollutants in an Arctic marine benthic food web, Sci. Total Environ. 542 108–120. https://doi.org/10.1016/j.scitotenv.2015.10.092.

[7] K. Kim, E. Kabir, S. Ara. (2017). Science of the Total Environment Exposure to pesticides and the associated human health effects, Sci. Total Environ. 575 525–535. https://doi.org/10.1016/j.scitotenv.2016.09.009.

[8] K. Vikrant, D.C.W. Tsang, N. Raza, B.S. Giri, D. Kukkar, K. Kim. (2018). Potential Utility of Metal − Organic Framework-Based Platform for Sensing Pesticides. https://doi.org/10.1021/acsami.8b00664.

[9] Eddleston, M. (2019). Poisoning by pesticides Key points. Medicine, 48(3), 214–217. https://doi.org/10.1016/j.mpmed.2019.12.019

[10] A.S. Tsagkaris, J.L.D. Nelis, G.M.S. Ross, S. Jafari, J. Guercetti, K. Kopper, Y. Zhao, K. Rafferty, J.P. Salvador, D. Migliorelli, G.I.J. Salentijn, K. Campbell, M.P. Marco, C.T. Elliot, M.W.F. Nielen, J. Pulkrabova, J. Hajslova. (2019). Trends in Analytical Chemistry Critical assessment of recent trends related to screening and con fi rmatory analytical methods for selected food contaminants and allergens, Trends Anal. Chem. 121 115688. https://doi.org/10.1016/j.trac.2019.115688.

3 ELECTROCHEMICAL BIOSENSORS WITH A SMARTPHONE-BASED READOUT SYSTEM FOR POINT-OF-CARE DETECTION

3.1 INTRODUCTION

3.1.1 ELECTROCHEMISTRY

Electrochemistry is the study of the chemical response of a system to an electrical stimulation. It studies the reduction (gain of electrons) and oxidation (loss of electrons) reactions a material undergoes during the electrical stimulation. These reactions are commonly known as redox-reactions and can provide information about several different properties of a species in solution (e.g.: concentration, kinetics, reaction mechanisms, chemical status) and also about the electrode's surface [1].

Electrochemical techniques are being used extensively for their excellent capabilities to characterize the analytical performances of immunosensing molecules. In general, electrochemical studies are being carried out with trielectrode systems, meaning that there is a working, a counter (auxiliary) and a reference electrode for building the analytical circuit [2]. The working electrode (WE) is usually constructed of an inert material and is the place where the reactions of interest take place. During a measurement, the potential of the working electrode is being compared to the one of the reference electrode (RE), which is always at a known potential. (A typical reference electrode would be the saturated calomel electrode, which is commonly used in pH measurements.) During an electrochemical measurement the current flows in the electrolyte solution between the working and counter electrodes (CE), which are ususally constructed of platinum or other inert materials. The three electrodes (WE, RE, CE) are connected to a potentiostat, which is an instrument able to control the potential of the working electrode while measuring the resulting current [1].

The most commonly used electrochemical transducers are: i) Amperometric transducers, which measure the change in current resulting from the oxidation or reduction of an electroactive species in a biochemical reaction, ii) Potentiometric transducers that measure the potential or charge accumulation, iii) Conductometric transducers that measure the conductive properties of a medium, iv) Impedimetric transducers that measure the impedance and v) transistor-based sensors.

3.1.2 SMARTPHONE-BASED ANALYSIS

There are several advantages of using smartphone-based analysis, the most obvious one of them being its wide accessibility since there are around 3.8 billion smartphone users by 2021. Smartphones are simple, cost-effective, citizen science ready tools available for on-site measurements, thus fulfilling the growing need for a continuous real-time monitoring of different substances (Point-of-care testing and mobile diagnostics). Smartphones are similar to a mini-computer with their rich set of built-in sensors (e.g.: camera, microphone), powerful processors and memories, high resolution touch-screen displays and powerful data transmission capabilities (GSM, WiFi, USB, NFC, Bluetooth). They can be used as detectors or as instrumental readout interfaces in the development of smartphone-based biosensors. Among various smartphone-based sensing platforms electrochemistry stands out due to its high stability and accuracy and has allowed its use in quantitative detections of important biomarkers, contaminants, etc. An electrochemical analyzer/workstation coupled with a smartphone can significantly simplify the electronic design, reduce volume and decrease the cost of the system. In this case smartphones are mostly used as instrumental interfaces, which connect with wearable or portable electrochemical devices through interfaces such as Bluetooth, WiFi, USB or an audio port for power delivery, signal transmission, data processing, result displaying and internet connecting.

3.2 ELECTROCHEMICAL SENSORS WITH SMARTPHONE-BASED READOUT SYSTEMS

There are several different configurations of electrochemical sensors with a smartphone read-out system. In the following sections I will discuss the most common and relevant types.

3.2.1 SCREEN-PRINTED ELECTRODE BASED SENSORS

The most common electrochemical sensors with a smartphone-based readout system are screen-printed electrode (SPE) based sensors. They usually involve a SPE, a relatively small electrochemical detector and a smartphone as the readout interface.

One example of this configuration, an electrochemical sensor for the detection of levodopa (Figure 3.1/a) consists of a disposable sensor, a hand-held electrochemical detector and a smartphone that has a designed application [3]. In this case the SPEs are modified with single-wall carbon nanotubes and gold nanoparticles and they are being used to convert and amplify the electrochemical current signals upon the presence of levodopa molecules. The second element of the system, the electrochemical detector is used to generate electrochemical excitation signals and to detect the resultant currents. Finally, the last part of the system the smartphone is used to control the detector, calculate data and plot the graph in real-time. When the levodopa reacts on the surface of the electrode, the current values change, which results in a dose-dependent curve. This system is able to achieve a limit of detection (LOD) of 0.5 µM for levodopa in human serum.

Another example for an SPE based sensor is an on-site smartphone-connected water quality monitoring system (Figure 3.1/b) that allows for the quantification of Pb^{2+} ions and chemical oxygen demand (COD) [4]. This system consists of a whole-copper electrochemical sensor, a hand-held detector and a smartphone with a custom-made application and a cloud map website. Similarly to the previous example, the smartphone is used to control the detector and to visualize the results in real-time. The achieved LOD in water for Pb^{2+} was 45 nM and 9 mg L^{-1} for the COD.

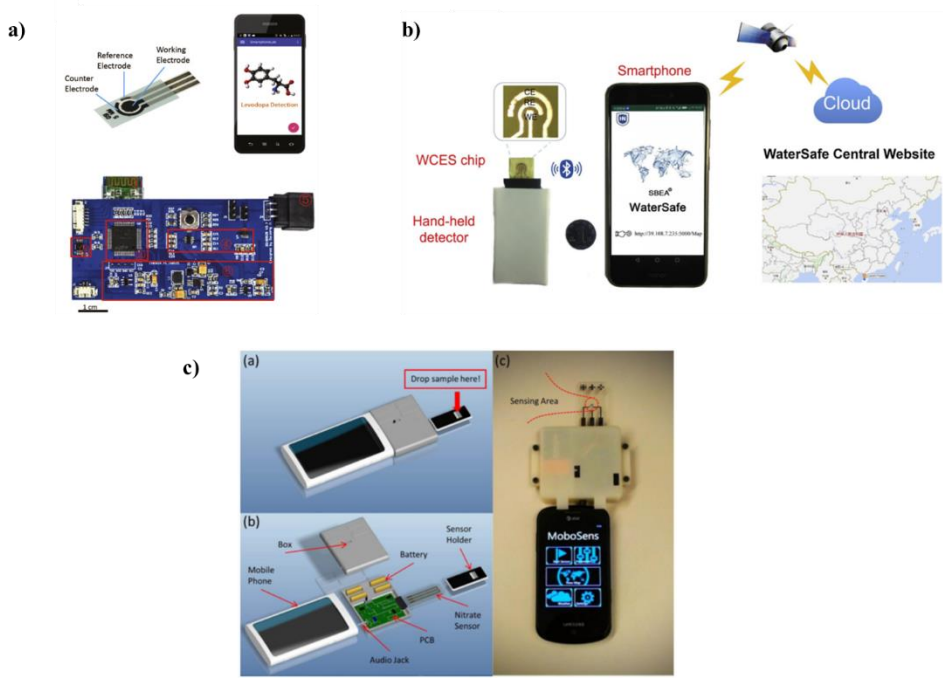

Figure 3.1. *Screen-printed electrode based sensors with a smartphone readout system.* ***a)*** *Photo of the different parts of the smartphone-based differential pulse amperometry system [3].* ***b)*** *Photograph of the smartphone-based water quality monitoring system, which consists of a WCES chip, a hand-held detector, a smartphone, and a WaterSafe central website.* ***c)*** *Illustration of the packaged MoboSens system [4]. a) Assembly view of MoboSens. b) Detailed components of MoboSens. c) Photograph showing the complete MoboSens system [5].*

A final example of this configuration (see Figure 3.1/c) is a mobile phone sensing platform (MoboSens), which has an integrated microelectronic ionic sensor that is able to perform electrochemical measurements using the audio jack of a smartphone [5]. In this case the smartphone is not only used to control the detection and the display of the results but the microfluidics of the system as well. This method was used to measure nitrate in water achieving an LOD of 0.2 ppm within 1 min. One of the main advantages of this system is that the results can be automatically saved on cloud servers.

3.2.2 PAPER-BASED BIOSENSORS

Another interesting concept are paper-based biosensors, which have the advantages of being small, low-cost and environment-friendly biosensors. They usually consist of a paper-based electrode and a smartphone-based electrochemical detection device [6]. In the case of the device shown in Figure 3.2, the three electrodes are directly drawn on chromatography paper using a carbon pencil. An enzyme layer can be found on the surface of the electrode, which contains glucose oxidase and potassium ferricyanide in PBS. (This layer is dropped on the sensor surface and then dried in an oven for 5 minutes.) The glucose concentration can be determined from the current after 120 sec. The detection system harvests its power from the smartphone and transfers its data through the audio jack. The advantage of this system is that it could be used for the detection of a number of target analytes by changing the enzymes and the electron transfer molecules.

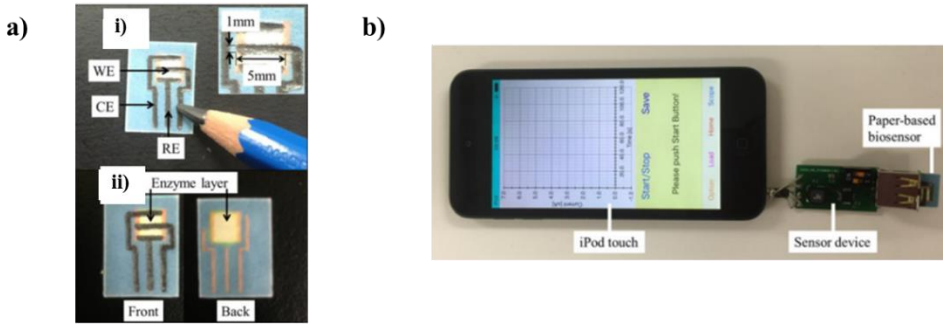

Figure 3.2. *Paper-based sensor with a smartphone readout system [6].**a)** i) Illustration of the three electrodes (WE, RE, CE) that are directly drawn on chromatography paper using a carbon pencil. ii) The enzyme solution is dropped on the hydrophilic area to provide the electrodes with an enzyme layer and the paper-based biosensor is dried in an oven at 60°C for 5 minutes. **b)** Overview of the sensing system showing the connection of iPod touch, sensor device and paper-based biosensor.*

3.2.3 CHIP-BASED SENSORS

A further type of electrochemical sensors with a smartphone readout system are chip-based sensors. An example for this is a fully integrated battery-free and flexible electrochemical tag (Figure 3.3) that was developed for wireless in situ

detections of heavy metal ions in various containers [7]. The system consists of a flexible screen printed electrode array that is connected to a circuit board. The circuit is integrated with square wave anodic stripping voltammetry technique and near field communication (NFC) module for wireless data transmission to the smartphone (or any other device). There are two carbon WEs on the SPE, modified with gold and bismuth nanoparticles, which ensure the high sensitivity and selectivity necessary for the detection of heavy metals such as lead and cadmium. The main advantage of this chip is that it can be attached to the inside of any food or drink container for a long time in order to realize wireless in situ monitoring of migrated lead and cadmium without the need for batteries or any external equipment.

Figure 3.3. *Design of the fully integrated battery-free chip-based sensor with a smartphone readout system [7]. a) Image of the electrochemical chip, including a flexible circuit board and an electrode array. b) Explosive view of the device. c) Curving of the flexible chip. d) The attachment of the tag to the inside surface of a glass. e) Illustration of the application scenario in real life. The tag is adhered onto the inside surface of a wine jar. Wireless in situ analysis of the migrated heavy metal ions is achieved by the proximity of an NFC-enabled smartphone outside the jar for wireless power delivery and data transmission.*

3.2.4 RE-USABLE SENSORS

A further example and a major development in the field of electrochemical detection are re-usable sensors. Bandodkar et al. have developed a smartphone-based reusable glucose meter (Figure 3.4), which includes a custom-built smartphone case, a permanent bare sensor chip, a stylus that is loaded with enzyme-carbon composite pellets, sensor instrumentation circuits and a custom designed app for the smartphone [8]. A typical test consists of the user first loading the software on the smartphone, then using the stylus to dispense an enzymatic pellet on top of the bare sensor chip, which is affixed to the case and finally introducing the sample (in this case a blood sample). Within a few seconds the electronic module acquires and wirelessly transmits the data to the application to be displayed on the screen. The deployed pellet is then discarded. The enzyme loaded in the pellets is stable for up to 8 months. The versatility of the system allows it to be easily modified to detect other analytes as well.

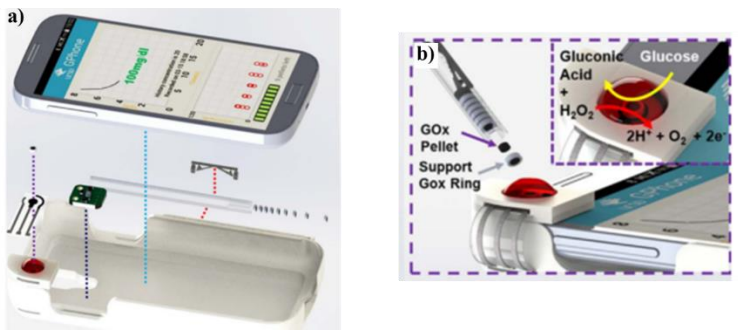

Figure 3.4. *Re-usable sensor with a smartphone based readout system [8]. a) Illustration of the smartphone-based glucose sensing system showing the smartphone case, the permanently-attached passive sensor strip, the enzyme-loaded pellet, the pellet-dispending stylus and the electronic readout circuits. b) The process of dispensing the carbon-composite pellets onto the bare carbon working electrode for the electrochemical analysis.*

3.2.5 MULTIPLEXED SENSORS WITH A SMARTPHONE READOUT SYSTEM

One of the most challenging parts of electrochemical detection systems is multiplexation and only a few examples can be found in the literature to this

date. Márquez et al. have developed a reconfigurable smartphone-interfaced electrochemical Lab-on-a-chip device (Figure 3.5/I) that has two working electrodes for dual analyte determination [9]. The biomarker selection is achieved by the electrodeposition of alginate hydrogels (which also have filtering capacity) containing glucose oxidase or lactate oxidase. Glucose or lactate samples can be measured in less than 1 min from whole blood samples with the use of this system. The main advantage of using alginate membranes is their high versatility and adaptability. Upon their immersion in a solution of calcium chelator the membrane can be regenerated, thus it can be used again for other measurements.

Another example for multiplex electrochemical detection is a smartphone-based integrated voltammetry system (Figure 3.5/II) using modified electrodes for the simultaneous detection of different biomolecules [10]. This system consists of a disposable sensor, a small detector and a smartphone that is equipped with a specific application program. Reduced graphene-oxide and gold nanoparticles are electrochemically deposited on the surface of the WEs by cyclic voltammetry. An excitation voltage is applied on the sensors and the current response is recorded by the detector. The Smartphone's main role is to communicate with the detector, calculate data and plot voltammograms in real-time. The practical applications of the system were tested through the detection of biomolecules in artificial urine. The system was able to simultaneously detect ascorbic acid, dopamine and uric acid in artificial urine samples due to the fact that the three electroactive substances oxidize on the modified electrodes at different potentials, thus resulting in different current peaks. The detector has the ability to transmit the obtained data via Bluetooth or on-the-go. The specifically designed App (for voltammetry detection) of the smartphone provides an interface between the users and the system. The interactive system allows the users to choose the detection method from the menu and set the parameters of each detection method according to the measurements.

A different example of multiplexed detection is a fully integrated electrochemical sensor array (Figure 3.5/III) that is able to monitor pH, temperature, free chlorine, emerging pharmaceutical contaminants and heavy metals [11]. This on-site water quality monitoring system consists of carbon nanotube based sensors that were fabricated on glass slides and are controlled by a custom designed readout circuit, a potentiostat and an Android app.

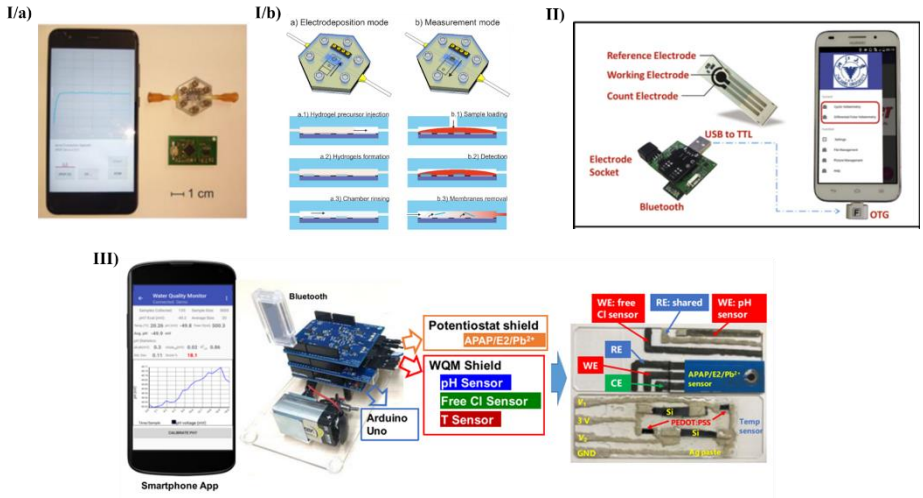

Figure 3.5. *Multiplexed sensors with a smartphone readout system.* ***I)*** *a) Picture of the parts of the reconfigurable multiplexed point of care system: mobile phone with the controlling application, PMMA-PDMS device and µPotentiostat circuit [9]. b) Scheme of the sample measurement. a) In the electrodeposition mode the gate remains closed, while the alginate membrane is electrodeposited. For real sample analysis b), the gate is open and a drop of blood is added. Once the measurement is finished, the gate is closed again and the chamber is cleaned with PBS.* ***II)*** *Illustration of the smartphone-based integrated voltammetry system using modified electrodes for the simultaneous detection of different biomolecules [10].* ***III)*** *A fully integrated water quality monitoring system with sensors on two glass slides connected to a customized smartphone app [11].*

3.2.6 WEARABLE SENSORS

Finally, as the last category of electrochemical sensors with a smartphone-based readout system, it is important to mention wearable sensors, which have become more and more popular in recent years and are revolutionizing the diagnostic field. Wearable electrochemical sensors can be adhered on the human body and detect analytes in accessible biological fluids. Several soft, flexible and stretchable electronic devices have been developed for the monitoring of clinically important indices of human health (Figure 3.6). Tattoo and patch sensors for example are low-cost and not intended for re-use, whereas band sensors are based on silicone and are therefore more durable and reliable and

also have the possibility of regenerating the sensor layer as well as multiplex detection of analytes [12].

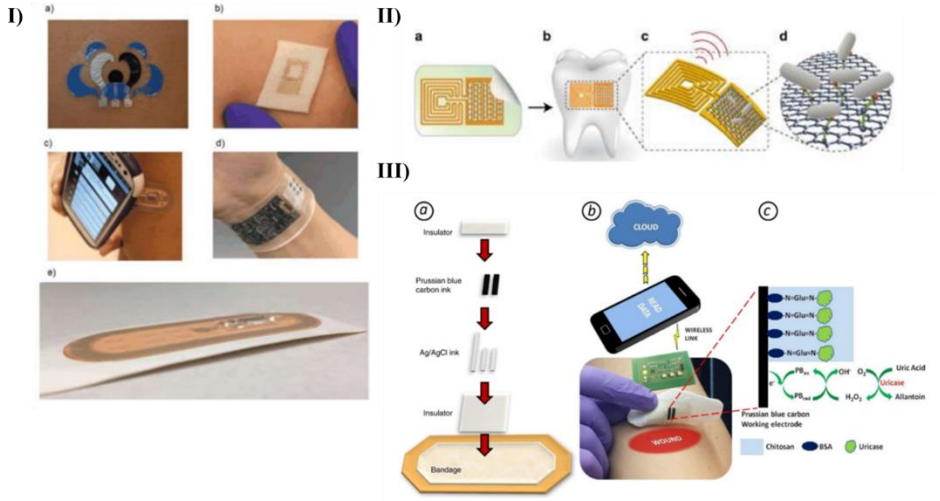

Figure 3.6. I) *Different types of wearable sensors: tattoo (a,b), patch (c), and band (d,e) [12]. a) An enzyme-based biosensor in the form of a flexible, printed temporary-transfer tattoo that is used for the determination of lactate in sweat. d) A multi-analyte potentiometric-amperometric sensor wristband platform to determine glucose, lactate, potassium and sodium in exercise-induced sweat.* ***II)*** *A graphene-based sensing element with a wireless readout coil on silk fibroin that could be transferred onto a tooth surface. It uses self-assembling antimicrobial peptides for the detection of Helicobacter pylori.* ***III)*** *A smart bandage for uric acid (UA) detection. UA level in wound exudate is highly correlated with wound severity and indicates the bacterial infection of it.*

Another fascinating example is a wearable glove-based sensor (Figure 3.7/I) that is able to electrochemically detect fentanyl on the fingertips [13]. The glove-based sensor consists of a flexible screen-printed carbon electrode that has been previously modified with a mixture of multiwalled carbon nanotubes. The sensor shows direct oxidation of fentanyl in both liquid and powder forms with an LOD of 10 µM using square-wave voltammetry. Combined with a portable electrochemical analyzer it is able to provide wireless data transmission to a smartphone. It has integrated sampling and sensing steps on different fingers and the measurements can be performed after completing the „electrochemical cell" by joining the thumb and the index fingers. It provides a rapid screening (1 min approx.), it is reproducible and selective.

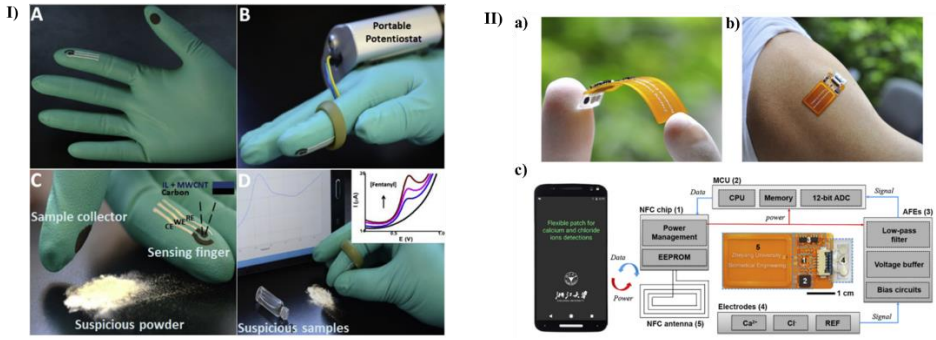

Figure 3.7. I) *Overview of the wearable glove-based sensor [13]. A) Photograph of the glove, which contains a sensing finger and a sample collector finger. B) The glove-based sensor with a portable electroanalyzer. The electrodes are connected via wires and a modified ring to a PalmSens potentiostat for on-site detection with wireless communication to a smartphone. C) Collection of the suspicious sample in powder phase. D) Joining of thumb (collector) and sensing (index) fingers after swiping a powder sample; direct detection of fentanyl in powder/liquid samples (voltammograms).* ***II)*** *Design of the wearable chip-based battery-free and flexible electrochemical patch [14]. a) Side-view of the patch, including an NFC-enabled flexible circuit board and a stretchable electrode array. b) Image of the patch when it was adhered on the arm of subject. c) Block diagram of the smartphone-based sensing system for Ca^{2+} and Cl^- detections.*

Finally, Xu et al. have developed a flexible smartphone-based battery-free electrochemical patch (Figure 3.7/II) for real-time detection of calcium and chloride ions in various biofluids [14]. The patch is integrated with near field communication (NFC) module, which enables both wireless power and data transmission. One of the main advantages of these devices is that they can get rid of the abundant batteries or wired connections and be totally flexible. NFC-enabled smartphones can wirelessly power the patch and get the detection results. The other component of the patch is an all-printed stretchable two-channel electrode array which can be comfortably mounted on skin surface and has the ability to maintain stable conductivity during stretching. They have carried out ex-situ measurements in serum, urine, tear and sweat. Additionally, they have realized real-time on-body sweat analysis further indicating the usability and stability of the device, which showed high sensitivity, repeatability, linearity and selectivity in the case of the detection of Ca^{2+} and Cl^-.

3.3 CONCLUSIONS

Smartphone-based sensors show great promise for possible development into stand-alone devices outside the laboratory, especially in the developing world. However, it is important to mention that to date smartphone-based sensing is still under development, thus their accuracy and sensitivity still has to be improved. The main challenges are the introduction of the sample, the integration of alternative power sources, the development of self-powered sensors, the ability of multiplexation and reusability and finally the quality of the App, which should be simple and easy to operate. Some commercial smartphone-based sensors have already been widely used for medical diagnostics and could also be applied for environmental and food safety monitoring in the near future.

3.4 BIBLIOGRAPHY

[1] Wang J. Analytical Electrochemistry, Second Edition. Wiley-VCH. (2000) ISBN: 0-471-22823-0 (Electronic).

[2] Mahato K. et al. Electrochemical Immunosensors: Fundamentals and Applications in Clinical Diagnostics. Handbook of Immunoassay Technologies, Elsevier (2018). http://doi.org/10.1016/B978-0-12-811762-0.00014-1

[3] D. Ji, N. Xu, Z. Liu, Z. Shi, S. Shin, J. Liu, Biosensors and Bioelectronics Smartphone-based differential pulse amperometry system for real-time monitoring of levodopa with carbon nanotubes and gold nanoparticles modified screen-printing electrodes, Biosens. Bioelectron. 129 (2019) 216–223. https://doi.org/10.1016/j.bios.2018.09.082.

[4] J. Liao, F. Chang, X. Han, C. Ge, S. Lin, Sensors and Actuators B : Chemical Wireless water quality monitoring and spatial mapping with disposable whole-copper electrochemical sensors and a smartphone, Sensors Actuators B. Chem. 306 (2020) 127557. https://doi.org/10.1016/j.snb.2019.127557.

[5] X. Wang, M. Ranjan, J. Jiang, T. Chang, J. Qian, Y. Liu, X. Liu, G. Logan, Sensors and Actuators B: Chemical Audio jack based miniaturized mobile phone

electrochemical sensing platform, Sensors Actuators B. Chem. 209 (2015) 677–685. https://doi.org/10.1016/j.snb.2014.12.017.

[6] T. Fujimoto, S. Kawahara, Y. Fuchigami, S. Shimokawa, Y. Nakamura, Portable Electrochemical Sensing System Attached to Smartphones and Its Incorporation with Paper-based Electrochemical Glucose Sensor, 7 (2017) 1423–1429. https://doi.org/10.11591/ijece.v7i3.pp1423-1429.

[7] G. Xu, X. Li, C. Cheng, J. Yang, Z. Liu, Z. Shi, L. Zhu, Y. Lu, S.S. Low, Q. Liu, Sensors and Actuators B : Chemical Fully integrated battery-free and flexible electrochemical tag for on-demand wireless in situ monitoring of heavy metals, Sensors Actuators B. Chem. 310 (2020) 127809. https://doi.org/10.1016/j.snb.2020.127809.

[8] A.J. Bandodkar, S. Imani, R. Nuñez-flores, R. Kumar, C. Wang, A.M.V. Mohan, J. Wang, P.P. Mercier, Biosensors and Bioelectronics Re-usable electrochemical glucose sensors integrated into a smartphone platform, Biosens. Bioelectron. 101 (2018) 181–187. https://doi.org/10.1016/j.bios.2017.10.019.

[9] A. Márquez, J. Aymerich, M. Dei, R. Rodríguez-rodríguez, M. Vázquez-carrera, J. Pizarro-delgado, P. Giménez-gómez, Á. Merlos, L. Terés, F. Serra-graells, C. Jiménez-jorquera, C. Domínguez, X. Muñoz-berbel, Biosensors and Bioelectronics Reconfigurable multiplexed point of Care System for monitoring type 1 diabetes patients, Biosens. Bioelectron. 136 (2019) 38–46. https://doi.org/10.1016/j.bios.2019.04.015.

[10] D. Ji, Z. Liu, L. Liu, S. Shin, Y. Lu, X. Yu, L. Zhu, Biosensors and Bioelectronics. Smartphone-based integrated voltammetry system for simultaneous detection of ascorbic acid, dopamine, and uric acid with graphene and gold nanoparticles modified screen-printed electrodes, Biosens. Bioelectron. 119 (2018) 55–62. https://doi.org/10.1016/j.bios.2018.07.074.

[11] A.U. Alam, D. Clyne, H. Jin, N. Hu, M.J. Deen, Fully Integrated, Simple, and Low-Cost Electrochemical Sensor Array for in Situ Water Quality Monitoring, (2020). https://doi.org/10.1021/acssensors.9b02095.

[12] A.N. Kozitsina, T.S. Svalova, N.N. Malysheva, A. V Okhokhonin, M.B. Vidrevich, K.Z. Brainina, Sensors Based on Bio and Biomimetic Receptors in

Medical Diagnostic, Environment, and Food Analysis, (2018) 1–34. https://doi.org/10.3390/bios8020035.

[13] A. Barfidokht, R.K. Mishra, R. Seenivasan, S. Liu, L.J. Hubble, J. Wang, D.A. Hall, Sensors and Actuators B : Chemical Wearable electrochemical glove-based sensor for rapid and on-site detection of fentanyl, Sensors Actuators B. Chem. 296 (2019) 126422. https://doi.org/10.1016/j.snb.2019.04.053.

[14] G. Xu, C. Cheng, W. Yuan, Z. Liu, L. Zhu, X. Li, Y. Lu, Sensors and Actuators B : Chemical Smartphone-based battery-free and fl exible electrochemical patch for calcium and chloride ions detections in bio fl uids, Sensors Actuators B. Chem. 297 (2019) 126743. https://doi.org/10.1016/j.snb.2019.126743.

4 ELECTROCHEMICAL TRANSDUCER PRODUCTION, MODIFICATION AND CHARACTERIZATION

CHAPTER OVERVIEW

This chapter describes the production, modification and characterization of different carbon-based screen printed electrodes (SPE) that were later used for the development of immunosensors for the detection of pesticides in different food matrices (described in chapters 5-7).

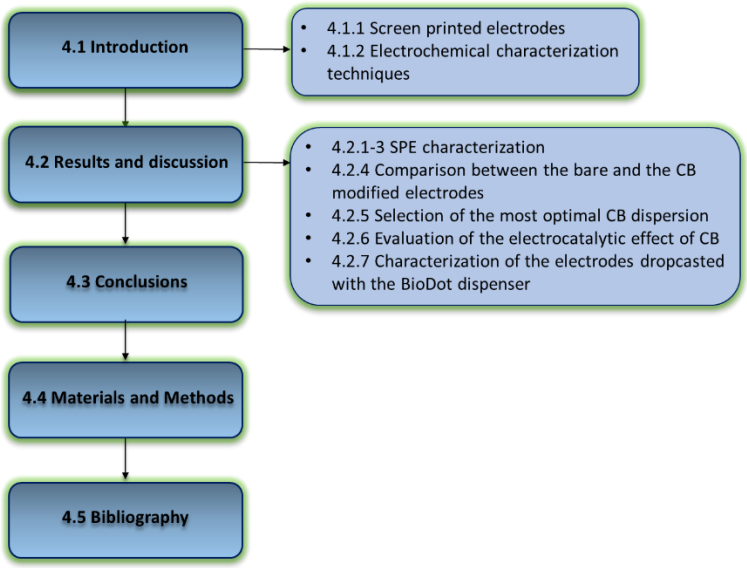

Figure 4.1. *Structure of this chapter related to the different sections.*

4.1 INTRODUCTION

4.1.1 SCREEN PRINTED ELECTRODES

Screen printed electrodes (SPEs) are small inexpensive electrochemical measuring tools that allow for the performance of quick in-situ measurements with high sensitivity, accuracy and reproducibility while requiring low sample volume [3]. Since most of these electrodes are designed for single use, there is no need for pre-treatment and maintenance procedures. Screen printed electrodes are produced by the printing of different types of inks on ceramic or

plastic substrates. The most commonly used materials for the printing of the working electrode are carbon, gold and platinum, but other metals could be used as well (e.g.: palladium, bismuth, nickel etc.). Due to their good reproducibility, SPEs can be integrated in various different sensing platforms such as enzyme, DNA or antibody-based sensors, which are most commonly used in the fields of environmental, food or medical analysis [4].

The use of carbon-based SPEs as electrochemical transducers is particularly ideal for the development of multiplexed electrochemical sensors for on-site analysis, since the mass production of these electrodes is well developed and relatively low cost, which drastically decreases the costs of the analysis [5]. Even though the unmodified carbon-based SPEs are normally less sensitive than other kinds of electrodes, their performance can easily be enhanced with modifications by nanomaterials, which are becoming more and more popular for the functionalization and the signal enhancement of the screen printed electrode surfaces [6].

During recent years the nanomaterial carbon black (CB) has started to become more and more popular due to its excellent conductive and electrocatalytic properties. It is a highly attractive candidate for SPE modification due to its high surface area, conductivity and low cost compared to other carbon materials (1 kg of CB costs ~1 € [7], whereas 1 kg of graphene costs ~100-1000 € depending on the quality [8] and 1 kg of carbon nanotubes cost ~1000 € [9]). The good dispersion stability (≈ 2 weeks) [10] combined with the excellent storage stability (>6 months) [11] and the possibility of automated mass-production of the modified SPEs make CB modified SPEs (CB-SPEs) excellent candidates for pesticide detection in the area of food safety.

4.1.2 ELECTROCHEMICAL CHARACTERIZATION TECHNIQUES

The most frequently used electroanalytical methods are voltammetric techniques, which are based on the fact that the current flowing through the system is a function of the potential applied across the electrodes. In voltammetric methods a range of potentials are being scanned and the generated current is directly proportional to the concentration of electroactive species in the sample of interest. Voltammetric methods are able to give both

qualitative and quantitative information, have high sensitivity and a wide linear dynamic range [2]. The most commonly used voltammetric techniques are cyclic voltammetry (CV), differential pulse voltammetry (DPV), linear sweep voltammetry (LSV) and square-wave voltammetry (SWV). In the case of amperometry, the evaluation is based on the interpretation of current as a function of time or potential applied across the electrodes, and this technique is mainly used to provide information about various sensing characteristics. The most commonly used amperometric technique is chronoamperometry (ChA).

During the development of this thesis the following electrochemical measurement techniques were used (All of them performed with a PalmSens 4 potentiostat (Palmsens, The Netherlands)):

4.1.2.1 Cyclic voltammetry

Cyclic voltammetry (CV) is one of the most commonly used electroanalytical techniques. It is usually being used during the development phases of a new method, thus its main advantage is its ability to characterize an electroanalytical system (e.g.: determination of Nernstian or non-Nernstian behaviour of a redox couple, number of electrons transferred in an oxidation or reduction, diffusion coefficients, etc.). In a CV experiment a range of potentials are being applied to the working electrode while the resulting current is being measured. These current values are being plotted versus the applied potential in the form of a CV graph (Figure 4.2).

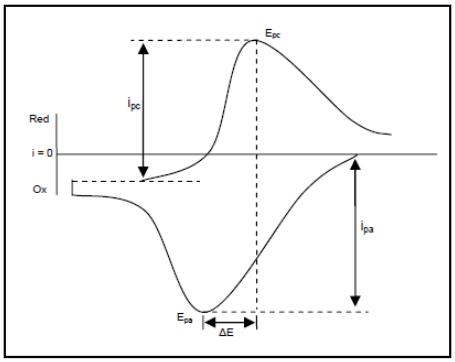

Figure 4.2. *A typical CV plot. The four important parameters are: cathodic peak height (I_{pc}), anodic peak height (I_{pa}), cathodic peak potential (E_{pc}) and anodic peak potential (E_{pa}).*

A singe CV is mostly used to determine whether or not a species is electroactive, thus a peak current response within the desired potential range indicates whether the material has been involved in a reaction or not. A single CV can also be used to determine the number of electrons transferred in a reaction. In general the peak separation is expressed by the following (Nernst) equation,

$$E = E° + \frac{RT}{nF} ln \frac{(Ox)}{(Red)}$$

which relates the potential of an electrochemical cell (E) to the standard potential of a species (E^0) and the relative activities of the oxidized (Ox) and reduced (Red) analyte in the system at equilibrium. In the equation F is Faraday's constant, R is the universal gas constant, n is the number of electrons transferred and T is the temperature. The Nernst equation is a powerful tool to predict how a system will respond to a change of concentration of species in solution or a change in the electrode potential [12].

Even though a lot of information can be exported from just a single CV, it is advised to perform multiple CV measurements in order to draw conclusions about the reversibility of a redox couple. For example, multiple CV measurements allow us to see chemical changes with time while also allowing the system to reach equilibrium before measurements are made. Varying the scan rate in a series of CV experiments for example is usually used to determine the diffusion coefficient of a species.

4.1.2.2 Electrochemical impedance spectroscopy

Electrochemical Impedance Spectroscopy (EIS) measures the impedance of an electrochemical system where dielectric properties and impedance are being quantified over a range of frequencies. It measures the electron transfer and mass transfer depending on the alternating frequency used. The information content of EIS is much higher than DC (direct current) techniques or single frequency measurements. It can identify diffusion-limited reactions, provide information about the electron transfer rate of a reaction and about the capacitive behavior of the system as well. The impedance circuit of an EIS measurement may be represented in a Nyquist or a Bode plot [2]. During the

development of this thesis, Nyquist plots (see Figure 4.3) were used for the EIS measurements:

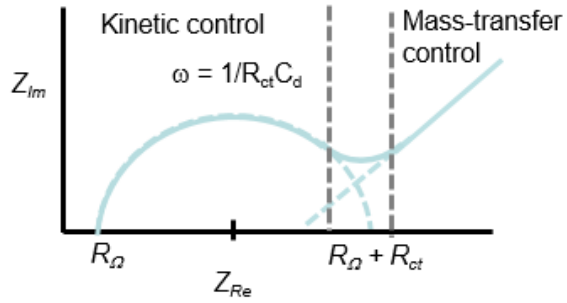

Figure 4.3. *Nyquist plot - If a system is kinetically slow, a large R_{ct} can be observed whereas in the case of a kinetically facile system a smaller R_{ct} can be observed.*

For the analyzation of the EIS data, the EIS response of an equivalent circuit is calculated and compared to the actual EIS response of the electrochemical cell.

4.1.2.3 Chronoamperometry

When a potential step large enough to cause an electrochemical reaction is applied to an electrode, the current changes with time. Chronoamperometry (CA) is the study of this current change as a function of time (Figure 4.4). A stationary WE and an unstirred solution are used for the measurement. The resulting current-time curve reflects the change in the concentration gradient in the close proximity of the electrode's surface and can be monitored by the Cottrel equation:

$$i = \frac{nFAD^{1/2}C^{b}}{(\pi t)^{1/2}}$$

n = number of electrons
F = Faraday's constant
D = diffusion coefficient
C^b = bulk concentration
A = area

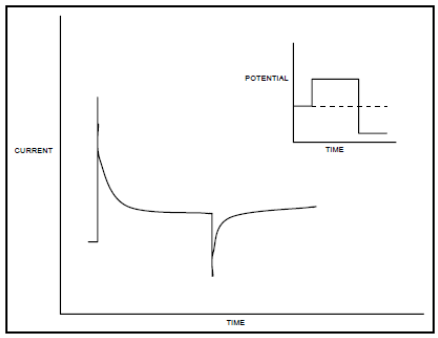

Figure 4.4. *A Typical chronoamperogram displaying the change of current as a function of time.*

Chronoamperometry is a useful tool for the determination of diffusion coefficients of electroactive species, for the measurement of the WE's surface area and for the investigation of reaction kinetics and mechanisms as well. As opposed to CV, CA is able to yield all this information in a single experiment [1].

4.1.2.4 Differential pulse voltammetry

In the case of Differential Pulse Voltammetry (DPV), fixed magnitude pulses are applied to the working electrode. The current is measured straight before the pulse application and again late in the pulse life (when the charging current has decayed). The first current is substracted from the second and this current difference is being plotted versus the applied potential (see Figure 4.5). The height of the resulting current peak is directly proportional to the corresponding analytes [2]. DPV is an extremely useful technique to measure trace levels of organic and inorganic species.

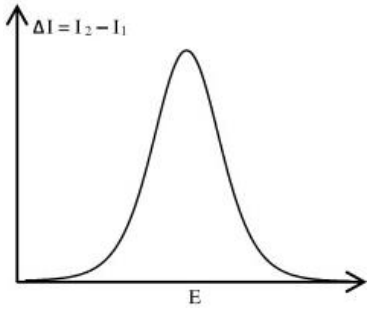

Figure 4.5. *A Typical differential pulse voltammetry graph displaying the current response versus the applied potential.*

4.2 RESULTS AND DISCUSSION

The main objective of this chapter was the printing, modification and characterization of different CB-SPEs. Afterwards, the best performing electrode was selected for the development of an electrochemical immunosensor for the detection of different pesticides in food matrices.

4.2.1 CHARACTERIZATION OF THE BARE SPEs

First, all four different typologies of screen printed electrodes (the combination of 2 different reference electrodes and 2 different dielectric layers) were characterized with CV and EIS measurements.

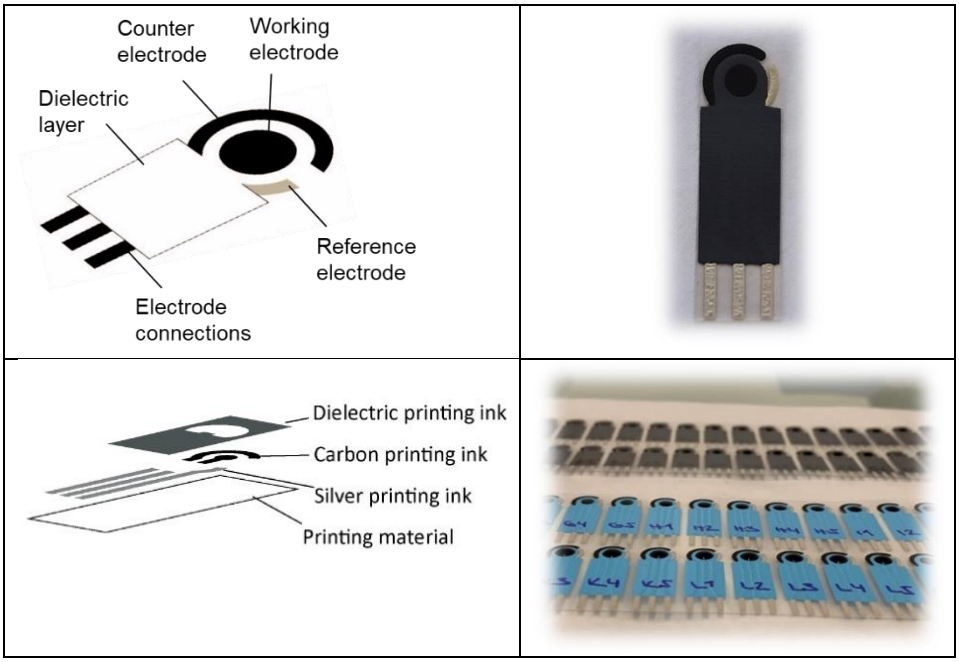

Figure 4.6. *Illustrations and photos demonstrating the different parts of a screen printed electrode (SPE).*

The characterization of the SPEs (Figure 4.6) was based on the electrocatalytic effect of the electrode's surface on the redox couple $[Fe(CN)_6]^{3-/4-}$. All of the different typologies of screen printed electrodes (detailed in section 4.4.2) were evaluated first by CV and then by EIS measurements according to the protocols described in section 4.4.4. In the CV, the $[Fe\ (CN)_6]^{4-/3-}$ oxidation and reduction current peaks and their potentials are indicative of the electron transfer rate on the electrode's surface. Thus, the parameters for the evaluation were the delta E (the difference in potential between the oxidation and reduction peaks) and the height of the anodic (I_A) and cathodic (I_C) current peaks (Figure 4.7). In electrochemically reversible one-electron transfer reactions, where the electron transfer is fast and the process follows the Nernst equation, the distance between the anodic and cathodic peak potentials at 25°C is 57 mV (2.22 RT⁄F). The results of these measurements are shown in Tabe 4.1.

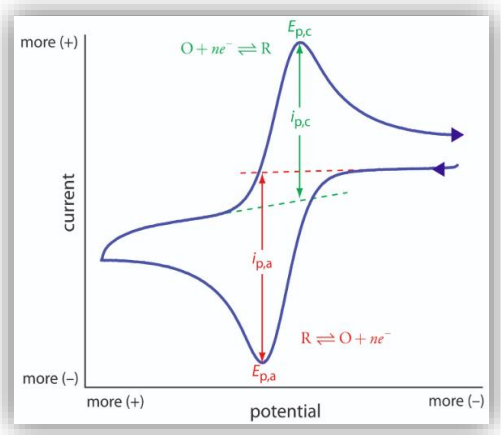

Figure 4.7. *CV graph highlighting the examined parameters for the evaluation of the screen printed electrodes.*

In the case of the EIS, the Nyquist plots (Figure 4.8 and 4.9) were fitted in the theoretical equivalent adapted Randles circuit in which the capacitor is replaced by a constant phase element (CPE) due to the non-homogeneus surface of the WE and is modelled as a non-ideal capacitor of capacitance C and roughness/non-uniformity factor α. In this model C_{dl} is the double layer capacitance, R_{ct} is the charge transfer resistance, R_s is the electrolyte resistance (where the Nyquist plot curve intercepts the real impedance axes) and Z_w is the diffusional resistance element (Warburg impedance). The parameter investigated was $R_{ct} – R_s$ (by Randles circuit fit), which is the diameter of the semi-circle indicative of the charge transfer resistance at the WE's surface. Thus, the aim was to select the electrode with the lowest resistivity (smallest semi-circle) upon performing the EIS measurements.

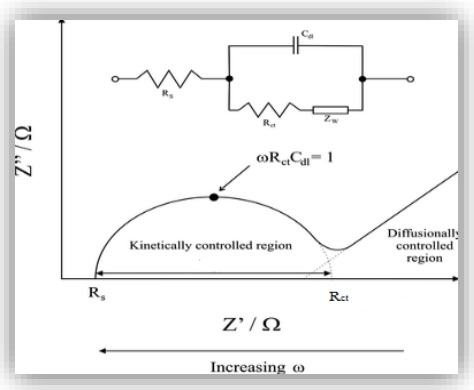

Figure 4.8. *EIS graph highlighting the parameters examined for the evaluation of the screen printed electrodes. C_{dl} is the double layer capacitance, R_{ct} is the charge transfer resistance, R_s is the ionic resistance and Z_w is the diffusional resistance element (Warburg impedance).*

Table 4.1. CV characterization of the four different typologies of electrodes (n=3).

	Capacitive current (µA)	Anodic peak (µA)	Catodic peak (µA)	E_{an} (V)	E_{cat} (V)	delta E (V)
Blue dielectric 80:20	0.043 ± 0.004	48.126 ± 1.072	-44.748 ± 0.589	0.293 ± 0.017	0.030 ± 0.014	0.267 ± 0.033
Blue dielectric 60:40	0.039 ± 0.001	51.874 ± 2.180	-48.140 ± 1.672	0.300 ± 0.000	0.007 ± 0.004	0.293 ± 0.004
Grey dielectric 80:20	0.034 ± 0.004	53.658 ± 1.231	-50.433 ± 1.694	0.297 ± 0.009	0.017 ± 0.001	0.280 ± 0.014
Grey dielectric 60:40	0.043 ± 0.002	51.259 ± 1.018	-47.413 ± 0.904	0.313 ± 0.005	0.007 ± 0.004	0.307 ± 0.005

As it can be observed from the values obtained by CV and EIS in Table 4.1 and Table 4.2, the electrochemical properties of the different typologies of electrodes are fairly similar. Thus, the modifications were performed with all four different typologies.

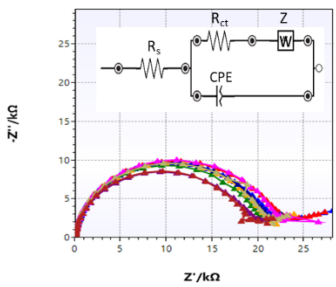

Table 4.2. EIS characterization of the four different typologies of electrodes (n=3).

	R_{ct}-R_s (kΩ)	RSD (%)
Blue dielectric 80:20	23296 ± 2689	12
Blue dielectric 60:40	23284 ± 4708	20
Grey dielectric 80:20	18711 ± 1458	8
Grey dielectric 60:40	20106 ± 1291	6

Figure 4.9. *EIS characterization of the four different typologies of electrodes.*

4.2.2 CHARACTERIZATION OF THE ELECTRODES DROPCASTED WITH CARBON BLACK (dCB-SPEs)

Different volumes of the nanomaterial carbon black (CB) were dropcasted on the surface of the working electrodes based on the protocol explained in section 4.4.3.

Table 4.3. Characterization of the different typologies of electrodes dropcasted with different volumes of carbon black (n=1).

	Amount of CB	Capacitive Current (µA)	Anodic Peak (µA)	Catodic Peak (µA)	E_{an} (V)	E_{cat} (V)	delta E (V)
Blue dielectric 60:40	4 µg	0.036	71.633	-65.900	0.260	0.060	0.200
	6 µg	0.024	77.352	-71.630	0.250	0.060	0.190
	8 µg	0.054	81.087	-75.699	0.250	0.060	0.190
	10 µg	0.029	76.820	-70.302	0.250	0.070	0.180
	15 µg	0.050	91.000	-86.000	0.240	0.080	0.160
	20 µg	0.073	101.00	-95.000	0.240	0.080	0.160
Grey dielectric 60:40	4 µg	0.044	68.241	-63.735	0.280	0.060	0.220
	6 µg	0.041	75.119	-71.616	0.250	0.070	0.180
	8 µg	0.047	76.781	-74.725	0.250	0.070	0.180
	10 µg	0.049	80.018	-75.165	0.250	0.070	0.180
	15 µg	0.028	91.000	-87.000	0.210	0.100	0.110
	20 µg	0.028	92.000	-86.000	0.220	0.100	0.120
Blue dielectric 80:20	4 µg	0.027	65.420	-59.333	0.280	0.050	0.230
	6 µg	0.036	69.776	-63.608	0.280	0.050	0.230
	8 µg	0.034	76.817	-69.979	0.270	0.060	0.210
	10 µg	0.036	79.130	-74.530	0.240	0.090	0.150
	15 µg	0.039	76.306	-70.801	0.240	0.090	0.150
	20 µg	0.062	93.800	-88.450	0.230	0.090	0.140
Grey dielectric 80:20	4 µg	0.038	67.604	-62.976	0.260	0.060	0.200
	6 µg	0.035	70.306	-65.739	0.260	0.060	0.200
	8 µg	0.030	72.172	-68.179	0.260	0.070	0.190
	10 µg	0.044	77.817	-73.478	0.250	0.070	0.180
	15 µg	0.052	84.434	-81.085	0.240	0.080	0.160
	20 µg	0.045	93.020	-90.260	0.230	0.090	0.140

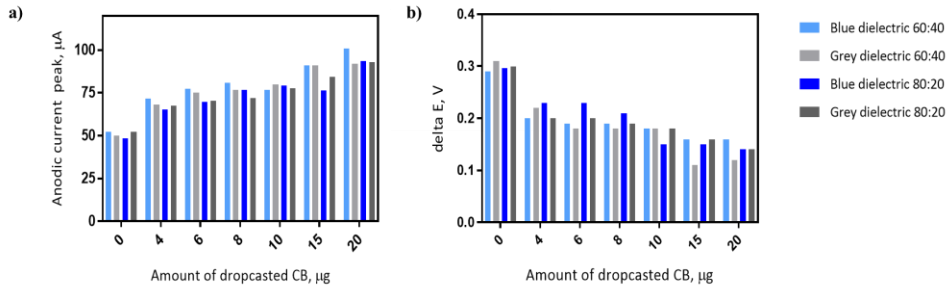

Figure 4.10. *Comparison of the different typologies of electrodes dropcasted with different volumes of CB by representing the values of their anodic current peak* ***a)*** *and their peak-to-peak separation (delta E)* ***b)*** *in relation to the amount of dropcasted CB.*

It can be seen from Table 4.3 and Figure 4.10 that in most cases the optimal amount of CB is 15 or 20 µg (highest anodic current peak and lowest delta E). However, the slightly better performance of the 20 µg CB is not significant enough to justify a second deposition step of CB. Thus, for future comparisons and experiments the use of the 15 µg CB is preferred, since in this case only one deposition step is necessary using a 3 mg mL^{-1} CB dispersion (further detailed in sections 4.2.5 and 4.4.3) for the dropcasting.

4.2.3 CHARACTERIZATION OF THE ELECTRODES WITH CB MODIFIED INK (iCB-SPEs)

After the characterization of the electrodes dropcasted with CB, the ones where the CB was mixed in the WE's ink (during the printing process) were characterized as well.

Table 4.4. CV characterization of the iCB-SPEs (n=3).

	Capacitive Current (µA)	Anodic Peak (µA)	Catodic Peak (µA)	E_{an} (V)	E_{cat} (V)	delta E (V)
Blue dielectric 80:20	0.079 ± 0.005	59.552 ± 0.589	-56.079 ± 0.932	0.277 ± 0.005	0.037 ± 0.005	0.240 ± 0.000
Blue dielectric 60:40	0.041 ± 0.002	56.640 ± 0.667	-51.472 ± 0.785	0.290 ± 0.000	0.013 ± 0.005	0.277 ± 0.005
Grey dielectric 80:20	0.055 ± 0.005	60.395 ± 4.174	-56.235 ± 2.550	0.277 ± 0.005	0.030 ± 0.010	0.247 ± 0.005
Grey dielectric 60:40	0.052 ± 0.002	62.892 ± 1.468	-57.489 ± 1.961	0.273 ± 0.005	0.030 ± 0.000	0.243 ± 0.005

Table 4.4 shows that the electrodes with the grey dielectric and 60:40 Ag/AgCl have the best electrochemical properties, even though the examined

electrochemical parameters had similar values for all of the different typologies of electrodes.

4.2.4 COMPARISON BETWEEN THE BARE AND THE CB MODIFIED ELECTRODES

Based on the results obtained in sections 4.2.1, 4.2.2 and 4.2.3, the electrode with 15 µg of dropcasted CB (from a dispersion of 3 mg mL^{-1} of CB) was selected for future experiments. On the different graphs and table below (Figure 4.11 and Table 4.5), a comparison of the bare SPEs, the electrodes with CB modified ink (iCB-SPE) and the electrodes that were modified with CB via dropcasting (dCB-SPE) can be seen.

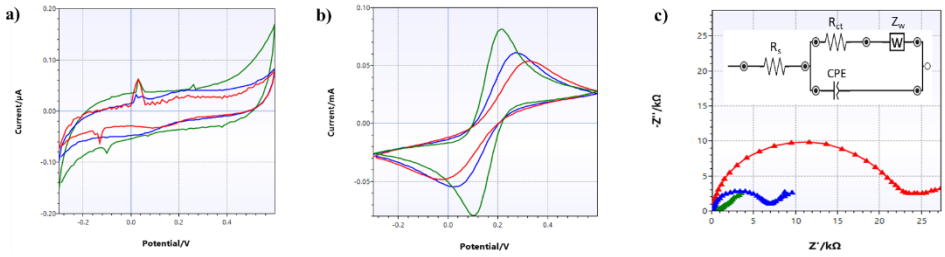

Table 4.5. CV and EIS characterization of the SPEs with 60:40 Ag/AgCl reference electrode and a grey dielectric layer (n=3).

Grey dielectric 60:40	Anodic peak (µA)	Catodic peak (µA)	delta E (V)	R_{ct}-R_s (kΩ)
Bare SPEs	51.3 ± 1.0	-47.4 ± 0.9	0.307 ± 0.005	20106 ± 1291
iCB-SPEs	62.9 ± 1.5	-57.5 ± 2.0	0.247 ± 0.005	6629 ± 723
dCB-SPEs	90.0 ± 3.0	-87.1 ± 2.3	0.130 ± 0.022	469 ± 74

Figure 4.11. *Characterization of the electrodes with 60:40 Ag/AgCl reference electrode and grey dielectric layer. a) CVs performed in KCl 0.1 M in the absence of $[Fe(CN)_6]^{3-/4-}$ 5 mM. b) CVs performed in KCl 0.1 M in the presence of $[Fe(CN)_6]^{3-/4-}$ 5 mM. c) EIS performed in $[Fe(CN)_6]^{3-/4-}$ 1 mM. The colour red corresponds to the bare SPEs, blue to the dCB-SPEs and green to the iCB-SPE. In the case of the graphs only one replica is shown (n=1) for clearer representation, whereas in Table 4.5 n=3 (representing all three replicates that were used for each measurement).*

Examining the CV results above, it can be observed that the dCB-SPEs show an improved reversibility of the redox reaction which means an improved electron transfer rate for reactions limited by diffusion, whereas in the case of the iCB-

SPEs the peak-to-peak separation remains bigger and only a slight increase in current can be detected compared to the bare SPEs (Figure 4.11/b). The capacitive current (Figure 4.11/a) has also increased in both cases of the CB modified electrodes, but it still remained in the nA range, thus perfectly acceptable.

In the case of the EIS analysis (Figure 4.11/c), a decrease in charge transfer resistance (R_{ct} - represented by the diameter of the semi-circle in the Nyquist plot) can be observed for the iCB-SPEs compared to the bare SPEs, and a further decrease in the case of the dCB-SPEs. Table 4.5 unequivocally shows the advantageous properties of the dCB-SPE, having the highest peaks in terms of current, the smallest delta E (from CV analysis) and the smallest semi-circle size (from EIS analysis).

As a result of the electrode characterization and evaluation (further detailed in section 4.2.6), the electrode with the best electrochemical properties: 60:40 Ag/AgCl with a grey dielectric layer, dropcasted with 15 µg of CB was chosen as the platform for the development of the immunosensors.

4.2.5 SELECTION OF THE MOST OPTIMAL CB DISPERSION

For the evaluation of the different CB dispersions, 15 µg of the different CB stock solutions (2 mg mL^{-1} and 3 mg mL^{-1}) were dropcasted on the surface of the working electrodes in order to evaluate the difference between having one or two layers of the dispersion on the WE.

Table 4.6. Comparison of the different concentrations of CB dispersions based on CV and EIS measurements (n=3).

Grey dielectric 60:40	Anodic peak (µA)	Catodic peak (µA)	delta E (V)	R_{ct}-R_s (kΩ)
Bare electrode	51.3 ± 1.0	-47.4 ± 0.9	0.307 ± 0.005	20106 ± 1291
2 mg mL^{-1} CB	88.7 ± 1.5	-84.0 ± 1.0	0.153 ± 0.005	448 ± 99
3 mg mL^{-1} CB	90.2 ± 0.6	-84.4 ± 0.6	0.153 ± 0.005	334 ± 52

As it can be observed from Table 4.6, both dispersions have the same properties regarding the height of the anodic current peak and the delta E, but using the 3 mg mL^{-1} stock gives us a lower resistivity of the surface, which can be explained by the fact that in this case only one layer of the CB ink was used. Thus, in the

future this CB dispersion will be used for the dropcasting of the electrodes. Using a more concentrated dispersion than 3 mg mL^{-1} is not be possible due to the fact that the solution would not be stable at a higher concentration (it would have precipitates of CB).

4.2.6 EVALUATION OF THE ELECTROCATALYTIC EFFECT OF CB

From the results obtained in the sections above, it is clear that the CB has an electrocatalytic effect on the potential (enhanced electron transfer) of the redox couple used, but we wanted to see if even the increase of the current peaks could be due to the electrocatalytic effect of the CB or is only due to the increased surface area that the CB provides.

First, the surface areas were calculated for the bare SPEs, for the iCB-SPEs and for the dCB-SPEs that were dropcasted with either 10 or 15 µg of CB. For this purpose, the Randles-Sevcik equation was used:

$$I_p = 2{,}69x10^5 \times n^{3/2} \times D^{1/2} \times C_0 \times A_{electrode} \times V^{1/2}$$

For electrochemically reversible electron transfer processes involving freely diffusing redox species, the Randles–Sevcik equation describes how the peak current I_p (A) increases linearly with the square root of the scan rate V (V s^{-1}), where A is the surface area of the electrode (cm^2), n the electron transfer per reaction (1 in the case of $[Fe(CN)_6]^{3-/4-}$), D the diffusion coefficient of $[Fe(CN)_6]^{3-/4-}$ (7.6 10-6 cm^2/s) and C_0 the concentration of $[Fe(CN)_6]^{3-/4-}$ (0.005 M).

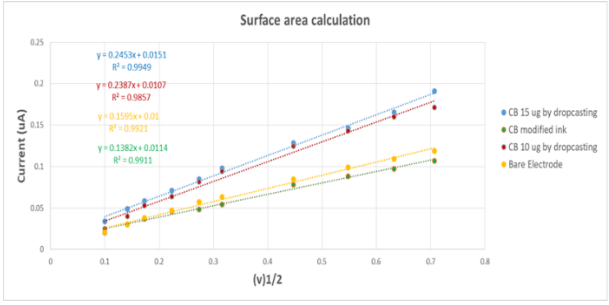

Table 4.7. Surface area calculations for the different typologies of electrodes.

Electrode types	A (cm^2)
Bare electrode	0.04
CB modified ink	0.04
10 µg dropcasted CB	0.06
15 µg dropcasted CB	0.07

Figure 4.12. *Surface area calculation for different SPEs from CV experiments with scan rates of: 10-20-30-50-75-100-200-300-400-500 mV/s.*

It can be seen from Figure 4.12 and Table 4.7, that indeed the surface area increases by dropcasting the CB on the surface of the WE. In order to verify if this is the only reason for the observed increase in anodic current peaks in the CV, a calibration curve for hydroquinone (HQ) was generated (the redox couple Hydroquinone/Benzoquinone was used due to the fact that HQ is the substrate of HRP, the enzyme used to label the secondary antibody in the immunoassay) using the concentrations 0.1, 0.5 and 1 mM of HQ and a ratio R was calculated by dividing the slopes of the HQ oxidation curves of the various modified SPEs in Figure 4.13/a by the corresponding active surface areas of those SPEs.

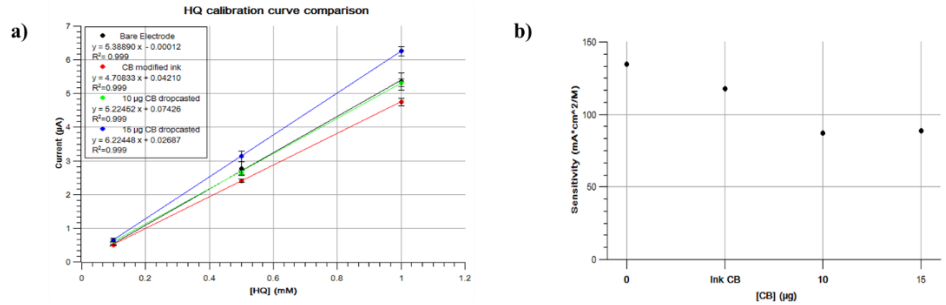

Figure 4.13. *Evaluation of the electrocatalytic effect of CB. a) Calibration curve for Hydroquinone. Applied potential, +0.120 V versus Ag/AgCl b) Correlation between the WE's surface area and the sensitivity.*

It can be detected from Figure 4.13/b that the sensitivity in terms of current is not given from the CB, since the electrodes modified with the highest concentration of CB (10 and 15 µg) show the lowest sensitivity. Thus, it is clear that the CB doesn't have any electrocatalytic effect on the increase of the current. The higher current is only due to the enhanced surface area that it provides.

4.2.7 CHARACTERIZATION OF THE ELECTRODES DROPCASTED WITH THE AUTOMATED BIODOT DISPENSER

In order to compare the efficiency of the manual dropcasting to the automated one, different amounts of CB (from the 3 mg mL^{-1} CB dispersion) were dropcasted on the surface of the WEs with the help of an automated BioDot dispenser, and

the electrochemical properties of these electrodes were also evaluated with CV and EIS measurements.

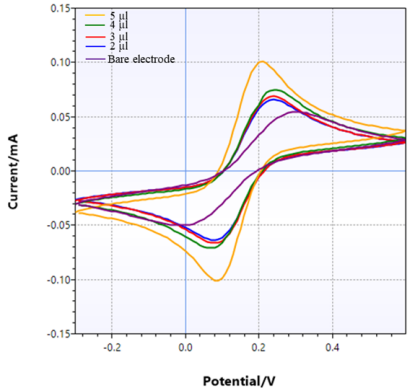

Table 4.8. Characterization of the electrodes dropcasted by the automated BioDot dispenser (n=3).

Amount of dropcasted CB	Capacitive current (µA)	Anodic peak (µA)	Catodic peak (µA)	E_{an} (V)	E_{cat} (V)	delta E (V)
2 µl	0.052 ± 0.002	75.300 ± 1.628	-71.121 ± 1.185	0.230 ± 0.010	0.083 ± 0.005	0.140 ± 0.022
3 µl	0.048 ± 0.002	75.961 ± 1.594	-72.665 ± 1.589	0.240 ± 0.000	0.080 ± 0.000	0.160 ± 0.000
4 µl	0.038 ± 0.004	81.154 ± 0.756	-76.563 ± 0.956	0.240 ± 0.000	0.073 ± 0.005	0.173 ± 0.005
5 µl	0.067 ± 0.019	111.000 ± 6.481	-112.333 ± 2.055	0.213 ± 0.005	0.087 ± 0.005	0.127 ± 0.005

Figure 4.14. *CV characterization of different amounts of CB dropcasted with the BioDot dispenser.*

It can be observed from the cyclic voltammograms above (Figure 4.14), that for the amounts 2, 3 and 4 µL of CB the height and the position of the anodic current peak is very similar, only in the case of the electrode that was dropcasted with 5 µL of CB, can an electrocatalytic effect be observed, which results in a higher anodic current peak (Table 4.8) and in a shift of the peaks.

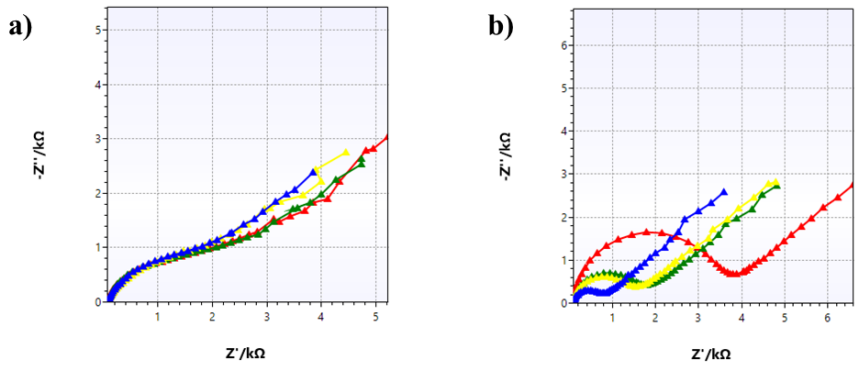

Figure 4.15. *a) EIS analysis of the electrodes dropcasted with CB by the BioDot dispenser b) EIS analysis of the electrodes manually dropcasted with CB. The colour red corresponds to the dropcasting of 2 µg of the nanomaterial CB, green to 3 µg, yellow to 4 µg and blue to 5 µg.*

The graphs above (Figure 4.15) show a comparison between the manual and the automated dropcasting of CB. It can be observed, that in the case of using an automated BioDot dispenser (Figure 4.15/a) the resistivity of the surfaces dropcasted with the nanomaterial CB is practically identical, even though they were dropcasted with different amounts of CB. This further proves that the BioDot dispenser is able to provide a homogeneous layer on the surface of the WE in contrast to the manual dropcasting procedure, where there is a clear difference in surface resistivity between the electrodes dropcasted with different amounts of CB (Figure 4.15/b). This can most probably be attributed to the capacity of the automatic dispenser to dispense a uniform and homogeneous layer of CB on the surface of the electrode.

Based on these results, from now on all the CB modifications will be performed with the Biodot dispenser.

4.3 CONCLUSIONS

Several different typologies of screen printed electrodes were produced, modified and characterized. The electrode modifications were carried out with the nanomaterial carbon black either during the printing process by directly mixing the particles in the ink or after the printing process by dropcasting these

nanoparticles on the surface of the working electrode. The evaluation of these SPEs was based on the electrocatalytic effect of the electrode's surface on the redox couple $[Fe(CN)_6]^{3-/4-}$. After selecting the electrodes with the best electrochemical properties in terms of peak-to-peak separation and height of the current peaks, surface area calculations were carried out and the electrocatalytic effect of CB was further investigated. Besides the enhancement of the electrochemical signal, CB also allows for the use of a potential close to zero due to the enhanced electron transfer, which is a big advantage during the analysis in real samples, since it helps in avoiding interferences with other electroactive species from the matrix.

4.4 MATERIALS AND METHODS

4.4.1 CONSUMABLES AND REAGENTS

Carbon black (N220) was obtained from Cabot Corporation (Ravenna, Italy). The graphite, the silver and the dielectric inks were provided by Gwent (Pontypool, UK). The substrate used for the printing was a flexible polyester sheet (Autostat CT, Wantage UK).

All solutions were prepared with MQ water from a MilliQ-system. $K_4Fe(CN)_6 \bullet 3H_2O$, $K_3Fe(CN)_6$, $C_6H_8O_7$, KCl, Na_2HPO_4, Hidroquinone (HQ) and Dimethylformamide (DMF) were purchased from Sigma Aldrich.

4.4.2 SCREEN PRINTED ELECTRODE PRODUCTION

All different typologies of SPEs were produced in-house at CSEM Landquart (Switzerland) using a DEK 248 semi-automatic screen-printing machine (DEK Printing Machines Ltd, UK). The first step of the electrode production was the printing of the reference electrodes with different ratios (80:20 and 60:40) of silver/silver-chloride based ink. The composition of the reference electrodes has an impact on their long-term stability. The following step was the printing of the working and the counter electrodes with a graphite based ink. Afterwards, as the

last step of the printing process, two different types of dielectric inks (grey coloured screen printable polymer dielectric (good flexibility properties) - blue coloured screen printable polymer dielectric (improved impermeability)) were used to insulate the electrodes and define the electrode's different areas. The material of the dielectric layer has an impact on the flexibility and impermeability of the electrode, the latter is particularly important upon developing immunosensors in a humid chamber. In between each printing step the electrodes were cured in an oven at 80 °C after the first two steps and at 130 °C after the last step.

4.4.3 SCREEN PRINTED ELECTRODE MODIFICATION

The SPEs were modified with the nanomaterial carbon black in two different ways. On one hand the SPEs were modified during the printing process by mixing the CB directly in the graphite based ink, reaching a 15 % concentration of the nanomaterial (iCB-SPEs).

On the other hand, another set of SPEs were only modified with the nanomaterial after the printing process by dropcasting (manually or with an automated BioDot dispenser) a dispersion of CB directly on the surface of the WE (dCB-SPEs). For this modification two different dispersions of CB (2 mg mL^{-1} and 3 mg mL^{-1}) were prepared in a solution of DMF:MQ (1:1, v/v) and then sonicated by using the "Ultrasonic processor HP 200 st" (Hielscher Ultrasonic GmbH) until a homogenous dispersion was obtained. In order to ensure a uniform coverage on the WE's surface, the dropcasted SPEs were dried in a humid chamber overnight (23-25 °C, 65% humidity).

For the 2 mg mL^{-1} CB dispersion the following volumes were dropcasted on the WEs:

Table 4.9. Dropcasted volumes of the 2 mg mL^{-1} CB dispersion

Volume	Resulting weight
2 µl	4 µg
3 µl	6 µg
4 µl	8 µg
5 µl	10 µg
5 µl + 2.5 µl	15 µg
2*5 µl	20 µg

In the case of the 3 mg mL^{-1} dispersion the same µg of CB per WE was reached by adding the following volumes:

Table 4.10. Dropcasted volumes of the 3 mg mL^{-1} CB dispersion

Volume	Resulting weight
1.3 µl	4 µg
2 µl	6 µg
2.7 µl	8 µg
3.3 µl	10 µg
5 µl	15 µg
5 + 1.7 µl	20 µg

4.4.4 ELECTROCHEMICAL CHARACTERIZATION AND MEASUREMENTS

All EC measurements were performed with a PalmSens 4 potentiostat (Palmsens, The Netherlands). i) *Cyclic voltammetry (CV)* measurements were performed in 0.1 M KCl in the absence or presence of 5 mM Ferro-Ferricyanide $[Fe(CN)_6]^{3-/4-}$. The potential was scanned from -0.3 V to 0.6 V with a step potential of 0.01 V and a scan rate of 0.05 V/s for two cycles. In the case of the active surface area calculation the following scan rates were used: 0.01, 0.02, 0.03, 0.05, 0.075, 0.1, 0.2, 0.3, 0.4 and 0.5 V/s. ii) *Electrochemical Impedance Spectroscopy (EIS)* measurements were executed in 1 mM $[Fe(CN)_6]^{3-/4-}$ in 0.1 M KCl. The following parameters were set: 0 V applied potential versus V_{ocp}, a frequency range from

100 kHz to 0.1 Hz, and an amplitude of 10 mV. Nyquist plots were fitted in a theoretical equivalent adapted Randles Circuit. iii) *Chronoamperometry (ChA)* measurements were employed for the quantification of the HQ and performed at a chosen fixed potential of +0.12 V for 30 seconds with a 0.1 s time interval.

4.4.5 DATA TREATMENT

For the electrochemical data obtained with the PalmSens4 potentiostat, the PSTrace v5.5 software was used. The above mentioned potentiostat has Bluetooth capabilities and next to PSTrace interface for computer it is also provided with a specific interface for Android's smartphone, PStouch, which can be downloaded free of charge from the Google Play Store. PStouch can communicate with the potentiostat directly via USB or wirelessly using the PalmSens Bluetooth dongle, thus, any smartphone or tablet with an Android operating system has the capabilities to function as a display for the results of the electrochemical measurements. For the data fitting of the EIS measurements the Z-view software (Scribner Associates, Inc., Southern Pines, NC, USA; www.scribner.com) was used.

4.5 BIBLIOGRAPHY

[1] Wang J. (2000). Analytical Electrochemistry, Second Edition. Wiley-VCH. ISBN: 0-471-22823-0 (Electronic).

[2] Mahato K. et al. (2018). Electrochemical Immunosensors: Fundamentals and Applications in Clinical Diagnostics. Handbook of Immunoassay Technologies, Elsevier. http://doi.org/10.1016/B978-0-12-811762-0.00014-1

[3] Renedo, O. Domínguez; Alonso-Lomillo, M.A.; Martínez, M.J. Arcos (2007). "Recent developments in the field of screen-printed electrodes and their related applications". Talanta. 73 (2): 202–219. doi:10.1016/j.talanta.2007.03.050

[4] Taleat, Zahra; Khoshroo, Alireza; Mazloum-Ardakani, Mohammad (July 2014). "Screen-printed electrodes for biosensing: a review (2008–2013)".

Microchimica Acta. 181 (9–10): 865–891. doi:10.1007/s00604-014-1181-1. ISSN 0026-3672

[5] Arduini, F.; Majorani, C.; Amine, A.; Moscone, D.; Palleschi, G. (2011). Hg^{2+} Detection by Measuring Thiol Groups with a Highly Sensitive Screen-Printed Electrode Modified with a Nanostructured Carbon Black Film. Electrochim. Acta, 2011, 56, 4209–4215

[6] Cinti, S.; Mazzaracchio, V.; Cacciotti, I.; Moscone, D.; Arduini, F. Carbon Black-Modified Electrodes Screen-Printed onto Paper Towel, Waxed Paper and Parafilm M®. Sensors (Switzerland), 2017, 17, 1–12

[7] Arduini, F.; Majorani, C.; Amine, A.; Moscone, D.; Palleschi, G. Hg2+ Detection by Measuring Thiol Groups with a Highly Sensitive Screen-Printed Electrode Modified with a Nanostructured Carbon Black Film. Electrochim. Acta, 2011, 56, 4209–4215.

[8] Ciriminna, R.; Zhang, N.; Yang, M.Q.; Meneguzzo, F.; Xu, Y.J.; Pagliaro, M. Commercialization of Graphene-Based Technologies: A Critical Insight. Chem. Commun., 2015, 51, 7090–7095.

[9] Smajda, R.; Mionic, M.; Duchamp, M.; Andresen, J.C.; Forró, L.; Magrez, A. Production of High Quality Carbon Nanotubes for Less than $1 per Gram. Phys. status solidi c, 2010, 7, 1236–1240.

[10] Arduini, F.; Di Nardo, F.; Amine, A.; Micheli, L.; Palleschi, G.; Moscone, D. Carbon Black-Modified Screen-Printed Electrodes as Electroanalytical Tools. Electroanalysis, 2012, 24, 743–751.

[11] J.L.D. Nelis, D. Migliorelli, L. Mühlebach, S. Generelli, L. Stewart, C.T. Elliott, K. Campbell, Talanta Highly sensitive electrochemical detection of the marine toxins okadaic acid and domoic acid with carbon black modified screen printed electrodes, Talanta. 228 (2021) 122215. https://doi.org/10.1016/j.talanta.2021.122215.

[12] Rountree, K. J., Mccarthy, B. D., Rountree, E. S., Eisenhart, T. T., & Dempsey, J. L. (2017). A Practical Beginner's Guide to Cyclic Voltammetry. Journal of Chemical Education. https://doi.org/10.1021/acs.jchemed.7b00361

5 DEVELOPMENT OF AN ELECTROCHEMICAL IMMUNOSENSOR FOR THE DETECTION OF ATRAZINE IN ORANGE JUICE

CHAPTER OVERVIEW

This chapter first describes the characterization of the immunoreagents necessary for the detection of the herbicide Atrazine. After the characterization process, the development of different immunochemical approaches such as electrochemical immunoassays and immunosensors is explained. Finally, the implementation of these methods into real food sample analysis is being discussed.

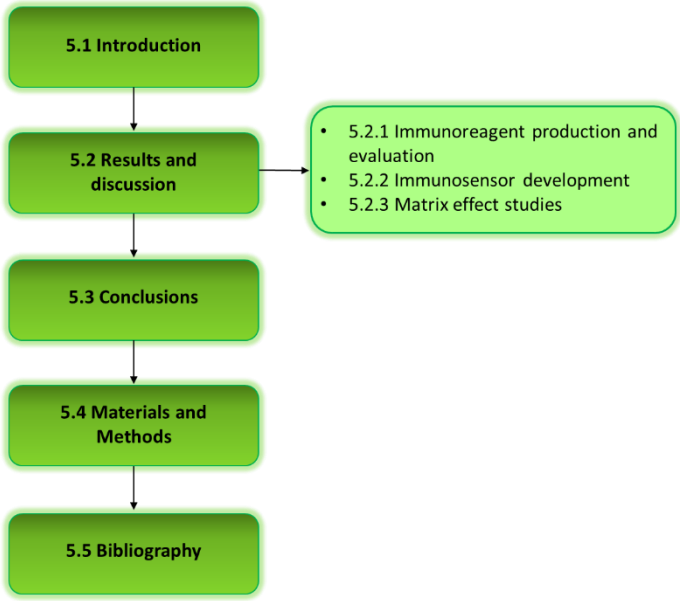

Figure 5.1. *The structure of this chapter regarding the different sections.*

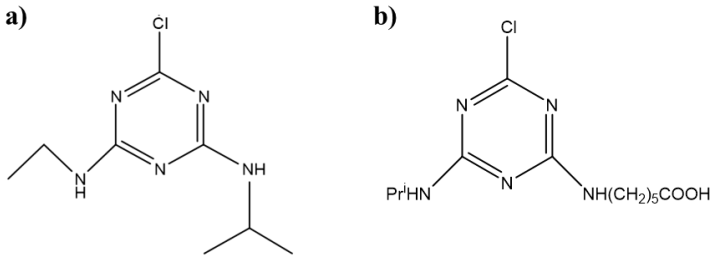

Figure 5.2. *a) Chemical structure of Atrazine. b) Chemical structure of the immunizing hapten for the detection of Atrazine.*

5.1 INTRODUCTION

5.1.1 THE ROLE OF ATRAZINE IN FOOD SAFETY MONITORING

Atrazine (Figure 5.2/a) is a widely used selective herbicide mainly used for the control of broadleaf plants and annual grasses, which would otherwise create hurdles in the normal growth of the desired crop [1]. It can be persistent in the environment for a long period and is commonly found in soil, water and agriculture due to its slow degradation and moderate water solubility. Its residues can cause harm to the reproductive, endocrine, central nervous and the immune system of animals and humans and they can even lead to cancer [2-5]. For this reason, the European Commission has decided to establish maximum residue limits (MRLs) for various different pesticides in a wide range of food matrices (EC Regulation 396/2005) [6]. In the case of atrazine the MRL was set to 0.05 mg kg^{-1} in fruit juices.

5.1.2 DETECTION METHODS FOR ATRAZINE IN THE LITERATURE

Traditionally, the detection of atrazine relies on analytical methods such as a solid-phase extraction technique followed by liquid chromatography or gas chromatography coupled to mass spectrometry (HPLC-MS or GC-MS) [7-9], potentiometry, capillary electrophoresis or flow injection calorimetry [10, 11]. Even though these techniques provide several advantages such as high sensitivity and accuracy with low detectability levels (ng L^{-1}), due to their drawbacks of being time-consuming, non-portable, relatively expensive, requiring high sample volumes, a complex pre-treatment of the samples, machinery and highly trained personnel, they cannot be implemented as on-site screening methods [12]. Hence there is a high demand for the development of rapid on-site screening tools that could serve as complementary warning techniques for food safety next to the chromatographic techniques. Attractive candidates for this purpose are immunoassays and immunosensors due to their numerous advantageous properties (high specificity, low detection limits, rapidity, reliability, simplicity, potentially low-cost and disposability, portability etc.), which make them suitable for on-site analysis [13, 14]. The incorporation

of nanomaterials into the development of sensors is also highly desirable due to their unique electrical and optical properties, their large surface area, diverse functionality, abundant active sites and multiple synthesis methods [1]. In fact, a number of sensors have already been successfully employed for the sensitive detection of herbicides based on the use of enzymes, antibodies, aptamers or different nanomaterials [15, 16].

For the detection of herbicides, such as atrazine, the use of immunoreagents (antibodies and antigens) is one of the most attractive options due to their high sensitivity and specificity. Additionally, the use of nanomaterials can further enhance the performance of these detection methods due to the distinct surface characteristics that they offer [13, 17-19]. As a result of their diverse properties, nanomaterials can be used for the fabrication of various sensortypes, such as electrochemical, surface plasmon resonance, piezoelectric, fluorimetric or chromatography-based sensors. Electrochemical immunosensors stand out due to their high specificity, sensitivity and quantifiable signals [1]. The most critical step in the development of an immunosensor is the efficient attachment of the analyte specific immunoreagent to the sensor's surface, in order to achieve an optimal response signal. One of the main advantages of using nanomaterials is that the functional groups on their surface allow for the immobilization of immunoreagents either through adsorption [19] or by chemical conjugation methods with the help of linker molecules [20, 21].

Various different nanomaterial-based electrochemical immunosensors have already been developed for the detection of atrazine, based on the use of sensing techniques such as cyclic voltammetry, differential pulse voltammetry [14], electrochemical impedance spectroscopy [15-17], conductometry [18], or square wave voltammetry [13]. However, there is still a great need for consumer-friendly on-site analytical devices with multiplexing capabilities that could detect a number of different pesticides in various food matrices integrated into a smartphone-based analytical device.

5.1.3 IMMUNOCHEMICAL ASSAYS

Immunochemical methods are based on the high affinity of an antibody towards a specific antigen. The specificity of this antigen-antibody interaction allows for the selective detection and/or quantification of the target molecule in complex samples or matrices. One of the most widespread immunochemical techniques is the enzyme-linked immunosorbent assay (ELISA). In the case of an ELISA, an enzyme label (e.g. horseradish peroxidase or alkaline phosphatase) is being used in order to detect the immunochemical reaction between the antigen and the antibody. The use of this enzyme catalyses a chemical reaction where a specific substrate is being converted into a colourful product that absorbs in the visible spectra (e.g. at 450 nm). This colorimetric change is proportional to the amount of antibody bound to the target analyte, which allows for the quantification of this target.

Depending on the molecular weight of the target molecule, different configurations of ELISAs could be used. The three main configurations of an ELISA are illustrated on the graph below (Figure 5.3). For the detection of analytes with a high molecular weight usually a sandwich-type ELISA is used. This method is based on the use of two primary antibodies, a capture (immobilized on the ELISA plate) and a detection antibody (free in solution) that binds to different epitopes of the target analyte. In the case of analytes with low molecular weight, the epitopes required for the recognition are too close to each other, which inhibits the use of a sandwich format (the analyte can not be simultaneously detected by two different antibodies). Thus, in this case the presence of a competitor (an antigen which is a hapten coupled to a protein) is needed and the use of a competitive ELISA format is preferred. This method is based on the competition between the target analyte and the competitor antigen for the binding sites of the antibody. A competitive ELISA can be direct, when the competitor antigen is labelled with an enzyme that catalyses the colorimetric reaction, or indirect, when the use of an enzyme-labelled secondary antibody is needed. This secondary antibody is specific to the constant fraction of the primary antibody (Figure 5.3). Due to the fact that atrazine is a compound with a low molecular weight, the competitive ELISA format was used for its detection.

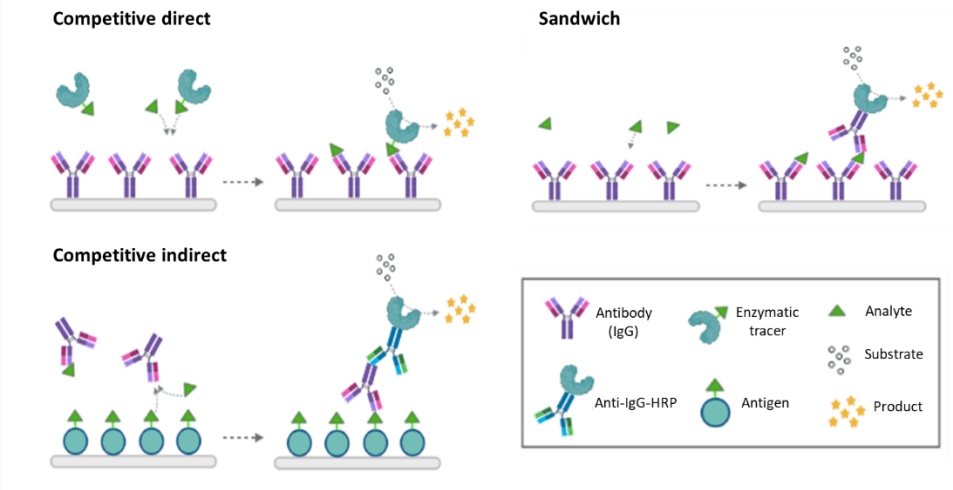

Figure 5.3. *Schematic representation of the three most commonly used ELISA formats. In the case of the competitive direct ELISA the antibody is being immobilized on the plate and the final signal can be obtained using an enzyme tracer. Whereas in the case of the competitive indirect ELISA the competitor antigen is immobilized on the surface of the 96 well plate and the use of a secondary antibody is necessary in order to obtain the final signal. Finally, in the case of the sandwich ELISA configuration, the detection of the analyte is achieved through the use of a capture and a detection antibody.*

ELISA experiments are usually performed in 96 well polystyrene microtiter plates that have been pre-treated in order to facilitate the adsorption of proteins. After the chemical adsorption of the coating antigen or the antibody, a sequential addition of reagents and washing steps (with the help of a detergent, in order to remove unbound materials and avoid non-specific interactions) are performed, finishing with the enzymatic reaction that produces the colorimetric signal, which is measured at the adequate wavelength by a spectrophotometer.

In competitive ELISAs the colorimetric signal is indirectly proportional to the concentration of the target analyte. The representation of the logarithm of the analyte concentration in respect to the measured signal (absorbance) results in a sigmoidal shaped inhibition curve that is fitted to a 4 parameter equation thus giving the main features of the assay (Figure 5.4).

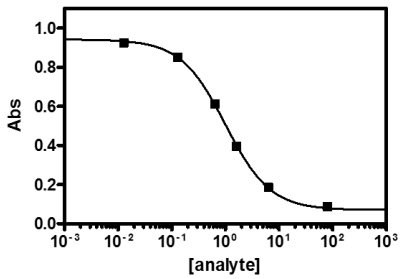

$$f(x) = A_{max}\frac{(A_{min} - A_{max})}{\left(1 - \left(\frac{x}{IC_{50}}\right)^{Hillslope}\right)}$$

Figure 5.4. *Calibration curve of a competitive ELISA and its fitted equation. A_{max}: maximum absorbance, A_{min}: minimum absorbance, IC_{50}: half maximal inhibitory concentration, Hillslope: slope of the linear part of the curve.*

5.2 RESULTS AND DISCUSSION

5.2.1 IMMUNOREAGENT PRODUCTION AND EVALUATION: 2D-BSA/AS11 ASSAY

The features of an antibody (specificity, affinity, etc.) determine the performance of a bioanalytical technique, thus they are the key molecules of any immunochemical assay/sensor. In the case of non-immunogenic small molecules, such as our target analyte atrazine, the features of the antibody are highly determined by the immunizing hapten used to raise the antibodies (Figure 5.5). The chemical structure of the hapten has a great impact on the affinity and specificity of the antibodies produced and therefore, on the detectability and selectivity of the developed immunochemical technique.

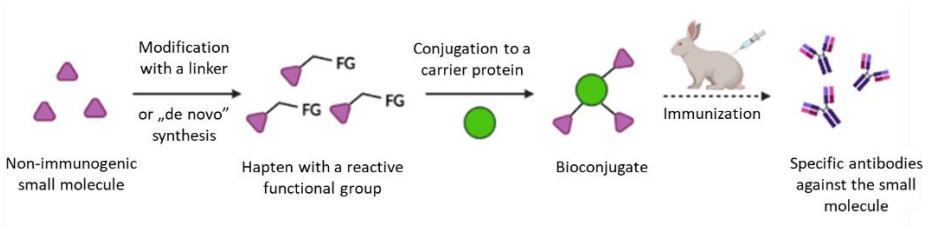

Figure 5.5. *Scheme representing the process required for the production of antibodies against non-immunogenic small molecules.*

5.2.1.1 Evaluation of the 2d-BSA/As11 assay

The immunoreagents for the detection of atrazine (coating/competitor antigen: 2d-BSA and antisera: As11) have already been developed by our research group (Nb4D) during previous years [23], thus only their evaluation had to be performed. Primary, non-competitive 2D checkerboard titration immunoassays were performed, in order to determine the appropriate concentrations of the immunoreagents. Subsequently, competitive indirect immunoassays were carried out to obtain the calibration curve of the assay. The standard deviation and the features of the assays are represented in the graph (Figure 5.6) and the table (Table 5.1) below. It can be observed that the assay shows extremely high detectability (in the pM-nM range) and there is practically no background noise.

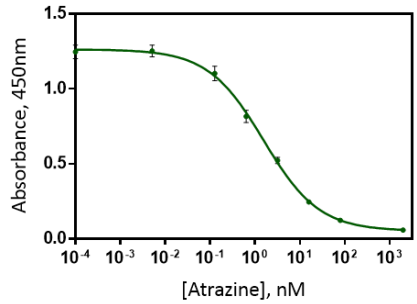

Table 5.1. Parameters of the assay 2d-BSA/As11) (n=3).

[Coating Ag], µg mL^{-1}	0.045
As dilution	1/1300000
Absorbance$_{min}$	0.055
Absorbance$_{max}$	1.830
Slope	-0.69
IC$_{50,}$ nM	1.84 ± 0.08
LOD, nM	0.10
R^2	0.990

Figure 5.6. *Analytical features of the 2d-BSA/As11 assay in PBST buffer. The data shown correspond to the average of three assays performed on three different days. Each assay was built using three well replicates. LOD corresponds to limit of detection, calculated as the concentration given at 90% of the maximum signal.*

5.2.2 IMMUNOSENSOR DEVELOPMENT

According to the procedure in section 5.4.3, for the development of the immunosensor directly on the surface of the SPEs, first the amounts of coating antigen, primary and secondary antibody had to be optimized.

5.2.2.1 Optimization of the immunosensor with HRP as label for the secondary antibody

For the development of the immunosensor directly on the surface of the screen printed electrodes with HRP as label for the secondary antibody, several experiments were dedicated to the optimization of the coating antigen, the primary and the secondary antibody concentrations. However, the reproducibility of these measurements was not optimal, in most of the cases no clear correlation could be observed between the different concentrations of the immunoreagents and the obtained current signal. In order to reduce this irreproducibility, different reagents (BSA, PVP, PVA etc.) were applied for the blocking step and the concentration of the detergent (Tween) was also changed in the washing step. Unfortunately, no improvement could be observed in regard to the correlation between the current signal and the immunoreagent concentrations, thus, the use of a different approach was suggested: i) using alkaline phosphatase (ALP) as label for the secondary antibody, and ii) continuing with the HRP labelled secondary antibody but instead of working directly on the electrode's surface, using magnetic beads as a platform for the assay.

5.2.2.2 Immunoassay development on the surface of magnetic beads (ELIME assay)

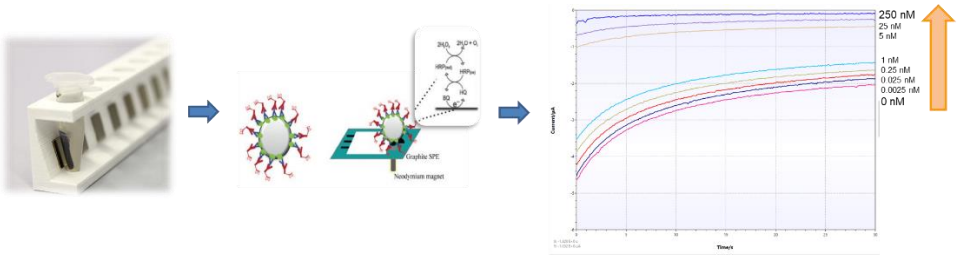

Figure 5.7. *Schematic representation of the development of an ELIME assay. On the first picture a magnetic rack and an Eppendorf tube can be seen, this is where the assay and the washing steps are being performed. On the second picture a SPE can be seen with the MBs that are concentrated on the WE by using a magnet underneath the SPE. On the third picture the signal acquisition can be seen in the form of chronoamperograms. The resulting signal is indirectly proportional to the amount of analyte in the examined sample.*

The immunoassay on the surface of the magnetic beads (Figure 5.7) was performed according to the procedure described in sections 5.4.2.2 and 5.4.2.3 of this chapter. First, the concentrations of the primary antibody, secondary antibody and magnetic beads had to be optimized. Afterwards, calibration curves were performed with the previously optimized concentrations of the immunoreagents.

Optimization of the ELIME assay

During the first step of the optimization process, the following primary antibody (Ab11) concentrations were tested: 0.05 µg mL^{-1}, 0.1 µg mL^{-1}, 0.25 µg mL^{-1}, 0.5 µg mL^{-1}, 1 µg mL^{-1}. The current signal was acquired by using chronoamperometry as electrochemical detection technique as explained in section 5.4.4.

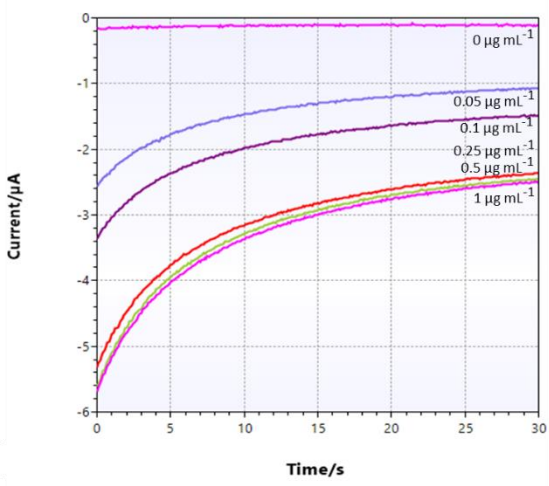

Figure 5.8. *Optimization of the Ab11 concentration for the ELIME assay. Chronoamperograms of 1mM HQ + 1 mM H_2O_2 in 0.05 M Citrate phosphate buffer, pH 5.0 + 0.1 M KCl.*

Based on the results of the experiment (see Figure 5.8) we have selected the 0.25 µg mL^{-1} concentration for the antibody, because this was the lowest concentration with which we could still obtain a relatively high signal. Further increase of the concentration of the antibody did not result in a significant increase of the amperometric signal.

For the optimization of the HRP-labelled secondary antibody, the following concentrations were tested: 5.3 µg mL^{-1}, 2.7 µg mL^{-1}, 1.3 µg mL^{-1}, 0.9 µg mL^{-1}, 0.6 µg mL^{-1}.

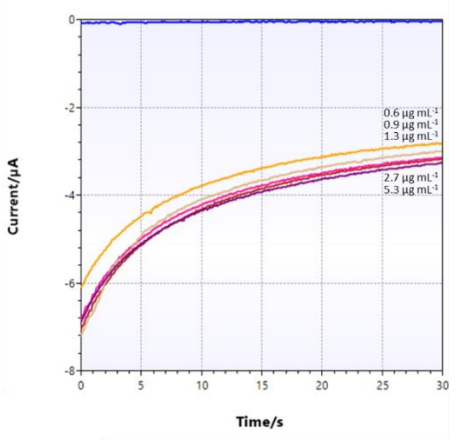

Figure 5.9. *Optimization of the anti-IgG-HRP concentration for the ELIME assay. Chronoamperograms of 1mM HQ + 1 mM H_2O_2 in 0.05 M Citrate phosphate buffer, pH 5.0 + 0.1 M KCl.*

As it can be seen from the figure above (Figure 5.9), no major difference can be observed between the different concentrations of the HRP-labelled secondary antibody. Thus, the lowest concentration (0.6 µg mL^{-1}) was used for further experiments.

For the optimization of the antigen coated magnetic beads, the following amounts were tested: 20 µg mL^{-1}, 10 µg mL^{-1}, 5 µg mL^{-1}, 2.5 µg mL^{-1}, 1 µg mL^{-1}.

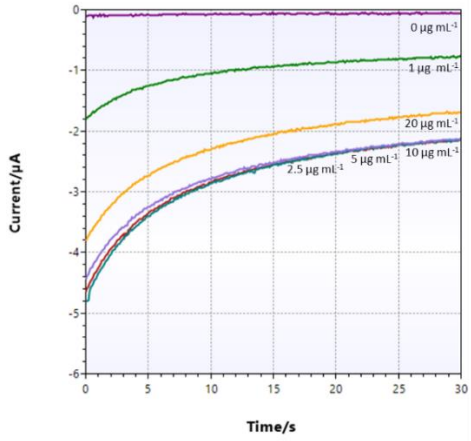

Figure 5.10. *Optimization of the MB concentration for the ELIME assay. Chronoamperograms of 1mM HQ + 1 mM H_2O_2 in 0.05 M Citrate phosphate buffer, pH 5.0 + 0.1 M KCl.*

In the case of the different MB concentrations it can be observed that too low (1 µg mL^{-1}) and too high (20 µg mL^{-1}) amounts of MBs both result in the drop of the electrochemical signal (Figure 5.10). The optimum signal was obtained with the amounts of 2.5, 5 and 10 µg mL^{-1} of MBs. Thus, for the next experiments we decided to use the 2.5 µg mL^{-1} MB concentration, which was the lowest concentration still providing us with a high signal.

After the optimization of the amount of coated MBs (2.5 µg mL^{-1}), primary antibody (0.25 µg mL^{-1}) and pAb-HRP (0.06 µg mL^{-1}), calibration curves were performed with different concentrations (from 0.0025 to 250 nM) of the analyte atrazine in PBS buffer using different dCB-SPEs (dropcasted either manually or by the BioDot). The current signal was acquired by using chronoamperometry as electrochemical detection technique as explained in section 5.4.4.

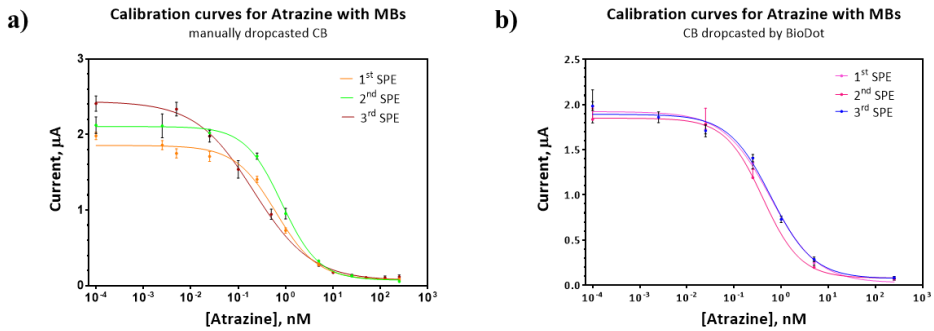

Figure 5.11. *Calibration curves for atrazine obtained by using the surface of MBs as platform for the immunoassay. a) CB manually dropcasted b) CB dropcasted by using an automated Biodot dispenser. The data shown correspond to the average of three assays performed on three different days. Each assay was built using three well replicates.*

It can be observed from the figures above that in the case where the electrodes were manually dropcasted with the nanomaterial carbon black (CB), the reproducibility between the calibration curves done with different electrodes is lower (Figure 5.11/a). This is most probably due to the fact that the manual dropcasting did not result in a completely homogeneous layer of CB on the WE's surface which has affected the electrochemical measurement. On the other hand, in the case of the SPEs where the CB was dropcasted by using the automated Biodot dispenser, an excellent reproducibility can be observed (Fig. 5.11/b) between the different electrodes. One of the main advantages of using the BioDot dispenser is the ability to obtain a homogenous layer on the surface of the WE, which manually could not be achieved.

5.2.2.3 Immunosensor development on the surface of the SPEs

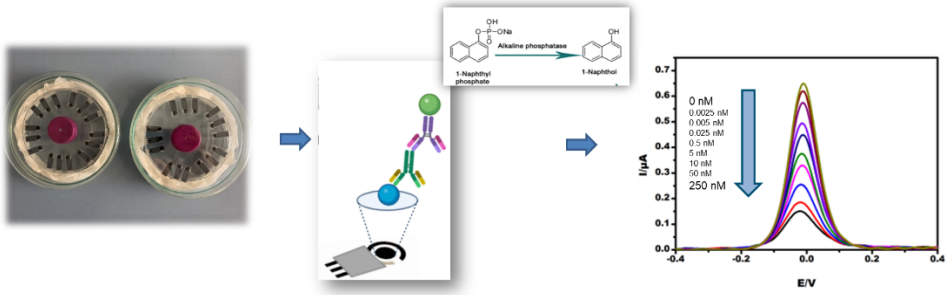

Figure 5.12. *Schematic representation of the process of immunosensor development on the surface of SPEs. On the first picture the incubation of the electrodes in a humid chamber can be seen. The second picture is a schematic graph of the immunochemical process that happens on the surface of the working electrode and finally the third picture illustrates the acquisition of the electrochemical signal (DPV graphs) which is indirectly proportional to the amount of analyte in the investigated sample.*

The development of the immunosensor directly on the surface of SPEs (Figure 5.12) was developed according to the procedure in section 5.4.3 of this chapter (Materials and Methods).

Optimization of the assay with ALP as label for the secondary antibody

For the optimization of this immunoassay, first the following dilutions of the ALP labelled secondary antibody were tested:

3 μg mL^{-1},
1 μg mL^{-1},
0.6 μg mL^{-1},
0.4 μg mL^{-1},
0.3 μg mL^{-1}.

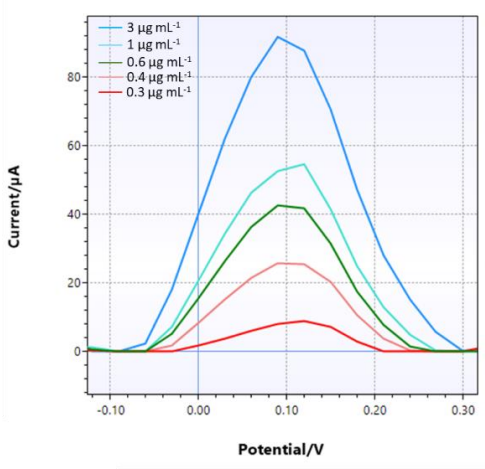

Figure 5.13. *Optimization of the anti-IgG-ALP concentration for the immunoassay directly on the WE. The differential pulse voltammograms were recorded on the 2d-BSA coated CB-modified electrodes.*

Based on the results shown in Figure 5.13, the concentration 1 µg mL^{-1} was chosen for future experiments, due to the fact that this concentration gives a high enough signal using a relatively low quantity of secondary antibody. Regarding the concentrations of the antigen and the primary antibody, the optimized concentrations were the following: 5 µg mL^{-1} of 2d-BSA and 5 µg mL^{-1} of Ab11.

After the optimization process, an indirect competitive assay was carried out and calibration curves were obtained using different concentrations of the analyte atrazine. The assay was performed on both the SPEs that were dropcasted with 5 µL of CB by the automated BioDot dispenser and on the surface of the bare SPEs for comparison as well. The current signal was acquired by using DPV as electrochemical detection technique as explained in section 5.4.4. It can be seen from the results obtained (Fig. 5.14) that the assay on the bare electrodes was less sensitive, the maximum signal has dropped down and also the IC_{50} has shifted, which proves that the use of CB increases the performance of the assay.

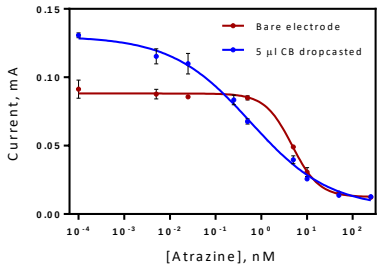

Figure 5.14. *Calibration curve for Atrazine obtained either on the surface of the bare SPE or on the surface of the SPE dropcasted with CB. The data shown correspond to the average of three assays performed on three different days. Each assay was built using three well replicates.*

5.2.2.4 Comparison of the two different detection methods

Comparing the two different approaches (MBs vs. ALP), the main advantage of using the MBs besides the enhancement of the surface area (which means an amplification of the final current signal) is the possibility to carry out the experiments in Eppendorf tubes instead of directly using the surface of the WE, which allows for more efficient washing steps and easier handling. Furthermore, during the use of MBs the sample is concentrated on the WE by using a magnet underneath it, which makes the system more sensitive and reproducible. In the case of the assay on the surface of the electrodes with ALP, the washing step is more time-consuming and less efficient, but the use of this system allows us to use DPV as electrochemical measuring technique, which is more sensitive than the ChA. DPV is able to distinguish even smaller changes in current due to the fact that it measures the difference between 2 pulses of current. Furthermore, for the future prospect of multiplexing and automatization (which are the requirements for the development of a portable smartphone-connected device which this project aims to achieve), this system would be more suitable than the approach with the MBs. Thus, for future experiments this approach is going to be further investigated and optimized.

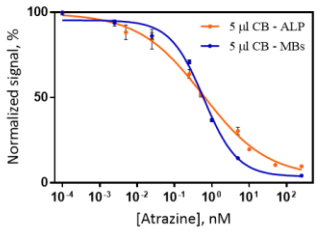

Table 5.2. Parameters of the two different approaches.

	5 µl CB - ALP	5 µl CB - MBs
IC_{50}, nM µg L^{-1}	0.75 ± 0.20 0.162	0.59 ± 0.06 0.127
LOD, nM µg L^{-1}	0.03 0.006	0.03 0.006
WR, nM µg L^{-1}	(0.02 ± 0.00)-(11.83 ± 1.72) (0.004)-(2.551)	(0.12 ± 0.03)-(2.99 ± 0.35) (0.026)-(0.645)

Figure 5.15. *Comparison of the two different immunochemical approaches for the detection of Atrazine (directly on the surface of the SPEs and on the MBs). The data shown correspond to the average of three assays performed on three different days. Each assay was built using three well replicates. LOD corresponds to limit of detection, calculated as the concentration given at 90% of the maximum signal.*

To obtain a comparison (see Fig. 5.15) between the two assays, the signal had to be normalized due to the different scales of the current range (mA vs. µA), but the two graphs are comparable. Even though the slopes of the two assays are different, their IC_{50}-s are very similar (see Table 5.2) and both fulfill the requirements of the EU regulations (MRL for atrazine in cereals is 0.05 mg L^{-1}), which is important from the view of the real sample analysis. In the case of the approach with ALP, the background noise is a bit higher but it is still in the nA range, thus acceptable.

5.2.2.5 Development of an Immunosensor with a new electrode design

Furthermore, the use of a new electrode design (Figure 5.16) was explored for the performance enhancement of the already developed immunosensor. The main differences of this new electrode design are the size of the working electrode, which has a 2 mm diameter instead of the 3 mm of the previous design and the shape of the reference electrode, which also became circular and a bit bigger, having the same size as the WE (2 mm diameter). The main objective with this design change was to enhance the reproducibility between the measurements performed on different days and also to mimic the characteristics of a multiplexed SPE which will be the next step of the immunosensor development.

Figure 5.16. *A new electrode design with a smaller working electrode and a round reference electrode.*

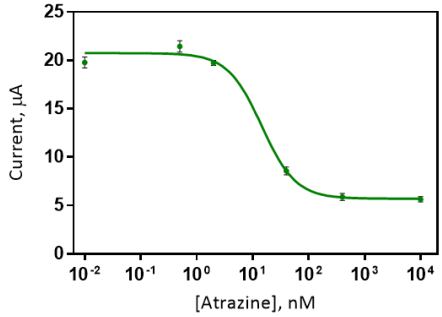

Table 5.3. Parameters of the electrochemical immunosensor developed in PBST buffer (n=3).	
[2d-BSA], µg mL^{-1}	2.5
[Ab11], µg mL^{-1}	5
Signal$_{min}$	5.699 ± 0.363
Signal$_{max}$	20.750 ± 0.435
Slope	-1.428 ± 0.290
IC$_{50}$, nM	14.48 ± 0.10
LOD, nM	2.09
R^2	0.989

Figure 5.17. *Analytical features of the electrochemical immunosensor developed in PBST buffer for the detection of Atrazine with the new electrode design. The data shown correspond to the average of three assays performed on three different days. Each assay was built using three replicates. LOD corresponds to limit of detection, calculated as the concentration given at 90% of the maximum signal.*

Observing the graph and the table above (Figure 5.17, Table 5.3) and comparing it to the previous results it can be seen that even though the maximum signal of the assay has decreased and the IC_{50} has increased, it is still well within the desired range and the shape of the calibration curve has also remained very similar.

5.2.3 RECOVERY STUDIES IN ORANGE JUICE

In order to study the accuracy of the developed immunosensor, spiked samples were prepared with the matrix orange juice. The experiment was carried out according to the protocol described in section 5.4.3.1.

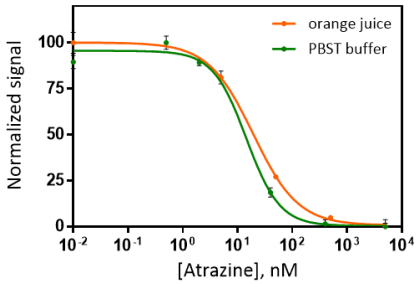

Table 5.4. Comparison of the parameters of the immunosensors developed in PBST bufffer and in orange juice (n=3).

	PBST buffer	Orange juice (1:5 dilution)
IC_{50}, nM	14.48 ± 0.10	19.34 ± 0.07
µg L^{-1}	3.12	4.17
LOD, nM	2.09	2.47
µg L^{-1}	0.45	0.53
WR, nM	(4.63)-(37.23)	(5.28)-(74.17)
µg L^{-1}	(1.00)-(8.03)	(1.14)-(16.00)

Figure 5.18. *Comparison of the calibration curve performed in PBST buffer and in a 1:5 dilution of orange juice.*

It can be observed from the graph (Figure 5.18) and the table (Table 5.4) above that the characteristics of the two assays are very similar, using a 1:5 dilution of orange juice only results in minor changes regarding the calibration curves, such as a slight shift in IC_{50} and LOD. The limit of detection obtained with the orange juice sample is still well below the MRL (0.05 mg L^{-1}) established by the current European legislations.

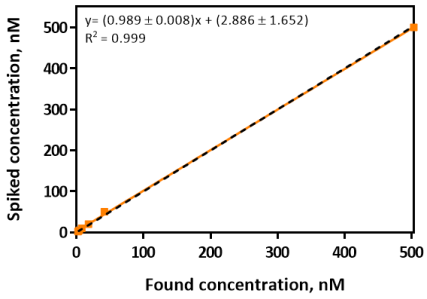

Table 5.5. Recovery values of the electrochemical immunosensor developed in orange juice (n=3).

Spiked concentration (nM)	Found concentration (nM)	Recovery (%)
2	2.15 ± 0.14	108
5	4.55 ± 0.50	91
10	8.78 ± 1.21	88
20	18.90 ± 1.11	94
50	44.99 ± 3.62	90
500	506.89 ± 3.92	101

Figure 5.19. *Recovery values of the electrochemical immunosensor developed in a 1:5 dilution of orange juice. The graph shows the correlation between the spiked and measured concentration values. The dotted line corresponds to a perfect correlation (m = 1). The data correspond to the average of at least three replicates from 3 different days.*

The graph (Figure 5.19) and the recovery values shown above (Table 5.5) demonstrate the applicability of the developed immunosensor for the detection of even trace levels (2 nM = 0.45 µg L^{-1}) of atrazine in orange juice well below the established MRL (0.05 mg L^{-1}) by the current European legislations. Even though in most cases an underestimation of the spiked values is observed, the results are still very close to the spiked values.

5.2.3.1 Comparison with ELISA

As a comparison to the immunosensor, the matrix effect studies were also performed in the ELISA format.

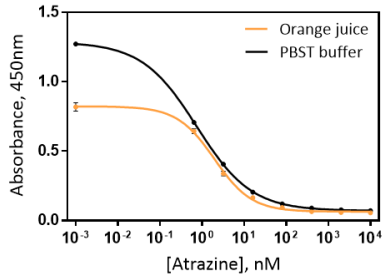

Table 5.6. Comparison of the main characteristics of the immunoassays in PBST buffer and in orange juice.

	PBST Buffer	Orange juice (1:5 dilution)
Absorbance $_{min}$	0.069	0.063
Absorbance $_{max}$	1.286	0.823
Slope	-0.669	-0.980
LOD, nM	0.007	0.048
IC_{50}, nM	0.745	1.966

Figure 5.20. *Calibration curves for the detection of Atrazine in PBST and in a 1:5 dilution of orange juice.*

Observing the figure and the table above (Figure 5.20 and Table 5.6), it can be seen that in this case the matrix effect of the orange juice results in a drop of the maximum signal and in a small shift of the IC_{50}, however still maintaining the main characteristics of the assay. Comparing the features of the assays to the ones of the sensors, it can be observed that in the case of the ELISA the LOD and IC_{50} values are slightly lower, but the two different detection methods still remain comparable.

5.3 CONCLUSIONS

Different formats of immunoassays (ELISA and ELIME) and electrochemical immunosensors were developed for the detection of the herbicide atrazine in PBST buffer and in orange juice, achieving LOD-s of 0.45 and 0.53 µg L^{-1}, respectively in the case of the immunosensor (both values are well below the MRL established by the European Commission (0.05 mg L^{-1})). Various different configurations were investigated for the development of the electrochemical immunosensor resulting in the selection of the one which directly uses the SPE's surface, an ALP labelled secondary antibody and DPV as electrochemical detection technique. Aside from having the desired sensitivity and specificity, the use of these parameters also provides an excellent applicability in terms of multiplexing and automatization, which are the requirements for the development of a portable smartphone-connected device, which this project aims to achieve.

5.4 MATERIALS AND METHODS

5.4.1 CONSUMABLES, REAGENTS AND EQUIPMENT

For the development of the immunoassays and immunosensors, all solutions were prepared with MQ water from a MilliQ-system. Phosphate buffer saline tablets (PBS), TWEEN® 20, anti-IgG horse radish peroxidase conjugated polyclonal antibody (pAb-HRP), sodium Citrate, sodium borate, NaCl, $CaCl_2$, KH_2PO_4, HCl (37%), NaOH, H_2O_2 (30%), $K_4Fe(CN)_6 \bullet 3H_2O$, $K_3Fe(CN)^6$, $CaSO_4$, citric acid, KCl, Na_2HPO_4, sodium carbonate decahydrate, bovine serum albumin (BSA), Hidroquinone (HQ), Dimethylformamide (DMF), Diethanolamine buffer, $MgCl_2$, 1-Naphthyl phosphate disodium salt and 1-Naphthol were purchased from Sigma Aldrich (St. Louis, MO, USA). The BSA conjugated antigen for atrazine (2d-BSA) and the polyclonal anti-Atrazine antibodies (Ab11) were produced in-house at the Nb4D research group (IQAC-CSIC). The anti-IgG alkalyne phosphatase conjugated polyclonal antibody (pAb-ALP) was obtained from Jackson

Immunoresearch. Magnetic beads were obtained from ThermoFisher Scientific (MyOne Dynabeads).

Buffers. Unless otherwise indicated, phosphate buffer saline (PBS) is 0.01 M phosphate buffer in a 0.8% saline solution, pH 7.5. Coating buffer is a 0.05 M carbonate-bicarbonate buffer, pH 9.6. PBST is PBS with 0.05% Tween 20, pH 7.5. Citrate buffer is 0.04 M sodium citrate, pH 5.5. The substrate solution contains 0.01% 3,3',5,5'-tetramethylbenzidine (TMB) and 0.004% H_2O_2 in citrate buffer. Hydroquinone solutions (0.1 mM, 0.5 mM, 1 mM) were prepared in 0.05 M citrate-phosphate buffer + KCl 0.1 M, pH 5.0. Diethanolamine buffer (DEA) is 1 M diethanolamine with 1 mM $MgCl_2$, pH 9.8. The substrate solution for the sensor is a 5 mg mL^{-1} 1-Naphthyl phosphate disodium salt (1-NPP) solution in DEA buffer.

The pH and the conductivity of all buffers and solutions were measured with a pH-meter pH 540 GLP and a conductimeter LF 340, respectively (WTW, Weilheim, Germany). Polystyrene microtiter plates were purchased from Nunc (Maxisorp, Roskilde, Denmark). Dilution plates were purchased from Nirco (Barberà del Vallés, Spain). Washing steps were performed with a Biotek ELx465 (Biotek Inc.). Absorbances were read on a SpectramaxPlus (Molecular Devices, Sunnyvale, CA, USA).

5.4.2 IMMUNOASSAY DEVELOPMENT

5.4.2.1 ELISAs

Non-competitive indirect ELISA. This method was used to evaluate the avidity of the antisera As11 with the coating antigen 2d-BSA. The two-dimensional titration assays (2D-assay) were carried out based on measuring the binding of a series of dilutions (starting from 1/1000 to 1/64000 and zero; 100 µL $well^{-1}$) of the antisera against different concentrations (dilutions from 10 µg mL^{-1} to 10 ng mL^{-1}, and zero; 100 µL $well^{-1}$) of the antigen. Depending on the results of these experiments, the optimum concentrations for coating antigens and antisera dilutions were chosen, generating around 0.8-1 units of absorbance.

Competitive ELISA 2d-BSA/As11 for the detection of atrazine. First, 96-well microtiter plates were coated with the antigen 2d-BSA (0.045 µg mL^{-1} in coating

buffer, 100 µL well^{-1}) and stored overnight at 4 °C, covered with adhesive plate sealers. The following day, the plates were washed four times with PBST (300 µL well^{-1}), and the solution of atrazine (stock from 2000 to 0 µM in DMSO and diluted 200 times in PBST or 1:5 diluted orange juice) was added (50 µL well^{-1}), followed by the solution of antisera As11 (1/1300000 both in PBST, 50 µL well^{-1}). After 30 min at room temperature (RT), the plates were washed as mentioned before, and a solution of anti-IgG-HRP (1/6000 in PBST) was added to the wells (100 µL well^{-1}) and incubated for 30 minutes at RT. The plates were washed again, and the substrate solution was added (100 µL well^{-1}). After 30 min the colour development was stopped with 4N H_2SO_4 (50 µL well^{-1}) at RT, and the absorbance was read at 450 nm with a spectrophotometer. The standard curves were fitted to a four-parameter equation according to the following formula: $y = (A - B/[1 - (x/C)D] + B$, where A is the maximal absorbance, B is the minimum absorbance, C is the concentration producing 50% of the maximal absorbance, and D is the slope at the inflection point of the sigmoid curve. Unless otherwise indicated, data presented corresponds to the average of at least three wells replicates.

Antibody purification. The produced antisera was precipitated with ammonium-sulfate and purified by affinity chromatography with the use of protein A columns. After a desalting purification step, the antibodies were lyophilized in order to be ready for the experiments with the electrodes.

5.4.2.2 Magnetic bead coating

During this procedure the 2d-BSA conjugate and the BSA (as negative control) were covalently coupled with the Dynabeads MyOne tosyl-activated magnetic beads. For this purpose first the tosyl-activated magnetic beads (with a 1 µm diameter) stock solution was vortexed and 5 mg of the MBs was resuspended in 200 µL of coating buffer (sodium borate buffer, 0.1 M, pH=9.5) and placed in a magnetic rack for 1 min. The supernatant was discarded and 227 µL of the coating buffer was added to the MBs. 200 µg of 2d-BSA in PBS (pH=7.4) was added and was followed by an addition of 223 µL of sodium borate buffer (0.1 M; pH=9.5) containing 3 M ammonium sulfate. The mixture was incubated for 24 hours at 37 °C with slow tilted rotation. After the incubation time the Eppendorf tube was placed in a magnetic rack for 2 minutes and the supernatant was discarded. Next, 650 µL of blocking buffer (PBS with 0.5% BSA and 0.05% Tween

20; pH=7.4) was added and the solution was incubated again for 24 hours at 37 °C with slow tilted rotation. After the incubation the tube was again placed in the magnetic rack for 2 min and the supernatant was discarded. Next, the MBs were washed 3 times with the washing/storage buffer (PBS containing 0.1 % BSA and 0.05 % Tween; pH=7.4). Finally, the MBs were resuspended in 200 µL of washing/storage buffer obtaining a final concentration of 25 mg MBs mL^{-1} with approximately 40 µg 2d-BSA $mgMBs^{-1}$ and stored at 4 °C for further experiments. The same procedure was followed to coat the MBs with BSA used as a negative control.

5.4.2.3 Enzyme-Linked-Immunomagnetic-Electrochemical (ELIME) assay

First, 2.5 µg of 2d-BSA coated MBs were dissolved in 200 µL of washing/storage buffer (PBS with 0.1 % BSA and 0.05 % Tween 20; pH=7.4), then 20 µL of this solution was incubated with the primary antibody (Ab11) and with different concentrations of the analyte atrazine in reagent buffer (PBS BSA 1%) for 1 hour at RT with a continuous slow tilting rotation. After the incubation time the Eppendorf tubes were put on the magnetic rack for 2 minutes and the supernatant was removed. The MBs were then suspended in 1 mL of the washing buffer and put back on the magnetic rack for 2 min after which the supernatant was removed again. The washing step was performed three times in total and was followed by a 30 min incubation (at RT with slow rotation) with the HRP labelled secondary antibody in 100 µL of reagent buffer. After this step the previously described washing step was repeated and the MBs were resuspended in 40 µL of citrate buffer (0.05 M, pH=5). For the electrochemical measurement, 10 µL of the MB suspension was dropped on the WE of the SPE under which a magnet was attached. Immediately after the addition of the MBs, 35 µL of the substrate solution (0.1 M KCl, 1 mM HQ and 1 mM H_2O_2 in citrate-phosphate buffer) was also added and mixed carefully so that all three electrodes would be covered. After 2 min of incubation time the chronamperometric measurement (according to section 5.4.4) was started (n=3).

5.4.3 IMMUNOSENSOR DEVELOPMENT

As the first step of the immunosensor development, the WEs were coated with the optimized concentration of the corresponding antigen by dropcasting 2 µL of the prepared solution (2.5 µg mL^{-1} 2d-BSA in carbonate buffer) on its surface. The prepared electrodes were incubated for 45 min at room temperature (RT). All of the incubation steps were performed in a humid chamber at RT. Afterwards, the WEs were washed twice with 100 µL of PBST (pH 7.5) and once with 100 µL of PBS (pH 7.5). The next step was the blocking of the WE's surface by dropping 2 µL of carbonate buffer containing 2 % BSA, after which the electrodes were incubated for another 30 min at RT. The WEs were washed again twice with 100 µL of PBST and once with 100 µL of PBS. Next, 2 µL of the primary antibody (5 µg mL^{-1} Ab11 in PBS) and different concentrations of the analyte atrazine (from 0.5 nM to 10 µM and 0 nM in PBS with BSA 1%) were incubated on the WE for 30 min at RT to allow for the competition to happen. The SPEs were washed again using the same procedure as explained above. The next step was the addition of 2 µL of the alkaline phosphatase (ALP) labelled secondary antibody (in PBS BSA 1%) and its incubation for 30 min at RT. After this step the SPEs were washed twice with 100 µL of PBST and once with 100 µL of PBS. Finally, the electrodes were dropcasted with 2 µL of PBS until the start of the DPV measurement in order to avoid drying them out. Afterwards, 60 µL of the enzymatic substrate containing solution (5 mg mL^{-1} 1-naphthyl phosphate disodium salt in diethanolamine buffer with 1 mM $MgCl_2$) was dropped on the SPE's surface (covering all 3 electrodes). After 2 min of incubation time, the DPV measurement was started according to the procedure explained in section 5.4.4 and the resulting current was recorded (n=3).

Recovery studies. Non-specific interferences produced by the parameters associated with the matrix of interest were studied by preparing a standard curve in orange juice. The orange juice samples were obtained from a local retail store and characterized regarding pH and conductivity. First, the pH was adjusted to 7.5 (original pH was around 3.5), since an acidic pH would have interfered with the measurements. Afterwards, the juice sample was filtered through a 0.22 µm filter and diluted five times with PBST buffer before the measurements. Six different orange juice solutions were spiked with the pesticide atrazine (at the concentrations: 500 nM, 50 nM, 20 nM, 10 nM, 5 nM, 2 nM) and measured using

the dCB-SPEs. Three replicates were used for every concentration and the experiment was performed on three different days.

5.4.4 ELECTROCHEMICAL CHARACTERIZATION AND MEASUREMENTS

All EC measurements were performed with a PalmSens 4 potentiostat (Palmsens, The Netherlands).

The Chronamperometric (ChA) measurements were performed at a chosen fixed potential of +0.12 V for 30 seconds with a 0.1 s time interval.

In the case of the Differential Pulse Voltammetry (DPV) measurements, the selected potential range was from -0.1 to 0.3 V with a potential step of 0.02 V, a pulse potential of 0.07 V, a time pulse of 0.05 s and a scan rate of 0.2 V/s.

5.4.5 DATA TREATMENT

For the electrochemical data obtained with the PalmSens4 potentiostat, the PSTrace v5.5 software was used.

The statistical analysis, the normalization of the calibration curves and their fitting to a four-parameter dose-response curve was performed using the GraphPad Prism software v.7. LOD, IC_{50} and the working range were obtained by interpolating 90%, 50% and 20-80% signal values from the fitted normalised curves respectively.

5.5 BIBLIOGRAPHY

[1] Kumar, V., Vaid, K., Anil, S., & Kim, K. (2020). Biosensors and Bioelectronics Nanomaterial-based immunosensors for ultrasensitive detection of pesticides/ herbicides: Current status and perspectives. Biosensors and Bioelectronics, 165(May), 112382. https://doi.org/10.1016/j.bios.2020.112382

[2] T.R. Steinheimer, Hplc determination of atrazine and principal degradates in agricultural soils and associated surface and ground-water, J. Agric.Food Chem. 41 (1993) 588–595.

[3] A. Kaune, R. Bruggemann, M. Sharma, A. Kettrup, Soil adsorption coefficients of s-triazines estimated with a newgradient HPLC method, J. Agric. Food Chem. 46 (1998) 335–343.

[4] A. Moore, C.P.Waring, Mechanistic effects of a triazine pesticide on reproductive endocrine function in mature male Atlantic salmon (Salmo salar L.) parr, Pesticide Biochem. Physiol. 62 (1998) 41–50.

[5] S.K. Papiernik, R.F. Spalding, Atrazine, deethylatrazine, and deisopropylatrazine persistence measured in groundwater in situ under low-oxygen conditions, J. Agric. Food Chem. 46 (1998) 749–754.

[6] Tsagkaris, A. S., Nelis, J. L. D., Ross, G. M. S., Jafari, S., Guercetti, J., Kopper, K., … Hajslova, J. (2019). Trends in Analytical Chemistry. Critical assessment of recent trends related to screening and con fi rmatory analytical methods for selected food contaminants and allergens. Trends in Analytical Chemistry, 121, 115688. https://doi.org/10.1016/j.trac.2019.115688

[7] Tran, A. T. K., Hyne, R. V, Pablo, F., Day, W. R., & Doble, P. (2007). Optimisation of the separation of herbicides by linear gradient high performance liquid chromatography utilising artificial neural networks, 71, 1268–1275. https://doi.org/10.1016/j.talanta.2006.06.031

[8] Zhao, E., Shan, W., Jiang, S., Liu, Y., & Zhou, Z. (2006). Determination of the chloroacetanilide herbicides in waters using single-drop microextraction and gas chromatography, *83*, 105–110. https://doi.org/10.1016/j.microc.2006.03.008

[9] Ferrer, C., Jose, M. G., Garc, J. F., Ferrer, I., Thurman, E. M., & Fern, A. R. (2005). Determination of pesticide residues in olives and olive oil by matrix solid-phase dispersion followed by gas chromatography/mass spectrometry and liquid chromatography/tandem mass spectrometry, 1069, 183–194. https://doi.org/10.1016/j.chroma.2005.02.015

[10] Andreescu, S., Marty, J., Sciences, B., Andreescu, S., & Marty, J. (2006). Trends in Flow-based Biosensing Systems for Pesticide Assessment, (iv), 1161–1186.

[11] Chang, P., Hsieh, M., & Chiu, T. (2016). Recent Advances in the Determination of Pesticides in Environmental Samples by Capillary Electrophoresis. https://doi.org/10.3390/ijerph13040409

[12] Valera, E., Ramón-Azcón, J., Rodríguez, Á., Castañer, L. M., Sánchez, F. J., & Marco, M. P. (2007). Impedimetric immunosensor for atrazine detection using interdigitated µ-electrodes (IDµE's). Sensors and Actuators, B: Chemical, 125(2), 526–537. https://doi.org/10.1016/j.snb.2007.02.048

[13] Chuc, N. Van, Binh, N. H., Thanh, C. T., & Tu, N. Van. (2016). Journal of Materials Science & Technology Electrochemical Immunosensor for Detection of Atrazine Based on Polyaniline / Graphene. Journal of Materials Science & Technology, 32(6), 539–544. https://doi.org/10.1016/j.jmst.2016.04.004

[14] Liu, X., Li, W., Li, L., Yang, Y., Mao, L., & Peng, Z. (2014). Sensors and Actuators B : Chemical. A label-free electrochemical immunosensor based on gold nanoparticles for direct detection of atrazine. Sensors & Actuators: B. Chemical, 191, 408–414. https://doi.org/10.1016/j.snb.2013.10.033

[15] Valera, E., Muñiz, D., & Rodríguez, Á. (2010). Fabrication of flexible interdigitated l -electrodes (FID l Es) for the development of a conductimetric immunosensor for atrazine detection based on antibodies labelled with gold nanoparticles. Microelectronic Engineering, 87(2), 167–173. https://doi.org/10.1016/j.mee.2009.07.001

[16] Madianos, L., Skotadis, E., Tsekenis, G., Patsiouras, L., Tsigkourakos, M., & Tsoukalas, D. (2018). Microelectronic Engineering l mpedimetric nanoparticle aptasensor for selective and label free pesticide detection. *Microelectronic Engineering*, *189*, 39–45. https://doi.org/10.1016/j.mee.2017.12.016

[17] Deep, A., Saraf, M., & Kumar, S. (2014). Electrochimica Acta Styrene Sulphonic Acid Doped Polyaniline Based Immunosensor for Highly Sensitive Impedimetric Sensing of Atrazine. Electrochimica Acta, 146, 301–306. https://doi.org/10.1016/j.electacta.2014.09.048

[18] Kim, K., & Deep, A. (2015). Immunosensing of Atrazine with Antibody-Functionalized Cu-MOF Conducting Thin Films. https://doi.org/10.1021/acsami.5b07692

[19] Ionescu, R. E., Gondran, C., Bouffier, L., Jaffrezic-renault, N., Martelet, C., & Cosnier, S. (2010). Electrochimica Acta Label-free impedimetric immunosensor for sensitive detection of atrazine. Electrochimica Acta, 55(21), 6228–6232. https://doi.org/10.1016/j.electacta.2009.11.029

[20] Belkhamssa, N., Justino, C. I. L., Santos, P. S. M., Cardoso, S., Lopes, I., Duarte, A. C., … Ksibi, M. (2016). Talanta Label-free disposable immunosensor for detection of atrazine. Talanta, 146, 430–434. https://doi.org/10.1016/j.talanta.2015.09.015

[21] Biju, V. (2014). Chem Soc Rev, 43(3). https://doi.org/10.1039/c3cs60273g

[22] Howard, C. B., Fletcher, N., Houston, Z. H., Fuchs, A. V, Boase, N. R. B., Simpson, J. D., … Thurecht, K. J. (2016). Overcoming Instability of Antibody-Nanomaterial Conjugates: Next Generation Targeted Nanomedicines Using Bispecifi c Antibodies, 2055–2068. https://doi.org/10.1002/adhm.201600263

[23] Gascón, J., Oubiña, A., Ballesteros, B., Camps, F., Marcoa, M., González-Martínez, M. A., … Maquieira, A. (1997). Development of a highly sensitive enzyme-linked immunosorbent assay for atrazine Performance evaluation by flow injection immunoassay, 2670(97).

6 DEVELOPMENT OF AN ELECTROCHEMICAL IMMUNOSENSOR FOR THE DETECTION OF CHLORPYRIFOS IN FLOUR SAMPLES

6.1 CHAPTER OVERVIEW

This chapter first describes the characterization of the immunoreagents necessary for the detection of the insecticide Chlorpyrifos. After the characterization process by ELISA, the development of an electrochemical immunosensors is described. Finally, the application of this sensor for the analysis of different flour samples is being discussed by evaluating the matrix effect and performing an in-house sample validation and recovery studies.

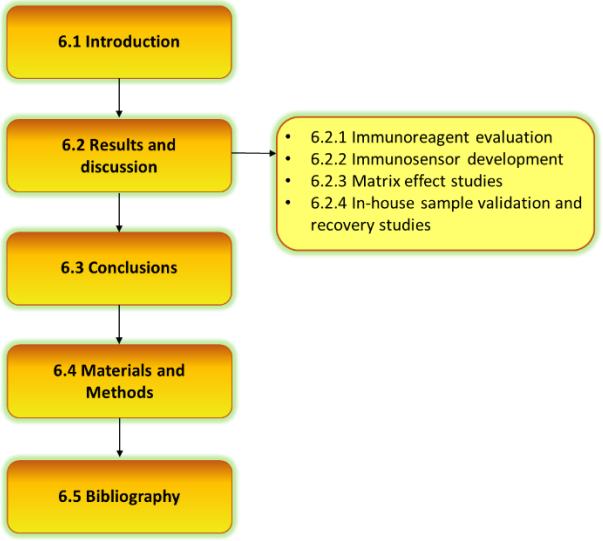

Figure 6.1. *The structure of this chapter realted to the different sections.*

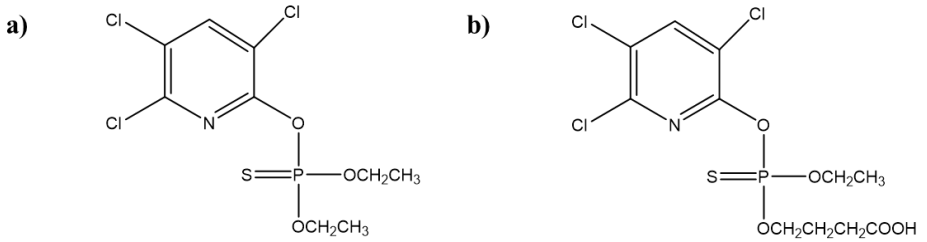

Figure 6.2. *I/a) Chemical structure of Chlorpyrifos. I/b) Chemical structure of the immunizing hapten for the detection of Chlorpyrifos.*

6.2 INTRODUCTION

6.2.1 THE ROLE OF CHLORPYRIFOS IN FOOD SAFETY MONITORING

Chlorpyrifos (O,O-diethyl-O-(3,5,6-trichloro-2-pyridyl)-phosphorothioate) is a widely used organophosphorus insecticide in agriculture to control pests and enhance production on a variety of crops, fruits and vegetables [1]. Organophosphorus pesticides are one of the most commonly used pesticides around the world, especially in developing countries. These pesticides have the ability to inhibit the activity of the enzyme acetylcholinesterase (AChE) or cholinesterase (ChE) in the nervous system, thus destroying the normal nerve impulse conduction, causing various symptoms such as spasms, abnormal excitement, paralysis, reproductive disorders, cancer or even death [2]. Chlorpyrifos (see Figure 6.2) is one of the most commonly used broad-spectrum organophosphorus pesticides in spite of its high toxicity and long retention time. Its widespread use has led to contaminations of drinking water, air and soil. The presence of these pesticide residues in food and environment can cause serious health threats to humans and animals [3]. Furthermore, it also has a poisonous effect on bees which mainly occurs when the insecticide is being applied to crops during the blooming period. Its residues can remain toxic for the honey bees for up to 4-6 days. For all of the above mentioned reasons, maximum residue limits (0.5 mg kg^{-1} in cereals) have been established by the European Commission and there is a high need for the development of rapid detection tools with high sensitivity and specificity [4,5].

6.2.2 DETECTION METHODS FOR CHLORPYRIFOS IN THE LITERATURE

Traditionally, the detection of organophosphorus pesticides relies on analytical methods, such as liquid chromatography (LC), high-performance liquid chromatography (HPLC) [6], gas chromatography (GC), mass spectrometry (MS) [7], capillary electrophoresis, infrared micro-imaging [8], photoelectrochemical sensing [9], thin-layer chromatography [10] and enzyme-based assay [11-14]. Even though these methods are highly sensitivite, specific and can be potentially

extended to multi-group screening/quantitation strategies for the detection of mycotoxins, pesticides and veterinary drugs [15,16], they are not suitable for on-site measurements due to their disadvantages of being time consuming, having high costs, needing complex sample preparation and highly trained professionals for their operation in addition to requiring the necessary equipment in specialized laboratories. For this reason, the development of more convenient, rapid, reliable, low cost but still highly sensitive screening tools has received growing interest. An excellent candidate for this purpose are immunoassays, such as ELISAs [17,18], fluorescence immunoassays based on signal amplification of gold nanoparticles [19], immunochromatographic devices based on up-converting nanoparticles [20], enzymatic lateral flow systems [21] or analytical tools assembled to microfluidic systems [22].

Electrochemical biosensors are also excellent candidates for the rapid on-site detection of pesticides [23-26] due to their several adventageous properties (fast response time, potential low cost and ease of operation). Enzyme-based sensors in general are gaining importance due to their high sensitivity and quick response but are limited to a certain class of pesticides [27-28]. As it has been explained in Chapter 5 before, immunosensors on the other hand work on the principle of antigen-antibody (Ag-Ab) interaction and stand out due to their high specificity and sensitivity, which make them applicable for the detection of various different molecules such as pesticides, narcotic drugs, bacteria and viruses [3]. Several different formats of electrochemical immunosensors have been explored in previous years for chlorpyrifos detection based on the use of gold nanoparticles [5], multiwall carbon nanotubes [29] or silica gel film modified SPEs [4]. However, there is still a great need for the development of end-user friendly electrochemical sensors that have the capabilities to be integrated in a multiplexed smartphone-based on-site detection tool.

6.3 RESULTS AND DISCUSSION

The first objective of this chapter was the characterization of the immunoreagents necessary for the detection of chlorpyrifos by ELISA experiments. Afterwards, these immunoreagents were used for the development of an electrochemical immunosensor. Finally, the application of

this sensor for the analysis of different flour samples is being discussed by evaluating the matrix effect and performing an in-house sample validation and recovery studies.

6.3.1 IMMUNOREAGENT EVALUATION: BSA-PO/LIB-PO ASSAY

The immunoreagents for the detection of chlorpyrifos (coating antigen: BSA-PO and monoclonal anti-chlorpyrifos antibody: LIB-PO) were developed by the research group of Ángel Montoya in the Universidad Politècnica de València [17,18].

For the evaluation of these immunoreagents, primarly non-competitive 2D checkerboard titration immunoassays were performed, in order to determine the appropriate concentrations for the immunosensor development. Subsequently, competitive indirect immunoassays were carried out to obtain the calibration curve of the assay. The standard deviation and the features of the assays are represented in the graph (Figure 6.3) and the table (Table 6.1) below.

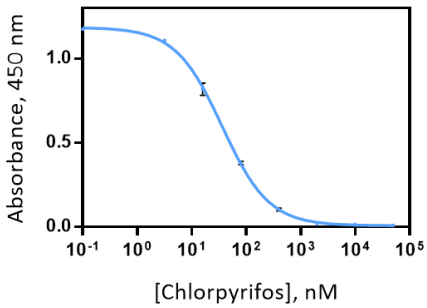

Table 6.1. Parameters of the assay (BSA-PO/LIB-PO)

Coating Ag, µg mL^{-1}	0.6125
mAb, µg mL^{-1}	0.0625
Absorbance$_{min}$	0.008
Absorbance$_{max}$	1.186
Slope	-1.012
IC$_{50}$, nM	36.48 ± 0.46
IC$_{50}$, µg kg^{-1}	12.79
LOD, nM	4.55
LOD, µg kg^{-1}	1.60
R^2	0.999

Figure 6.3. *Analytical features of the BSA-PO/LIB-PO assay in PBST buffer. The data shown correspond to the average of three assays performed on three different days. Each assay was built using three well replicates. LOD corresponds to limit of detection, calculated as the concentration given at 90% of the maximum signal.*

The results of the assay demonstrate (Figure 6.3) that the interday variability is very low, resulting in a final IC_{50} value of 12.79 µg kg^{-1} and a limit of detection of 1.60 µg kg^{-1}, much below the maximum residue limit established by the EC.

6.3.2 IMMUNOSENSOR DEVELOPMENT

According to the procedure described in section 6.4.3, in order to develop the immunosensor directly on the surface of the screen printed electrodes (SPEs), an indirect competitive assay was carried out (using the previously optimized concentrations of the coating antigen, primary and secondary antibody) and calibration curves were obtained using different concentrations of the analyte chlorpyrifos.

6.3.2.1 Anti-IgG-ALP optimization

For the optimization of the immunoassay, first the following concentrations of the alkalyine-phosphatase labelled secondary antibody were investigated:

3 µg mL^{-1},
1 µg mL^{-1},
0.6 µg mL^{-1},
0 µg mL^{-1}.

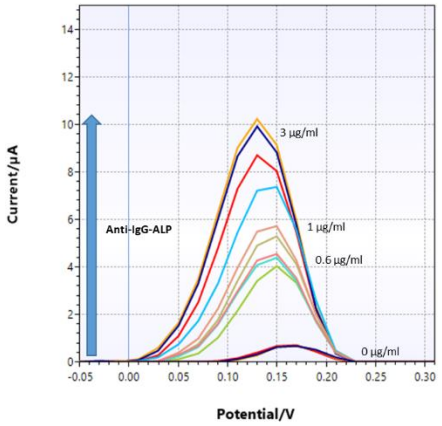

Figure 6.4. *Optimization of the anti-IgG-ALP concentration for the development of the immunosensor. The differential pulse voltammograms were recorded on the BSA-PO coated CB-modified electrodes.*

Based on the results shown in Figure 6.4, the concentration 3 µg mL^{-1} was used for future experiments, since the lower concentrations do not give a high enough

signal, thus they can not be used for the development of the immunosensor. Regarding the concentrations of the coating antigen and the primary antibody, the optimized concentrations were the following: 2.5 µg mL^{-1} of BSA-PO and 5 µg mL^{-1} of LIB-PO.

Subsequently to the optimization process, an indirect competitive assay was carried out and calibration curves were obtained using different concentrations of the analyte chlorpyrifos. The assay was performed on the SPEs that were dropcasted with 5 µL of CB by the automated BioDot dispenser. The current signal was acquired by using DPV as electrochemical detection technique as explained in section 5.4.4.

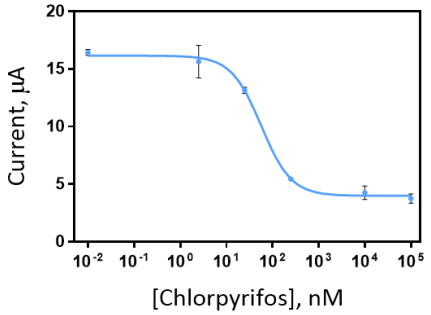

Table 6.2. Parameters of the electrochemical immunosensor developed in PBST buffer (n=3).

[BSA-PO], µg mL^{-1}	2.5
[LIB-PO], µg mL^{-1}	5
$Signal_{min}$	3.98
$Signal_{max}$	16.16
Slope	-1.331
IC_{50}, nM	56.97 ± 2.60
IC_{50}, µg kg^{-1}	19.97 ± 0.91
LOD, nM	9.17
LOD, µg kg^{-1}	3.22
R^2	0.981

Figure 6.5. *Analytical features of the electrochemical immunosensor developed in PBST buffer for the detection of Chlorpyrifos. The data shown correspond to the average of three assays performed on three different days using three replicates in each case.*

The features of the sensor (see Figure 6.5) are similar to the ones of the ELISA shown before (Figure 6.4), the main difference being the increased background noise, which has lead to a slight increase in other parameters as well, such as the limit of detection (3.22 µg kg^{-1}) or the IC_{50} (19.97 µg kg^{-1}) of the assay. However, the developed sensor still fulfills the requirements established by the European commission regarding the MRL, which was set at 0.5 mg kg^{-1} for chlorpyrifos in wheat flour.

6.3.3 MATRIX EFFECT STUDIES: WHEAT FLOUR SAMPLES

The accuracy of the developed immunosensor was studied using wheat flour samples obtained and previously analysed/validated by the company Barilla

(Parma, Italy), a partner organization of the FoodSmartphone project. The sample treatment procedure of the electrochemical immunosenor was carried out using the QuEChERS method according to the protocol described in section 6.4.4.

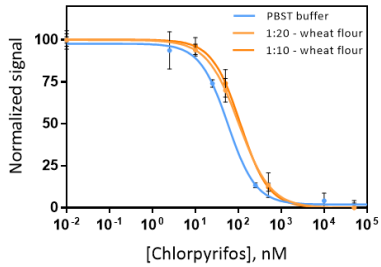

Table 6.3. Parameters of the electrochemical immunosensor developed in wheat flour (n=3).

	1:20 dilution	1:10 dilution
IC_{50}, nM	102.70 ± 5.61	111.30 ± 5.74
IC_{50}, µg kg^{-1}	36.01 ± 1.97	39.02 ± 2.01
LOD, nM	15.82	21.22
LOD, µg kg^{-1}	5.55	7.44
R^2	0.967	0.971

Figure 6.6. *Performance of the electrochemical immunosensor in wheat flour. The data shown correspond to the average of three assays performed on three different days using three replicates in each case.*

Comparing the calibration curves performed in wheat flour to the one in PBST buffer (see Figure 6.6), a slight shift can be observed in the case of the flour samples. This shift mainly results in the increase of the IC_{50}, whereas the other parameters of the assays (e.g.: LOD) remained fairly similar to the one performed in PBST.

The matrix effect studies were also performed in the ELISA format for comparison according to the protocol described in section 6.4.4.

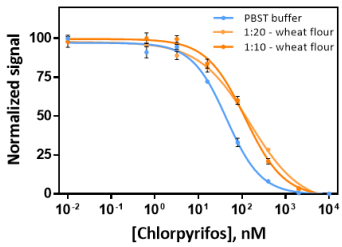

Table 6.4. Parameters of the immunoassays developed in wheat flour (n=3).

	PBST	1:10	1:20
IC_{50}, nM	41.41 ± 0.80	112.61 ± 1.91	120.01 ± 2.42
IC_{50}, µg kg^{-1}	14.52 ± 0.28	39.48 ± 0.67	42.07 ± 0.85
LOD, nM	4.29	11.63	5.10
LOD, µg kg^{-1}	1.51	4.08	1.79
R^2	0.996	0.996	0.996

Figure 6.7. *Performance of the BSA-PO/LIB-PO assay in wheat flour using 1:10 and 1:20 dilutions in PBST buffer. The data shown correspond to the average of three assays performed on three different days using three replicates in each case.*

As it can be observed from Figure 6.7, the features of the assays are very similar to the ones of the sensors, the only difference being the slightly lower LOD values in the case of the ELISA.

In the case of chromatography-based methods the most commonly used detection technique for chlorpyrifos in cereals is GC-MS or GC-MS/MS. These methods have reportedly achieved LOD values of 2.5 to 12 µg kg^{-1} [30-32], which are in the same range of values as we have obtained with the electrochemical immunosensor.

6.3.4 IN-HOUSE SAMPLE VALIDATION AND RECOVERY STUDIES

The in-house sample validation was carried out by measuring 20 blank and 20 spiked flour samples according to the protocol described in section 6.4.4. Five different kind of flour samples were analysed (wheat flour, wholewheat flour, buckwheat flour, corn flour and oat flour), each of them on different days using three replicates in all cases. The results below (see Figure 6.8) demonstrate a clear difference between the blank and the spiked samples, no false negatives or false positives can be observed. Since none of the responses of the spiked samples overlaps with the range of responses of the blanks, it can be stated that the CCß of this screening method is less than or equal to the STC.

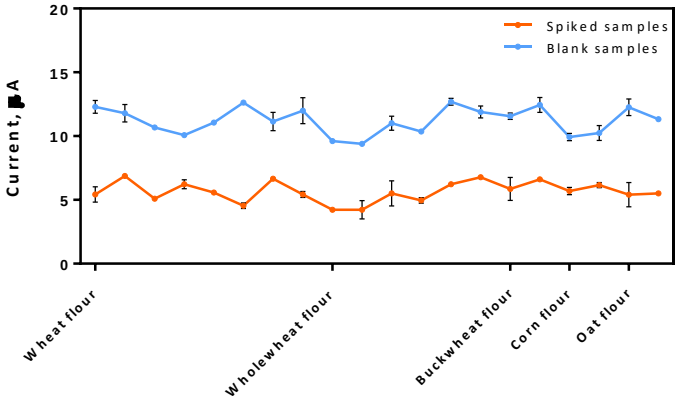

Figure 6.8. *In-house sample validation for Chlorpyrifos in different flour samples. The y-axis corresponds to the acquired current signal in relation to the different flour samples*

represented on the x-axis. The results shown are from different days using three replicates in each case.

Recovery studies were performed using blank and contaminated wheat flour samples (also obtained from Barilla) according to the procedure described in section 6.4.4. Blank samples were spiked at the screening target concentration (STC = 245.41 µg kg^{-1}) and at half of the STC (122.71 µg kg^{-1}) in order to validate the developed electrochemical immunosensor. Furthermore, two previously validated (by GC-MS) contaminated samples were also studied with the immunosensor, achieving good recovery values.

Table 6.5. Recovery studies performed in wheat flour samples (n=3).

Blank samples	Spiked concentraion (µg kg^{-1})	Found concentration (µg kg^{-1})	Recovery (%)
Sample I	122.7	150.0 ± 4.5	122
Sample II	245.4	235.9 ± 3.69	96
Sample III	245.4	247.9 ± 3.29	101
Sample IV	245.4	235.4 ± 3.00	96

Contaminated samples	Measured concentration by GC-MS (µg kg^{-1})	Found concentration (µg kg^{-1})	Recovery (%)
Contaminated sample I	118.2	104.6 ± 1.2	89
Contaminated sample II	268.6	241.7 ± 2.5	91

Figure 6.9. *Recovery values of the electrochemical immunosensor developed in wheat flour samples. The data correspond to the average of three replicates from 3 different days.*

The recovery values above (Table 6.5) demonstrate the applicability of the developed electrochemical immunosensor for the detection of chlorpyrifos in flour samples. As it can be observed from Table 6.5, the recovery values resulted between 89 and 122 % and around 90 % for the contaminated samples. Even though in most cases a slight underestimation of the spiked or contaminated values can be detected, the results measured with the sensor are still close in value.

6.4 CONCLUSIONS

An electrochemical immunosensor was developed for the detection of the insecticide chlorpyrifos in wheat flour samples achieving LOD values around 5 µg kg^{-1}, well below the MRL of 0.5 mg kg^{-1} established by the European Commission. The features of the sensor are comparable to the ones acquired by other detection methods such as ELISA and different MS techniques. Recovery studies and an in-house sample validation was also performed using validated blank and naturally contaminated samples. The in-house validation showed no false positives or false negatives and the recovery values varied between 90 and 120 %. Furthermore, the use of the QuEChERS method for the extraction of the sample avoids the need of bringing the sample to a laboratory and enables the analysis of various different crops on the field. Thus, the developed electrochemical immunosensor is an excellent candidate for the on-site detection of chlorpyrifos in crop samples and could be easily implemented into a multiplexed on-site detection tool with a smartphone-based detection system.

6.5 MATERIALS AND METHODS

The parameters of the electrochemical measurements and the data treatment are identical to the ones described in sections 5.4.4 and 5.4.5 of Chapter 5.

6.5.1 CONSUMABLES AND REAGENTS

For the development of the immunoassays and immunosensors, all solutions were prepared with MQ water from a MilliQ-system. Acetonitrile, acetic acid, $MgSO_4$, sodium acetate, sodium citrate, and the anti-IgG horse radish peroxidase conjugated monoclonal antibody (mAb-HRP) were purchased from Sigma Aldrich (St. Louis, MO, USA). The BSA conjugated antigen for chlorpyrifos (BSA-PO) and the monoclonal anti-chlorpyrifos antibodies (LIB-PO) were obtained from the research group of Ángel Montoya from the Universidad Politècnica de València. The anti-IgG alkalyne phosphatase conjugated monoclonal antibody (mAb-ALP) was obtained from Jackson Immunoresearch.

The rest of the reagents, buffers and equipments used have already been described in section 5.4.1 of Chapter 5.

Wheat samples. The validated blank and contaminated flour samples were selected within the monitoring plans of 2020 Italian wheat harvesting campaign and analysed for determining precisely their pesticide content through an official valildated method (EN 15662:2018).

[*EN 15662:2018 - Foods of plant origin - Multimethod for the determination of pesticide residues using GC- and LC-based analysis following acetonitrile extraction/partitioning and clean-up by dispersive SPE - Modular QuEChERS-method* - *https://standards.cen.eu/dyn/www/f?p=CENWEB:110:::::FSP_ORG_ID,FSP_PROJECT:6256,61387&cs=1A5F8BA6D83DC028C76EB868855FCCF57*

CEN - Standards Development - Technical Bodies - CEN/TC 275 - Catalogue of Published Standards]

6.5.2 IMMUNOASSAY DEVELOPMENT

Non-competitive indirect ELISA. This method was used to evaluate the avidity of the antibody LIB-PO with the coating antigen BSA-PO. The two-dimensional titration assays (2D-assay) were carried out based on measuring the binding of a series of concentrations (starting from 1 μg mL^{-1} to 0.016 ng mL^{-1} and zero; 100 μL $well^{-1}$) of the monoclonal antibody against different concentrations (dilutions from 10 μg mL^{-1} to 10 ng mL^{-1}, and zero; 100 μL $well^{-1}$) of the antigen. Depending on the results of these experiments, the optimum concentrations for the coating antigen and the monoclonal antibody were chosen, generating an absorbance around 0.8-1 units.

Competitive ELISA BSA-PO/LIB-PO for the detection of Chlorpyrifos. First, 96-well microtiter plates were coated with the antigen BSA-PO (0.6125 μg mL^{-1} in coating buffer, 100 μL $well^{-1}$), overnight at 4 °C and covered with adhesive plate sealers. The following day, the plates were washed four times with PBST (300 μL $well^{-1}$), and the solution of Chlorpyrifos (stock from 2000 to 0 μM in DMSO and diluted 200 times in PBST or in the flour samples) were added (50 μL $well^{-1}$), followed by the solution of the antibody LIB-PO (0.0625 μg mL^{-1} in PBST, 50 μL $well^{-1}$). After

30 min of incubation at room temperature (RT), the plates were washed as mentioned before, and a solution of anti-IgG-HRP (1/6000 in PBST) was added to the wells (100 µL well^{-1}) and incubated for another 30 minutes at RT. The plates were washed again, and the substrate solution was added (100 µL well^{-1}). After 30 min, colour development was stopped with 4N H_2SO_4 (50 µL well^{-1}) at RT, and the absorbance was read at 450 nm with a spectrophotometer. The standard curves were fitted to a four-parameter equation according to the following formula: y = (A − B/[1 − (x/C)D] + B, where A is the maximal absorbance, B is the minimum absorbance, C is the concentration producing 50% of the maximal absorbance, and D is the slope at the inflection point of the sigmoid curve. Unless otherwise indicated, data presented correspond to the average of at least three well replicates.

6.5.3 IMMUNOSENSOR DEVELOPMENT

As the first step of the sensor development, similarly to the ELISA, the working electrode (WE) was functionalized with the optimized concentration of the corresponding antigen by dropcasting 2 µL of the prepared solution (2.5 µg mL^{-1} BSA-PO in carbonate buffer) on its surface. All the electrodes were incubated for 45 minutes at RT. All of the incubation steps were performed in a humid chamber at RT. Afterwards, the WEs were washed twice with 100 µL of PBST and once with 100 µL of PBS. The next step was the blocking of the electrode's surface by dropping 2 µL of 2 % BSA in carbonate buffer, after which the electrodes were incubated for 30 minutes at RT. The WEs were washed again twice with 100 µL of PBST and once with 100 µL of PBS. Next, 2 µL of the primary antibody solution (5 µg mL^{-1} LIB-PO in PBS) and different concentrations of the analyte chlorpyrifos (from 2.5 nM to 10 µM and 0 nM in PBS with BSA 1%) were incubated on the WE for 30 minutes at RT for the competition step. The SPEs were washed again using the same procedure as explained above. The next step was the addition of the alkaline phosphatase (ALP) labelled secondary antibody (in PBS with BSA 1%) for 30 minutes at RT. This step was also followed by a washing step (twice with 100 µL of PBST and once with 100 µL of PBS) and finally the electrodes were dropcasted with 2 µL of PBS until the start of the electrochemical measurement in order to avoid drying them out. Afterwards, 60 µL of the enzymatic substrate containing solution (5 mg mL^{-1} 1-Naphthyl phosphate disodium salt in

diethanolamine buffer with 1 mM $MgCl_2$) was dropped on the SPE's surface (covering all 3 electrodes) and after 2 minutes of incubation time, the DPV measurement was started according to the procedure explained in section 5.4.4 and the resulting current was recorded (n=3).

6.5.4 MATRIX EFFECT STUDIES AND IN-HOUSE SAMPLE VALIDATION

Analysis of validated reference samples by GC-MS/MS. The analytical method used is based on EN 15662:2018. The principle of the method is: homogenization of 5 g samples by lab grinder, water-acetonitrile extraction by shaking and addition of mix of internal standards, liquid-liquid partition (adding salts and buffers), purification on a dispersed solid phase, instrumental analysis carried out with a GC-MS/MS (triple quadrupole). LOD/LOQ: 0.003/0.01 mg kg^{-1}.

Matrix effect studies. Non-specific interferences produced by the parameters associated with the matrix of interest were studied by preparing a standard curve in wheat flour samples. The validated blank and contaminated flour samples were obtained from the company Barilla (Parma, Italy). For the preparation of the samples, the QuEChERS ("quick, easy, cheap, effective, rugged, and safe") solid phase extraction method was used. First, 5 g of the flour sample was weighed and homogenized with 10 mL of MilliQ water in a 50 mL centrifuge tube. Afterwards, 10 mL of acetonitrile containing 1% of acetic acid was added to the solution and hand-shaken for 1 min. The following step was the addition of 3 g $MgSO_4$ and the mixture was immediately hand-shaken for 20 sec. Subsequently, 1.7 g of sodium-acetate and 1 g of sodium-citrate were added and the tube was hand-shaken for an additional 1 min. It was followed by an 8 min centrifugation step at 4000 rpm, which resulted in a well-defined phase separation. Afterwards, the supernatant was taken and diluted in PBST (1:10 or 1:20) for the analysis of the sample either by ELISA or by the developed electrochemical immunosensor.

Recovery studies. The recovery of the chlorpyrifos concentration subsequently to the sample treatment was assessed by spiking four different blank wheat flour samples at either 350 nM (half of the screening target concentration, STC) or at 700 nM (STC) before the sample extraction procedure and then analysed by the immunosensor. The sample concentrations were then calculated by interpolating the results to the chlorpyrifos standard curve that was previously

prepared in the corresponding flour samples. On the other hand, two naturally contaminated and previously validated (by GC-MS) samples were also analysed. The final recovery values were obtained using a recovery factor (RF) of 10 due to the dilution of the samples.

In-house sample validation. For the in-house validation of the developed immunosensor, the guidelines from 2002/657/EC were followed. First, twenty different blank wheat flour samples were selected. At the same time twenty other samples (replicates of the blank samples) were spiked at the STC, (700 nM = 245.41 µg kg^{-1}) which was set around half of the Maximum Residue Limit (MRL) of chlorpyrifos in cereals (0.5 mg kg^{-1}). The 20 blank samples all had to be negative and at least 19 of the 20 spiked samples had to be classified as "suspect", thus resulting in a false compliant rate lower than 5 %.

6.6 BIBLIOGRAPHY

[1] Jiao, Y., Hou, W., Fu, J., Guo, Y., & Sun, X. (2017). Sensors and Actuators B: Chemical A nanostructured electrochemical aptasensor for highly sensitive detection of chlorpyrifos. Sensors & Actuators: B. Chemical, 243, 1164–1170. https://doi.org/10.1016/j.snb.2016.12.106

[2] Xu, G., Huo, D., Hou, C., Zhao, Y., Bao, J., Yang, M., & Fa, H. (2018). Talanta A regenerative and selective electrochemical aptasensor based on copper oxide nano fl owers-single walled carbon nanotubes nanocomposite for chlorpyrifos detection. Talanta, 178(August 2017), 1046–1052. https://doi.org/10.1016/j.talanta.2017.08.086

[3] Islam, S., Shukla, S., Bajpai, V. K., Han, Y., & Huh, Y. S. (2019). Microfluidic-based graphene field effect transistor for femtomolar detection of chlorpyrifos. Scientific Reports, (August 2018), 1–7. https://doi.org/10.1038/s41598-018-36746-w

[4] Wei, W., Zong, X., Wang, X., Yin, L., Pu, Y., & Liu, S. (2012). A disposable amperometric immunosensor for chlorpyrifos-methyl based on immunogen / platinum doped silica sol – gel film modified screen-printed carbon electrode.

Food Chemistry, 135(3), 888–892. https://doi.org/10.1016/j.foodchem.2012.06.037

[5] Talan, A., Mishra, A., Eremin, S. A., Narang, J., Kumar, A., & Gandhi, S. (2018). Biosensors and Bioelectronics Ultrasensitive electrochemical immuno-sensing platform based on gold nanoparticles triggering chlorpyrifos detection in fruits and vegetables. Biosensors and Bioelectronic, 105(January), 14–21. https://doi.org/10.1016/j.bios.2018.01.013

[6] He, L., Luo, X., Xie, H., Wang, C., Jiang, X., & Lu, K. (2009). Analytica Chimica Acta Ionic liquid-based dispersive liquid – liquid microextraction followed high-performance liquid chromatography for the determination of organophosphorus pesticides in water sample, 655, 52–59. https://doi.org/10.1016/j.aca.2009.09.044

[7] S. Rai, A.K. Singh, A. Srivastava, S. Yadav, M.H. Siddiqui, M.K.R. Mudiam, Comparative evaluation of QuEChERS method coupled to DLLME extraction for the analysis of multiresidue pesticides in vegetables and fruits by gas chromatography- mass spectrometry, Food Anal. Method. 9 (2016) 2656–2669.

[8] X.T. Li, D.Z. Zhu, Z.H. Ma, L.G. Pan, D. Wang, J.H. Wang, Feasibility study of the detection of chlorpyrifos residuals on apple skin based on infrared micro-imaging, Opt. Eng. 51 (2012) 8.

[9] G. Xu, D. Huo, C. Hou, Y. Zhao, J. Bao, M. Yang, H. Fa, Talanta A regenerative and selective electrochemical aptasensor based on copper oxide nano fl owers-single walled carbon nanotubes nanocomposite for chlorpyrifos detection, Talanta. 178 (2018) 1046–1052. https://doi.org/10.1016/j.talanta.2017.08.086.

[10] S. Li, W. Liang, F. Zheng, X. Lin, J. Cai, Ascorbic acid surface modified TiO 2-thin layers as a fully integrated analysis system for visual simultaneous detection of organophosphorus pesticides, Nanoscale 6 (2014) 14254–14261.

[11] Mostafalou, S. & Abdollahi, M. Pesticides and human chronic diseases: evidences, mechanisms, and perspectives. Toxicol Appl Pharmacol 268, 157–177 (2013).

[12] Chen, J. et al. Electrochemical Biosensor for Detection of BCR/ABL Fusion Gene Using Locked Nucleic Acids on 4-Aminobenzenesulfonic Acid-Modified Glassy Carbon Electrode. Anal Chem 80, 8028–8034 (2008).

[13] Sirtori, C., Ana, A., Irene, C., José, A. & Sanchéz, P. Application of liquid chromatography quadrupole time-of-flight mass spectrometry to the identification of acetamiprid transformation products generated under oxidative processes in different water matrices. Anal Bioanal Chem 406, 2549–2558 (2014).

[14] Watanabe, E., Miyake, S., Baba, K., Eun, H. & Endo, S. Evaluation of performance of a commercial monoclonal antibody-based fenitrothion immunoassay and application to residual analysis in fruit samples. Anal Bioanal Chem 386, 1441–1448 (2006).

[15] De Dominicis, E.; Commissati, I.; Gritti, E.; Catellani, D.; Suman, M. (2015). Quantitative targeted and retrospective data analysis of relevant pesticides, antibiotics and mycotoxins in bakery products by liquid chromatography – single stage Orbitrap mass spectrometry. Food Additives and Contaminants, 32(10), pp. 1617-1627

[16] Moretti, S.; Cavanna, D.; Lambertini, F.; Catellani, D.; Sammarco, G.; Barola, C.; Paoletti, F.; Saluti, G.; Galarini, R.; Suman, M. (2020). Practical approach to develop a multi-group screening method for detection of mycotoxins, pesticides and veterinary drugs in food. Journal of Mass Spectrometry, 55(11). https://doi.org/10.1002/jms.4618

[17] Manclu, J. J., Primo, J., & Montoya, A. (1996). Development of Enzyme-Linked Immunosorbent Assays for the Insecticide Chlorpyrifos. 1. Monoclonal Antibody Production and Immunoassay Design, 4052–4062.

[18] Manclu, J. J., Montoya, A., Valencia, D., & Vera, C. De. (1996). Development of Enzyme-Linked Immunosorbent Assays for the Insecticide Chlorpyrifos. 2. Assay Optimization and Application to Environmental Waters.

[19] C. Zhang, Z. Jiang, M. Jin, P. Du, G. Chen, X. Cui, Y. Zhang, Fluorescence immunoassay for multiplex detection of organophosphate pesticides in agro-products based on signal amplification of gold nanoparticles and

oligonucleotides, Food Chem. 326 (2020) 126813. https://doi.org/10.1016/j.foodchem.2020.126813.

[20] K. Sankar, D. Lenisha, G. Janaki, J. Juliana, R.S. Kumar, M.C. Selvi, G. Srinivasan, Talanta Digital image-based quantification of chlorpyrifos in water samples using a lipase embedded paper based device, Talanta. 208 (2020) 120408. https://doi.org/10.1016/j.talanta.2019.120408.

[21] R. Zou, Y. Chang, T. Zhang, F. Si, Y. Liu, Y. Zhao, Up-Converting Nanoparticle-Based Immunochromatographic Strip for Multi-Residue Detection of Three Organophosphorus Pesticides in Food, 7 (2019) 1–10. https://doi.org/10.3389/fchem.2019.00018.

[22] L.F. Capitán-vallvey, A.L. Ogunneye, N.A.A. Babarinde, M.M. Erenas, Talanta Bioactive microfluidic paper device for pesticide determination in waters, Talanta. 218 (2020) 121108. https://doi.org/10.1016/j.talanta.2020.121108.

[23] Suri, C. R., Kaur, J., Gandhi, S. & Shekhawat, G. S. Label-free ultra-sensitive detection of atrazine based on nanomechanics. Nanotechnol 19, 235502 (2008).

[24] Suri, C. R. et al. Immunoanalytical techniques for analyzing pesticides in the environment. TrAC Trends in. Anal Chem 28, 29–39 (2009).

[25] Thakur, S., Gandhi, S., Paul, A. K. & Suri, C. R. A flow injection immunosensor for the detection of atrazine in water samples. Sens Trans 131, 91–100 (2011).

[26] Hu, W., Chen, Q., Li, H., Ouyang, Q. & Zhao, J. Fabricating a novel label-free aptasensor for acetamiprid by fluorescence resonance energy transfer between NH_2-NaYF4: Yb, Ho@SiO_2 and Au nanoparticles. Biosens Bioelectron 80, 398–404 (2016).

[27] Yuce, M., Ullah, N. & Budak, H. Trends in aptamer selection methods and applications. Analyst 140, 5379–5399 (2015).

[28] Li, X. et al. A simple highly sensitive and selective aptamer-based colorimetric sensor for environmental toxins microcystin-LR in water samples. J Hazard Mater 304, 474–480 (2016).

[29] X. Sun, Y. Cao, Z. Gong, X. Wang, Y. Zhang, J. Gao, An Amperometric Immunosensor Based on Multi-Walled Carbon Nanotubes-Thionine-Chitosan Nanocomposite Film for Chlorpyrifos Detection, (2012) 17247–17261. https://doi.org/10.3390/s121217247.

[30] D.I. Kolberg, O.D. Prestes, M.B. Adaime, R. Zanella, Development of a fast multiresidue method for the determination of pesticides in dry samples (wheat grains , flour and bran) using QuEChERS based method and GC – MS, Food Chem. 125 (2011) 1436–1442. https://doi.org/10.1016/j.foodchem.2010.10.041.

[31] S. Walorczyk, Development of a multi-residue method for the determination of pesticides in cereals and dry animal feed using gas chromatography – tandem quadrupole mass spectrometry II. Improvement and extension to new analytes, 1208 (2008) 202–214. https://doi.org/10.1016/j.chroma.2008.08.068.

[32] R. Zamora-Sequeira, R. Starbird-Pérez, O. Rojas-Carillo, S. Vargas-Villalobos, What are the Main Sensor Methods for Quantifying Pesticides in Agricultural Activities? A Review, Molecules. 24 (2019) 2659. https://doi.org/10.3390/molecules24142659

7 DEVELOPMENT OF ELECTROCHEMICAL IMMUNOSENSORS FOR THE DETECTION OF BROMOPROPYLATE AND PARAQUAT

CHAPTER OVERVIEW

This chapter first describes the production and characterization of the immunoreagents necessary for the detection of the herbicide paraquat and the insecticide bromopropylate. Subsequently to the characterization process (by ELISA), the immunoreagents are used for the development of electrochemical immunosensors for the detection of the above mentioned pesticides. Finally, the application of these detection methods in juice and jam samples is decribed by evaluating the matrix effect and the recovery values of the system.

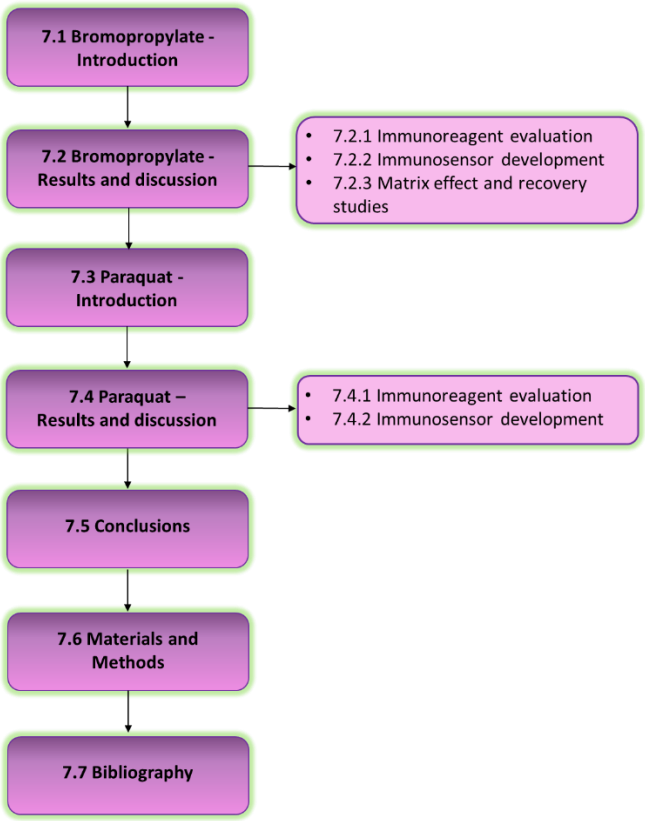

Figure 7.1. *The structure of this chapter in relation to the different sections.*

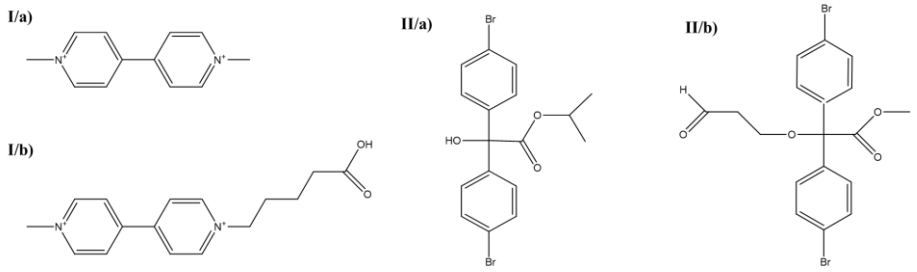

Figure 7.2. *I/a) Chemical structure of paraquat. I/b) Chemical structure of the immunizing hapten for the detection of Paraquat. II/a) Chemical structure of Bromopropylate. II/b) Chemical structure of the immunizing hapten for the detection of Bromopropylate.*

7.1 BROMOPROPYLATE - INTRODUCTION

7.1.1 THE ROLE OF BROMOPROPYLATE IN FOOD SAFETY

Bromopropylate (isopropyl-4,4'-dibromobenzilate) is a contact acaricide that has been extensively used in agriculture against all stages of mites [1]. It is a non-penetrating and non-systemic compound that remains on the peel of fruits and vegetables without migrating into the pulp. Moreover, bromopropylate (BP) is fairly persistent in the environment in acid and neutral media (resulting in half-lives of 50 days and >3 years, respectively) [2]. It has also shown low acute toxicity in rats and rabbits [3,4], but the effects of BP on humans are still unknown. BP was first tested in the field for the controlling of mites in 1966 and its use was banned in the European Union in 2011. However, despite the regulations of the European legislation, several member states have negotiated essential uses of the compound; therefore, some countries in Europe enable authorized BP use while alternatives are sought (Regulation 2076/2002/EC). For the above mentioned reasons the International Programme on Chemical Safety (INCHEM) has established a maximum recommended BP daily intake of 0-0.03 mg kg^{-1} of body weight/day for humans. In order to fulfill these recommendations and accommodate an essential use of the pesticide, maximum residue levels (MRLs) have been established in marketed products such as wine grapes, citrus, stone and pome fruits (Reg. (EU) No 310/2011 - MRL 0.01 mg kg^{-1}). Nevertheless, data of the European Commission show that there is still a

continuous use of BP in vineyards and that BP has been found in several countries such as Norway, Iceland, Denmark, Italy, and Lichtenstein in table grapes with residue levels exceeding the MRLs [5]. Thus, the monitoring of this pesticide is of utmost importance in our food products.

7.1.2 DETECTION METHODS FOR BROMOPROPYLATE IN THE LITERATURE

In order to follow the regulations of the European commission and to guarantee the quality of fruits and vegetables, the monitoring and analysis of BP in alimentary samples is mainly conducted using chromatographic techniques such as high-performance liquid chromatography [6], gas chromatography [7], or gas chromatography coupled to mass spectrometry [8-10]. One of the main advantages of these techniques is that their limits of detection is around the established MRLs. However, they also possess several drawbacks such as the need of an extraction method (e.g.: liquid-liquid or solid-phase extraction) prior to the analysis. As a result, chromatographic methods are time-consuming and also require high-cost equipment and trained personnel. On the other hand, immunochemical techniques are rapid, reliable, easy-to-use and low-cost. Furthermore, they also have the ability to simultaneously analyse multiple samples while achieving the necessary detectability and selectivity for the target analyte without an extensive sample treatment [1,7,11-14]. Even though several different immunochemical detection formats (e.g.: ELISA, lateral-flow, microarray etc.) have been explored for the detection of Bromopropylate, to this date no electrochemical immunosensor has been developed, thus one of the objectives of this thesis was to achieve that.

7.2 BROMOPROPYLATE - RESULTS AND DISCUSSION

7.2.1 IMMUNOREAGENT EVALUATION

In the case of the analyte bromopropylate, the production of a new conjugate (coating antigen) was necessary. The conjugation was performed by a reductive amination strategy between an aldehyde and the amino groups of the protein's lysines. The conjugates were purified by chromatography and then characterized with MALDI-TOF-MS.

Regarding the antisera, after the immunoreagent evaluation process both of them (As174 and As198) were purified based on the protocol explained in section 7.4.2.

The immunoreagents necessary for the detection of bromopropylate were evaluated by the performance of non-competitive 2D checkerboard titration immunoassays (in order to obtain their optimal concentrations), which were followed by competitive indirect immunoassays in order to obtain the calibration curve of the assay.

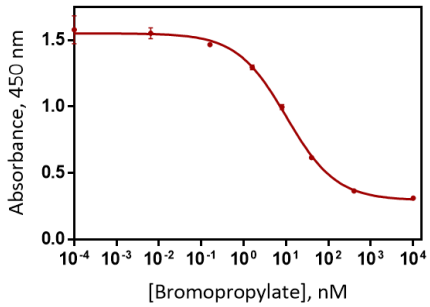

Table 7.1. Parameters of the assay (h9-BSA/As174)

Coating Ag, µg mL^{-1}	0.35
As dilution	1/15000
Absorbance$_{min}$	0.293
Absorbance$_{max}$	1.550
Slope	-0.74
IC$_{50}$, nM	10.17 ± 1.07
IC$_{50}$, µg L^{-1}	4.35 ± 0.46
LOD, nM	0.37
LOD, µg L^{-1}	0.16
R^2	0.992

Figure 7.3. *Analytical features of the h9-BSA/As174 assay in PBST buffer. The data shown correspond to the average of three assays performed on three different days. Each assay was built using three well replicates. LOD corresponds to limit of detection, calculated as the concentration given at 90% of the maximum signal.*

The results of the assay (see Figure 7.3) demonstrate that the interday variability is fairly low, resulting in a final IC$_{50}$ of 4.35 ± 0.46 µg L^{-1} and an LOD of 0.37 µg L^{-1} which still fulfils the requirements regarding the MRL of this pesticide (0.01 mg

L^{-1}). However, it is also important to mention that there is a relatively high background noise, which is most probably due to the different properties of the immunoreagents and could in fact pose a potential difficulty upon developing the electrochemical immunosensors for the detection of the analyte.

7.2.2 IMMUNOSENSOR DEVELOPMENT

Similarly to the other analytes, the first step of the immunosensor development was the optimization of the alkaline-phosphatase labelled secondary antibody for which the following concentrations were studied:

3 µg mL^{-1},
1 µg mL^{-1},
0.6 µg mL^{-1},
0 µg mL^{-1}.

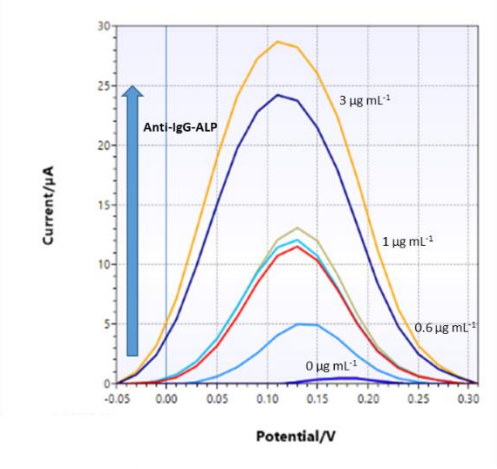

Figure 7.4. *Optimization of the anti-IgG-ALP concentration for the development of the immunosensor. The differential pulse voltammograms were recorded on the h9-BSA coated CB-modified electrodes.*

According to the results shown in Figure 7.4, the concentration 3 µg mL^{-1} was used for future experiments, since using a lower concentration would not give a high enough signal for the development of the immunosensor. Regarding the

concentrations of the coating antigen and the primary antibody, the optimized concentrations were 2.5 µg mL^{-1} of h9-BSA and 10 µg mL^{-1} of Ab174.

After the optimization process, an indirect competitive assay was carried out and calibration curves were obtained using different concentrations of the analyte bromopropylate.

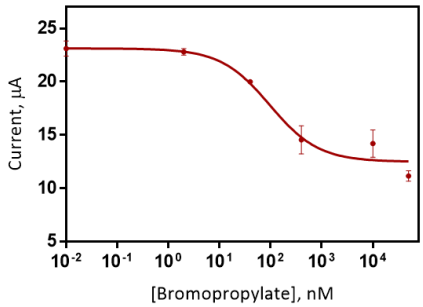

Table 7.2. Parameters of the electrochemical immunosensor developed in PBST buffer (n=3).

h9-BSA, µg mL^{-1}	2.5
Ab174, µg mL^{-1}	10
$Signal_{min}$	12.48
$Signal_{max}$	23.12
Slope	-0.91
IC_{50}, nM	96.42 ± 1.71
IC_{50}, µg L^{-1}	54.82 ± 0.73
LOD, nM	10.08
LOD, µg L^{-1}	4.32
R^2	0.902

Figure 7.5. *Analytical features of the electrochemical immunosensor developed in PBST buffer for the detection of Bromopropylate. The data shown correspond to the average of three replicates.*

The results of the developed sensor (see Figure 7.5) show a significant increase in terms of IC_{50}, LOD and background noise compared to the parameters of the ELISA.

Even though the developed sensor fulfills the requirements of the European Commission regarding the MRL, the interday variability (most probably due to the high background noise) made it difficult to perform reproducible measurements. In order to overcome this issue, different new conjugation strategies were explored to produce new coating antigens in the hope of minimizing the background noise and increasing the reproducibility of the assay.

The hapten h9 was conjugated to aminodextran (AD) using the protocol explained in section 7.4.2 and a successful conjugation could be observed, which was followed by the performance of non-competitive 2D and competitive indirect immunoassays in order to obtain the calibration curves of the assay.

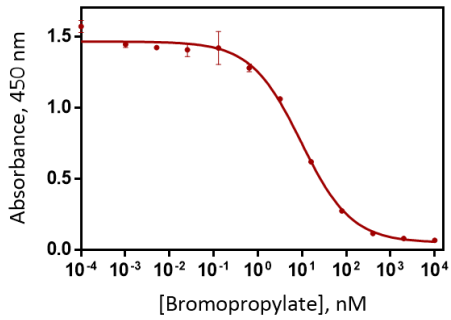

Table 7.3. Parameters of the assay (h9-AD/As174)	
Coating Ag, µg mL^{-1}	0.625
As dilution	1/8000
Absorbance$_{min}$	0.049
Absorbance$_{max}$	1.465
Slope	-0.76
IC$_{50}$, nM	9.54 ± 1.15
IC$_{50}$, µg L^{-1}	4.08 ± 0.49
LOD, nM	0.11
LOD, µg L^{-1}	0.05
R^2	0.991

Figure 7.6. *Analytical features of the h9-AD/As174 assay in PBST buffer. The data shown correspond to the average of three assays performed on three different days. Each assay was built using three well replicates. LOD corresponds to limit of detection, calculated as the concentration given at 90% of the maximum signal.*

It can be seen from the analytical features of the assay (Figure 7.6) that using the conjugate h9-AD has helped in eliminating the background noise and has also significantly decreased the other parameters of the assay such as the IC_{50} and the LOD. Unfortunately however, due to its physico-chemical properties this conjugate could not be immobilized to the surface of the screen printed electrodes by simple adsorption (which was used in the case of the other analytes), thus the matrix effect and recovery studies were only performed using the ELISA format in this case.

7.2.3 MATRIX EFFECT AND RECOVERY STUDIES FOR BROMOPROPYLATE: JUICES AND JAMS

In order to study the accuracy of the developed immunoassay, different kinds of juices and jams were purchased from a local store and prepared for the measurements according to the protocol described in section 7.4.4.

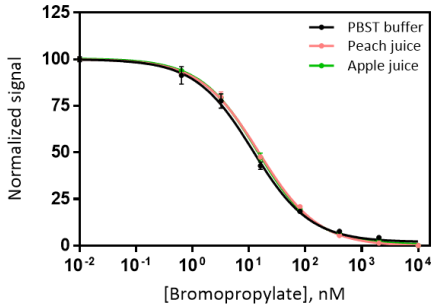

Table 7.4. Comparison of the main parameters of the immunoassay in PBST buffer, in peach and in apple juice (n=3).

	PBST Buffer	Peach juice (1:5 dilution)	Apple juice (1:5 dilution)
IC_{50}, nM	11.74 ± 1.11	15.20 ± 1.05	14.32 ± 1.05
IC_{50}, µg L^{-1}	5.03 ± 0.48	6.51 ± 0.45	6.13 ± 0.45
LOD, nM	0.93	1.09	1.16
LOD, µg L^{-1}	0.40	0.47	0.50
R^2	0.996	0.999	0.999

Figure 7.7. *Performance of the immunoassay in peach and apple juice. The data shown correspond to the average of three assays performed on three different days using three replicates in each case.*

Comparing the calibration curves performed in apple and peach juices to the one in PBST buffer (see Figure 7.7), only a slight shift in terms of IC_{50} and LOD can be observed, demonstrating a practically null matrix effect.

Recovery studies were performed using blank peach and apple juice samples spiked at 4 different concentrations according to the protocol described in section 7.4.4.

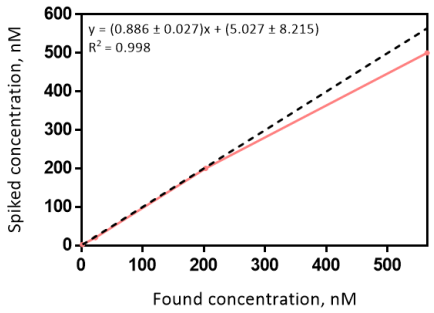

Table 7.5. Recovery values of the immunoassay developed in peach juice (n=3).

Spiked concentration (nM)	Found concentration (nM)	Recovery (%)
2	1.73 ± 0.17	87
20	22.93 ± 2.03	115
200	202.94 ± 1.55	101
500	564.74 ± 10.51	113

Figure 7.8. *Recovery values of the immunoassay developed in a 1:5 dilution of peach juice. The graph shows the correlation between the spiked and measured concentration values. The dotted line corresponds to a perfect correlation (m=1). The data correspond to the average of three replicates from 3 different days.*

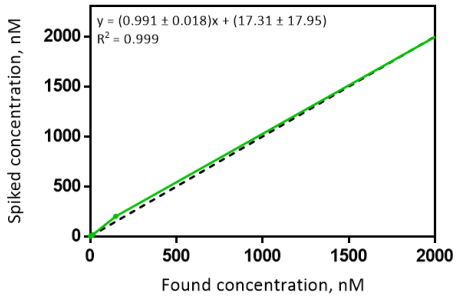

Table 7.6. Recovery values of the immunoassay developed in apple juice (n=3).

Spiked concentration (nM)	Found concentration (nM)	Recovery (%)
2	1.74 ± 0.18	87
15	13.92 ± 0.42	93
200	148.30 ± 11.51	74
2000	2002.48 ± 65.71	100

Figure 7.9. *Recovery values of the immunoassay developed in a 1:5 dilution of apple juice. The graph shows the correlation between the spiked and measured concentration values. The dotted line corresponds to a perfect correlation (m=1). The data correspond to the average of three replicates from 3 different days.*

The results of the recovery studies (Figure 7.8 and 7.9) demonstrate the applicability of the immunoassay for the detection of even trace levels (2nM = 0.86 µg L^{-1}) of bromopropylate in peach and apple juice, well below the established MRL (0.01 mg L^{-1}) by the current European legislations. Even though in the case of the peach juice samples (Table 7.5) a slight underestimation and in the case of the apple juice samples (Table 7.6) an overestimation of the spiked values can be observed, the results are still quite close to the spiked values.

As a proof-of-concept of the immunoassay, next to the different juice samples, jams were also tested and prepared according to the protocol in section 7.4.4.

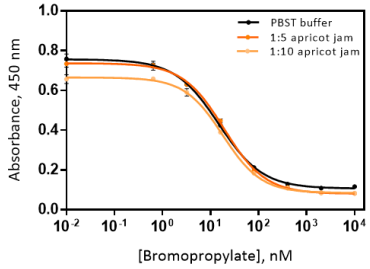

Table 7.9. Parameters of the immunoassays developed in different dilutions of apricot jam (n=3).

	PBST	1:5 apricot jam	1:10 apricot jam
IC_{50}, nM	14.80 ± 1.08	19.01 ± 1.06	17.98 ± 1.07
IC_{50}, µg kg^{-1}	6.33 ± 0.46	8.14 ± 0.45	7.70 ± 0.46
LOD, nM	1.42	2.25	2.65
LOD, µg kg^{-1}	0.61	0.96	1.13
R^2	0.995	0.997	0.996

Figure 7.10. *Performance of the immunoassay in different dilutions of apricot jam. The data shown correspond to the average of three assays performed on three different days using three replicates in each case.*

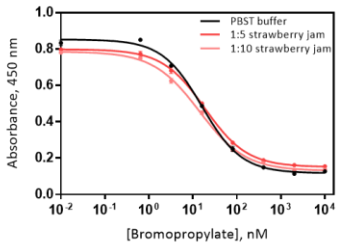

Table 7.8. Parameters of the immunoassays developed in different dilutions of strawberry jam (n=3).

	PBST	1:5 strawberry jam	1:10 strawberry jam
IC_{50}, nM	16.00 ± 1.08	53.65 ± 1.15	51.03 ± 1.19
IC_{50}, µg kg^{-1}	6. 85 ± 0.46	22.97 ± 0.49	21.85 ± 0.51
LOD, nM	1.67	1.72	1.70
LOD, µg kg^{-1}	0.71	0.74	0.73
R^2	0.996	0.981	0.985

Figure 7.11. *Performance of the immunoassay in different dilutions of strawberry jam. The data shown correspond to the average of three assays performed on three different days using three replicates in each case.*

It can be observed from the results above (Figure 7.10 and 7.11) that using a 1:5 dilution of the jams only results in a slight shift in terms of IC_{50} and LOD, thus demonstrating that the developed immunoassay is able to detect the pesticide bromopropylate not only in juice but in jam samples as well.

7.3 PARAQUAT - INTRODUCTION

7.3.1 THE ROLE OF PARAQUAT IN FOOD SAFETY

Modern agricultural production highly depends on the use of herbicides to control weeds in crops [15]. Paraquat (1,1'-dimethyl-4,4'-dipyridylium) is a broad-spectrum, non-selective bipyridine (quaternary nitrogen) herbicide used to control weeds in various different crops and can also be used as defoliant (cotton, hops) or for the destruction of potato stems [16,17]. Paraquat is a rapidly acting contact pesticide, which upon absorbtion by green shoots is able to destroy the shoots by interfering with the intracellular electron transfer system, inhibiting the reduction of NADP to NADPH during photosysnthesis [15,18,19]. As a result of its swift acting mechanism, paraquat was declared as an agricultural breakthrough when it was introduced in the 1960s. Since then, hundreds of millions of pounds have been used in the U.S. alone (see Figure 7.12). The main problem with paraquat is that it is also extraordinarily toxic to humans [20,21,22] and unlike some other poisons, paraquat has no antidote. People who accidentally drink just a little bit of it often die soon afterward.

Because it is so remarkably lethal, thousands of people around the world have used the pesticide to kill themselves. Its high toxicity is due to the formation of superoxide anions in the mitochondria and cytosol of yeast and mammalian cells leading to the formation of several reactive oxygen species (superoxide, hydroxyl, and hydrogen peroxide) through the reduction of bivalent cations [23,24]. Such radical species can lead to significant damage to the cell membranes, DNA, and other important biomolecules [25]. Furthermore, the highly water-soluble nature of these herbicides (35−60 mg kg^{-1} LD_{50} for humans [26]) is often responsible for the contamination of water sources near the cultivation fields. Thus, the toxicity effects of bispyridinium herbicides are more significant than those of their contemporaries, such as glyphosate, glufosinate, and organophosphorous compounds [25].

Moreover, human epidemiological [27, 28, 29] and animal studies indicate that paraquat might also be an environmental factor contributing to neurodegenerative disorders such as Parkinson's disease [30,31]. Paraquat can also lead to lung fibrosis, adenocarcinomas [32–34], and oxidative stress affecting liver functionality [32, 35]. Due to its adverse effects, since July 2007 the use of this pesticide in the EU has been banned, however farmers outside the EU (in more than 130 countries) are still using PQ and export their products to the EU. (China is the biggest producer with more than 100 000 tons of paraquat every year and its production is increasing every year worldwide) [26]. Therefore, PQ is included in the EU database between the compounds that should be monitored in food samples and maximum residue limits (MRL, 20 µg kg^{-1} for most crops) have been established for different commodities (Regulation (EC) No. 396/2005).

According to this requirement, and in order to protect public health, official laboratories should be able to efficiently process a high number of samples. Thus, the development of rapid, cost-effective and sensitive on-site analytical measuring tools with high sample throughput capabilities are required.

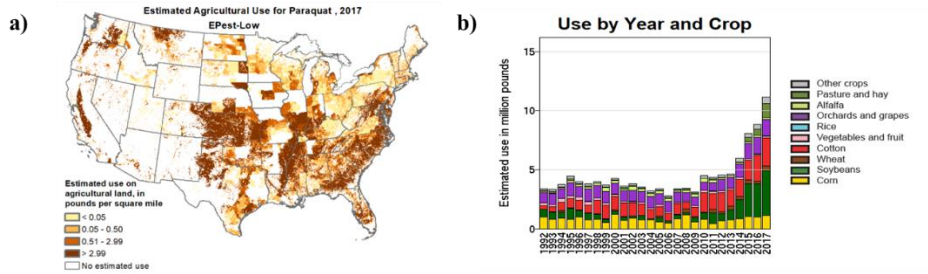

Figure 7.12. *Estimated annual agricultural use of Paraquat in 2017 [https://water.usgs.gov/nawqa/pnsp/usage/maps/show_map.php?year=2017&map=PARAQUAT&hilo=L&disp=Paraquat].*

7.3.2 DETECTION METHODS FOR PARAQUAT IN THE LITERATURE

Due to its physico-chemical properties such as permanent ionic character, high hydrophilicity and a tendency to interact with surfaces, the implementation of paraquat within multi-residue methods (MRMs) is very difficult [36,37]. It would require distinctive extraction and clean-up conditions, thus it is being excluded from the routine pesticide monitoring programs in spite of its high relevance [15]. Regarding analytical procedures, high-performance-liquid-chromatography (HPLC) or gascromatography (GC) coupled to mass spectrometry (MS) are the most commonly used methods [38,39]. UV detection is also used for certain biological studies [40] even though it presents certain limitations due to the particular physico-chemical properties of paraquat. Different alternative analytical methods, such as microwave assisted solvent extraction [41] combined with HPLC-MS, electrophoresis [42, 43] coupled to MS, electroanalytical systems [44], based on the particular electrochemical behaviour of paraquat, or high-performance thin-layer chromatography, radioimmunoassay [45], fluorescent probe titration [46], spectrophotometry [47], and more recently flow injection colorimetric assay [48], or surface enhanced Raman spectroscopy [49] have also been explored. However, these techniques often do not reach the necessary detectability and are time-consuming, since laborious sample extraction, concentration or clean-up procedures are required to perform accurate and reliable measurements. Moreover, they often involve sophisticated or complex equipment which highly increases the costs of the analysis.

Analyzing these toxic chemicals in remote places requires simpler methods that don't involve cumbersome procedures or expensive instruments [26]. In this regard immunochemical analytical techniques, including immunoassays [50] and immunosensors [51] have been demonstrated to be excellent candidates for PQ residue analysis in a variety of different environmental and biological matrices as complementary detection methods.

Combined with the latest advances in microelectronics and the recent knowledge in nanotechnology, electrochemical biosensors have revolutionized modern analysis due to their technical simplicity and rapid response time [52-55]. As it has been already described in previous chapters of this thesis (4,5,6), screen printed electrodes are excellent candidates for the miniaturization of electrochemical analytical systems due to their cost-effectiveness, high versatility and simple operation. Furthermore, the use of nanomaterials can enhance the performance of the SPEs in terms of selectivity ans sensitivity. Even though a number of reports are already available for the electrochemical detection of paraquat based on the use of screen printed electrodes [56-61], there is still a lack of devices that are capable of multiplex detection while maintaining their ease of use.

7.4 PARAQUAT - RESULTS AND DISCUSSION

7.4.1 IMMUNOREAGENT EVALUATION

The immunoreagents used for the detection of Paraquat were developed in-house by the Nb4D research group during previous years [16].

For the evaluation of these immunoreagents, primarly non-competitive 2D checkerboard titration immunoassays were performed, in order to determine the appropriate concentrations for the immunosensor development. Subsequently, competitive indirect immunoassays were carried out to obtain the calibration curve of the assay. The features of the assay are represented in the graph (Figure 7.13) and the table (Table 7.9) below.

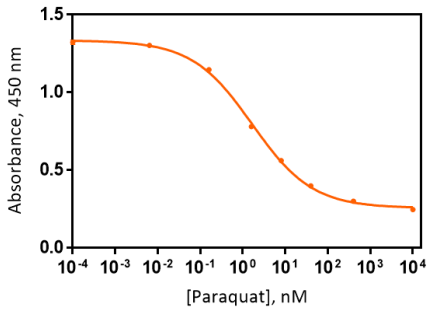

Table 7.9. Parameters of the assay (Hp-PQ_1-BSA/As198)	
Coating Ag, µg mL^{-1}	0.04
As dilution	1/150000
Absorbance$_{min}$	0.256
Absorbance$_{max}$	1.335
Slope	-0.61
IC_{50}, nM	1.67 ± 0.20
IC_{50}, µg L^{-1}	0.43 ± 0.05
LOD, nM	0.06
LOD, µg L^{-1}	0.02
R^2	0.998

Figure 7.13. *Analytical features of the Hp-PQ_1-BSA/As198 assay performed in PBST buffer. The data shown correspond to the average of three assays performed on three different days. Each assay was built using three well replicates. LOD corresponds to limit of detection, calculated as the concentration given at 90 % of the maximum signal.*

As it can be observed from Table 7.9, the standard deviation between the different assays is really low, resulting in a final IC_{50} value of 0.43 ± 0.05 µg L^{-1} and an LOD of 0.02 µg L^{-1} which is well below the MRL established by the European Commission (20 µg L^{-1}).

7.4.2 IMMUNOSENSOR DEVELOPMENT

According to the protocol described in section 7.4.5, in order to develop the electrochemical immunosensor, first of all the amounts of coating antigen, primary and secondary antibodies had to be optimized. The first step of this process was the optimization of the alkaline-phosphatase labelled secondary antibody for which the following concentrations were examined:

3 µg mL^{-1},
1 µg mL^{-1},
0.6 µg mL^{-1},
0 µg mL^{-1}.

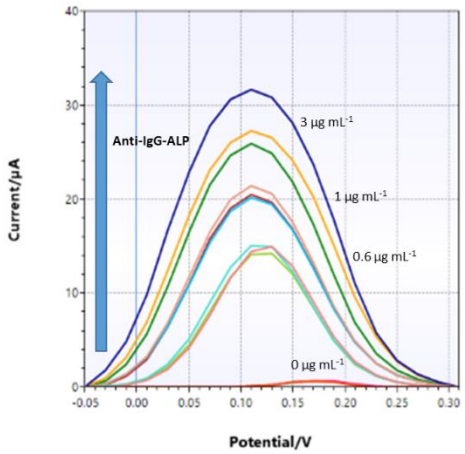

Figure 7.14. *Optimization of the anti-IgG-ALP concentration for the development of the immunosensor. The differential pulse voltammograms were recorded on the Hp-PQ_1-BSA coated CB-modified electrodes (n=3).*

Based on the results shown in Figure 7.14, the concentration 3 µg mL^{-1} was chosen for the development of the immunosensor because using this concentration gives a significantly higher signal compared to the other ones. In regard to the coating antigen and the primary antibody, the optimized concentrations were 2.5 µg mL^{-1} for Hp-PQ_1-BSA and 5 µg mL^{-1} in the case of Ab198.

After the optimization process, an indirect competitive assay was developed on the surface of the screen printed electrodes that were previously dropcasted with the nanomaterial carbon black using an automated BioDot dispenser (further described in Chapter 4). The calibration curves were obtained using different concentrations of the target analyte paraquat and the resulting current signal was acquired using differential pulse voltammetry as electrochemical detection technique (explained in detail in section 5.4.4).

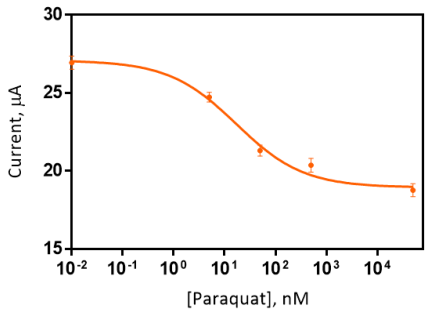

Table 7.10. Parameters of the electrochemical immunosensor developed in PBST buffer (n=3).	
Hp-PQ-BSA, µg mL^{-1}	2.5
Ab198, µg mL^{-1}	5
Signal$_{min}$	18.94
Signal$_{max}$	27.08
Slope	-0.67
IC$_{50}$, nM	16.99 ± 1.47
IC$_{50}$, µg L^{-1}	4.37 ± 0.63
LOD, nM	0.95
LOD, µg L^{-1}	0.24
R^2	0.960

Figure 7.15. *Analytical features of the electrochemical immunosensor developed in PBST buffer for the detection of the herbicide paraquat. The data shown correspond to the average of three replicates.*

The features of the electrochemical sensor (see Figure 7.7) show a further increase in background noise compared to the ELISA, which has also led to an increase of the parameters of LOD (0.24 µg L^{-1}) and IC$_{50}$ (4.37 ± 0.63 µg L^{-1}). Even though the developed sensor fulfills the requirements of the European Commission regarding the MRL, similarly to the bromopropylate sensor, the interday variability (most probably due to the high background noise) made it difficult to perform reproducible measurements.

In hopes of solving this problem, the hapten Hp-PQ was conjugated to aminodextran (AD) using the protocol explained in section 7.4.2, but unfortunately in this case the new conjugate did not improve the parameters of the assay, thus the experiments were not followed with this analyte.

7.5 CONCLUSIONS

Electrochemical immunosensors were developed in PBST buffer for the detection of both pesticides achieving LOD values of 0.24 µg L^{-1} in the case of paraquat and 4.32 µg L^{-1} in the case of bromopropylate, both of them well below the European Commission's MRLs (0.02 mg L^{-1} and 0.01 mg L^{-1} respectively). Due to the high background noise and the irreproducibility of the developed sensors, the matrix effect and recovery studies were only performed for the analyte bromopropylate with the use of a new conjugate in the ELISA format. Different

juice (apple and peach) and jam (apricot and strawberry) samples were used for these studies resulting in recovery values between 74 and 115 %.

7.6 MATERIALS AND METHODS

The parameters of the electrochemical measurements and the data treatment are identical to the ones described in sections 5.4.4 and 5.4.5 of Chapter 5.

7.6.1 REAGENTS, MATERIALS AND EQUIPMENT

$NaBH_3CN$ and sodium borate were purchased from Sigma Aldrich (St. Louis, MO, USA). Most of the immunoreagents were previously developed in-house by our research group [2,22], only in the case of bromopropylate was there need to prepare a new conjugate which is described below. For the matrix studies, the different juices and jams were obtained from a local retail store. The matrix-assisted laser desorption ionization time-of-flight mass spectrometer (MALDI-TOF-MS) was a Bruker autoflex III Smartbeam spectrometer (Billerica, Massachusetts).

The rest of the reagents, buffers and equipment used are identical to the ones described in section 5.4.1 of Chapter 5.

7.6.2 IMMUNOREAGENT PREPARATION

H9-BSA and H9-AD preparation by reductive amination method. First, 10 µmol of h9 was dissolved in 100 µL anhydrous DMF. The hapten was then added dropwise to a solution of 10 mg of bovine serum albumin (BSA) or 10 mg of aminodextran (AD) in 800 µl borate buffer (0.2 M). Subsequently, 100 µmol of sodium cyanoborohydride ($NaBH_3CN$) in 10 mM PBS (100 µL) was added to the solutions, which were allowed to react ON at 4°C with constant agitation. The following day an additional 100 µmol of $NaBH_3CN$ (in 10 mM PBS) was added to the solutions and agitated for 30 min at RT. Finally, the solutions were centrifuged at 4000 rpm for 10 min, the pellet was discarded and the supernatant

was used for the following experiments. The protein conjugate was then purified by dialysis against 0.5 mM PBS (4×5 L) and Milli-Q water (1×5 L) and was stored frozen at -40 °C. Unless otherwise indicated, working aliquots were stored at 4 °C in 0.01 M PBS at 1 mg mL^{-1}.

The hapten density of the BSA bioconjugate was estimated by measuring the molecular weight of the native protein and the MW of the conjugate by MALDI-TOF-MS. The mass spectrum was obtained by crystallization of the corresponding matrix (sinapinic acid, 2 µL of 10 mg mL^{-1} in a 70:30 solution of ACN/H_2O and 0.1% in HCOOH), followed by 2 µL of sample, or 2 µL of the reference sample (BSA, 5 mg mL^{-1} in 50:50 ACN/H_2O and 0.1% in HCOOH). Finally, after the evaporation of the solution deposited on the plate, 2 µL of the matrix was added again. The hapten densities (δ hapten) were calculated according to the following equation: [MW(conjugate)-MW(protein)]/MW(hapten).

Antibody purification. The produced antisera was precipitated with ammonium-sulfate and purified by affinity chromatography with the use of protein A. After a desalting purification step, the antibodies were lyophilized in order to be ready for the experiments with the electrodes.

7.6.3 IMMUNOASSAY DEVELOPMENT FOR PARAQUAT

Non-competitive indirect ELISA. This method was used to evaluate the avidity of the antisera As198 with the coating antigen Hp-PQ_1-BSA. The two-dimensional titration assays (2D-assay) were carried out based on measuring the binding of a series of dilutions (starting from 1/1000 to 1/64000 and zero; 100 µL $well^{-1}$) of the antisera against different concentrations (starting from 10 µg mL^{-1} to 10 ng mL^{-1}, and zero; 100 µL $well^{-1}$) of the antigen. Depending on the results of these experiments, the optimum concentrations for coating antigens and antisera dilutions were chosen, generating around 0.8-1 units of absorbance.

Competitive ELISA Hp-PQ-BSA/As198 for the detection of Paraquat. First, 96-well microtiter plates were coated with the antigen Hp-PQ_1-BSA (0.04 µg mL^{-1} in coating buffer, 100 µL $well^{-1}$), overnight at 4 °C and covered with adhesive plate sealers. The following day, the plates were washed four times with PBST (300 µL $well^{-1}$), and the solution of paraquat (from the stock solution in MQ) was added (50 µL $well^{-1}$), followed by the solution of antisera As198 (1/150000 both in PBST,

50 µL well^{-1}). After 30 min at room temperature (RT), the plates were washed as mentioned before, and a solution of anti-IgG-HRP (1/6000 in PBST) was added to the wells (100 µL well^{-1}) and incubated for 30 minutes at RT. The plates were washed again, and the substrate solution was added (100 µL well^{-1}). After 30 min colour development was stopped with 4N H_2SO_4 (50 µL well^{-1}) at RT, and the absorbance was read at 450 nm with a spectrophotometer. The standard curves were fitted to a four-parameter equation according to the following formula: y = (A − B/[1 − (x/C)D] + B, where A is the maximal absorbance, B is the minimum absorbance, C is the concentration producing 50% of the maximal absorbance, and D is the slope at the inflection point of the sigmoid curve. Unless otherwise indicated, data presented corresponds to the average of at least three wells replicates.

7.6.4 IMMUNOASSAY DEVELOPMENT FOR BROMOPROPYLATE

Non-competitive indirect ELISA. The avidity of the antisera As174 with the coating antigen h9-BSA or h9-AD was evaluated with this method. The two-dimensional titration assays (2D-assay) were carried out based on measuring the binding of a series of dilutions (starting from 1/1000 to 1/64000 and zero; 100 µL well^{-1}) of the antisera against different concentrations (starting from 10 µg mL^{-1} to 10 ng mL^{-1}, and zero; 100 µL well^{-1}) of the antigens. Depending on the results of these experiments, the optimum concentrations for coating antigens and antisera dilutions were chosen, generating around 0.8-1 units of absorbance.

*Competitive ELISA*s h9-*BSA/As174 or h9-AD/As174 for the detection of Bromopropylate*. First, 96-well microtiter plates were coated with the antigen h9-BSA or h9-AD (0.35 or 0.625 µg mL^{-1} in coating buffer, 100 µL well^{-1}), overnight at 4 °C and covered with adhesive plate sealers. The following day, the plates were washed four times with PBST (300 µL well^{-1}), and the solution of Bromopropylate (stock from 2000 to 0 µM in DMSO and diluted 200 times in PBST or in the target matrix) was added (50 µL well^{-1}), followed by the solution of antisera As174 (1/15000 or 1/8000 both in PBST, 50 µL well^{-1}). After 30 min at room temperature (RT), the plates were washed as mentioned before, and a solution of anti-IgG-HRP (1/6000 in PBST) was added to the wells (100 µL well^{-1}) and incubated for 30 minutes at RT. The plates were washed again, and the substrate solution was added (100 µL well^{-1}). After 30 min colour development

was stopped with 4N H_2SO_4 (50 µL $well^{-1}$) at RT, and the absorbance was read at 450 nm with a spectrophotometer. The standard curves were fitted to a four-parameter equation according to the following formula: y = (A − B/[1 − (x/C)D] + B, where A is the maximal absorbance, B is the minimum absorbance, C is the concentration producing 50% of the maximal absorbance, and D is the slope at the inflection point of the sigmoid curve. Unless otherwise indicated, data presented corresponds to the average of at least three wells replicates.

Matrix effect studies. Non-specific interferences produced by the parameters associated with the matrices of interest were studied by preparing standard curves in different juice (apple and peach) and jam samples (strawberry and apricot). Previously to the measurements the pH of the juices was set to 7.5, then the juices were filtered through a 0.22 µm filter and diluted five times in PBST. In the case of the jams a homogenization process (by heating them up in a microwave) had to be performed before the adjusting of the pH, filtration and dilution (1:5 in PBST buffer) of the samples.

Recovery studies. In the case of the juice samples, the recovery of the analyte (BP) concentration subsequently to the sample treatment was assessed by spiking blank juice samples at 4 different concentrations (from 2 to 2000 nM, including a zero). The sample concentrations were then calculated by interpolating the results to bromopropylate standard curves that were previously prepared in the corresponding juice samples. The results were fitted to a linear regression curve illustrating the correlation between the spiked and the found concentrations of the analyte.

7.6.5 IMMUNOSENSOR DEVELOPMENT

As the first step of the sensor development, similarly to the ELISA, the working electrode was coated with the optimized concentration of the corresponding antigen (2.5 µg mL^{-1} h9-BSA or 2.5 µg mL^{-1} Hp-PQ_1-BSA) by dropcasting 2 µL of the prepared solution in carbonate buffer. All the prepared electrodes were incubated for 45 minutes at RT. All of the incubation steps were performed in a humid chamber at RT. Afterwards, the WEs were washed twice with 100 µL of PBST and once with 100 µL of PBS. The next step was the blocking of the electrode's surface by dropping 2 µL of 2 % BSA in carbonate buffer, after which

the electrodes were incubated for 30 minutes at RT. The WEs were washed again twice with 100 µL of PBST and once with 100 µL of PBS. Next, 2 µL of the primary antibody solution (10 µg mL^{-1} Ab174 or 5 µg mL^{-1} Ab198 in PBS) and different concentrations of the analyte (from 2 nM to 50 µM of bromopropylate and from 5 nM to 50 µM of paraquat and 0 nM in PBS with BSA 1%) were incubated on the WE for 30 minutes at RT for the competition to allow. The SPEs were washed again using the same procedure as explained above. The next step was the addition of the alkaline phosphatase (ALP) labelled secondary antibody (in PBS BSA 1%) for 30 minutes at RT. This step was also followed by a washing step (twice with 100 µL of PBST and once with 100 µL of PBS) and finally the electrodes were dropcasted with 2 µL of PBS until the start of the electrochemical measurement in order to avoid drying them out. Afterwards, 60 µL of the enzymatic substrate containing solution (5 mg mL^{-1} 1-Naphthyl phosphate disodium salt in diethanolamine buffer with 1 mM $MgCl_2$) was dropped on the SPE's surface (covering all 3 electrodes) and after 2 minutes of incubation time, the DPV measurement was started according to the procedure explained in section 5.4.4 and the resulting current was recorded (n=3).

7.7 BIBLIOGRAPHY

[1] Ramón, J.; Sánchez, F.; Sanvicens, N.; Marco, M.-P. Development of an Enzyme-Linked Immunosorbent Assay for Determination of the Miticide, (2009) 375–384.

[2] Corta, E.; Bakkali, A.; Barranco, A.; Berrueta, L. A.; Gallo, B.; Vicente, F.; Bogdanov, S. Study of the degradation products of bromopropylate, chlordimeform, coumaphos, cymiazole, flu- methrin and Tau-fluvalinate in aqueous media. Talanta 2000, 52 (2), 169–180.

[3] Bathe, R.; Sachsse, K. Acute Dermal LD50 in the Rat; 790969; GS 19'851 tech: Oct 9, 1979; submitted to WHO by Ciba-Geigy Ltd., Basel, Switzerland.

[4] Kuhn, J. O. Acute Dermal Toxicity Study in Rabbits; 6032-89; Stillmeadow, Inc., Houston, TX, April 11, 1989; submitted to WHO by Ciba-Geigy Ltd., Basle, Switzerland.

[5] COMMUNITIES, C. O. T. E., Monitoring of Pesticide Residues in Products of Plant Origin in the European Union, Norway, Iceland, Denmark, Italy and Liechtenstein; 2005.

[6] Martel, A.-C.; Zeggane, S. Determination of acaricides in honey by high-performance liquid chromatography with photodiode array detection. J.Chromatogr., A 2002, 954 (1-2), 173–180.

[7] Lee, N. A.; Kennedy, I. R. Environmental monitoring of pesticides by immunoanalytical techniques: validation, current status, and future perspectives. J. AOAC Int. 2001, 84 (5), 1393–1406.

[8] Liapis, K. S.; Aplada-Sarlis, P.; Kyriakidis, N. V. Rapid multi- residue method for the determination of azinphos methyl, bro- mopropylate, chlorpyrifos, dimethoate, parathion methyl and phosalone in apricots and peaches by using negative chemical ionization ion trap technology. J. Chromatogr., A 2003, 996 (1- 2), 181–187.

[9] Jimenez, J. J.; Bernal, J. L.; del Nozal, M. J.; Alonso, C. Liquid- liquid extraction followed by solid-phase extraction for the determination of lipophilic pesticides in beeswax by gas chromatography-electron-capture detection and matrix-matched calibration. J.Chromatogr., A 2004, 1048 (1), 89–97.

[10] Rial-Otero, R.; Gaspar, E. M.; Moura, I.; Capelo, J. L. Gas chromatography mass spectrometry determination of acaricides from honey after a new fast ultrasonic-based solid phase micro- extraction sample treatment. Talanta 2007, 71 (5), 1906–1914.

[11] Korta, E.; Bakkali, A.; Berrueta, L. A.; Gallo, B.; Vicente, F.; Bogdanov, S. Determination of amitraz and other acaricide residues in beeswax. Anal. Chim. Acta 2003, 475 (1-2), 97–103.

[12] Oubina, A.; Ballesteros, B.; Bou, P.; Galve, R.; Gascón, J.; Iglesias, F.; Sanvicens, N.; Marco, M.-P. Inmunoassays for environmental analysis. Sample handling and trace analysis of pollutants. In Techniques, Applications and Quality Assurance; Barceló, D., Ed.; Elsevier Sciences: Amsterdam, The Netherlands, 2000; pp 289- 331.

[13] J. Ram, Sensitive and Spatially Multiplexed Detection System Based on Immunoreactions Platform, (2011) 1053–1060.

[14] J. Ramón-Azcón, T. Yasukawa, H. Jung, T. Matsue, F. Sánchez-Baeza, M. Marco, F. Mizutani, Biosensors and Bioelectronics Competitive multi-immunosensing of pesticides based on the particle manipulation with negative dielectrophoresis, 25 (2010) 1928–1933. https://doi.org/10.1016/j.bios.2010.01.006.

[15] R. Garcia-Febrero, E. Valera, A. Muriano, M. Pividori, F. Sanchez-Baeza, M. Marco, An electrochemical magneto immunosensor (EMIS) for the determination of paraquat residues in potato samples, (2013) 7841–7849. https://doi.org/10.1007/s00216-013-7209-2.

[16] R. Garcia-febrero, J. Salvador, F. Sanchez-baeza, M. Marco, Rapid method based on immunoassay for determination of paraquat residues in wheat, barley and potato, 41 (2014). https://doi.org/10.1016/j.foodcont.2014.01.008.

[17] Locke, E. A., & Wilks, M. F. (2001). Chapter 70: Paraquat.In Handbook of pesticide toxicology: Principles and agents (Vol. 1). New York: Academic Press.

[18] Fernández M, Ibáñez M, Picó Y, Mañes J (1998). Spatial and temporal trends of paraquat, diquat, and difenzoquat contamination in water from marsh areas of theValencian community (Spain). Arch Environ Contam Toxicol 35(3):377–384. doi:10.1007/s002449900391

[19] Fischer, B. B., Rüfenacht, K., Dannenhauer, K., Wiesendanger, M., & Eggen, R. I. L. (2010). Multiple stressor effects of high light irradiance and photosynthetic herbicides on growth and survival of the green alga Chlamydomonas reinhardtii. Environmental Toxicology and Chemistry, 29(10), 2211-2219.

[20] Erickson, T., Brown, K. M., Wigder, H., & Gillespie, M. (1997). A case of paraquat poisoning and subsequent fatality presenting to an emergency department. The Journal of Emergency Medicine, 15(5), 649-652.

[21] Philbey, A. W., & Morton, A. G. (2001). Paraquat poisoning in sheep from contaminated water. Australian Veterinary Journal, 79(12), 842-843.

[22] Taylor, P. J., Salm, P., & Pillans, P. I. (2001). A detection scheme for paraquat poisoning: validation and a five-year experience in Australia. Journal of Analytical Toxicology, 25(6), 456-460.

[23] Fukushima T, Tanaka K, Lim H, Moriyama M (2002). Mechanism of cytotoxicity of paraquat. Environ Health Prev Med 7(3):89–94. doi:10.1265/ehpm.2002.89

[24] Tawara T, Fukushima T, Hojo N, Isobe A, Shiwaku K, Setogawa T, Yamane Y (1996). Effects of paraquat on mitochondrial electron transport system and catecholamine contents in rat brain. Arch Toxicol 70(9):585–589. doi:10.1007/s002040050316

[25] N. Dey, D. Bhagat, D. Cherukaraveedu, S. Bhattacharya, Utilization of Red-Light-Emitting CdTe Nanoparticles for the Trace-Level Detection of Harmful Herbicides in Adulterated Food and Agricultural Crops, Chem. - An Asian J. 12 (2017) 76–85. https://doi.org/10.1002/asia.201601302.

[26] M. He, Mesoporous Silica Thin Films for Improved Electrochemical Detection of Paraquat, (2018). https://doi.org/10.1021/acssensors.7b00920.

[27] Cha, E. S., Lee, Y. K., Moon, E. K., Kim, Y. B., Lee, Y.-J., Jeong, W. C., et al. (2012). Paraquat application and respiratory health effects among South Korean farmers. Occupational and Environmental Medicine, 69(6), 398-403.

[28] Hsu, C.-W., Lin, J.-L., Lin-Tan, D.-T., Chen, K.-H., Yen, T.-H., Wu, M.-S., et al. (2012). Early hemoperfusion may improve survival of severely paraquat-poisoned patients. PLos One, 7(10), e48397.

[29] Lee, P.-C., Bordelon, Y., Bronstein, J., & Ritz, B. (2012). Traumatic brain injury, paraquat exposure, and their relationship to Parkinson disease. Neurology, 79(20), 2061-2066.

[30] Berry, C., La Vecchia, C., & Nicotera, P. (2010). Paraquat and Parkinson's disease. Cell Death and Differentiation, 17(7), 1115-1125.

[31] Brent, J., & Schaeffer, T. H. (2011). Systematic review of Parkinsonian syndromes in short- and long-term survivors of paraquat poisoning. Journal of Occupational and Environmental Medicine, 53(11), 1332-1336.

[32] Podder B, Kim Y-S, Zerin T, Song H-Y (2012). Antioxidant effect of silymarin on paraquat-induced human lung adenocarcinoma A549 cell line. Food Chem Toxicol 50(9):3206–3214. doi:10. 1016/j.fct.2012.06.007

[33] Jian X, Ruan Y, Guo G, Zhang Y (2008). Anti-TGF-[beta]1 anti- body: an effective treatment for lung injury caused by paraquat in the future. Med Hypotheses 70(3):705

[34] Kim KS, Suh GJ, KwonWY, Kwak YH, Lee K, Lee HJ, Jeong KY, Lee MW (2012). Antioxidant effects of selenium on lung injury in paraquat intoxicated rats. Clin Toxicol 50(8):749–753. doi:10. 3109/15563650.2012.708418

[35] Novaes RD, Goncalves RV, Santos Marques DC, MdC C,MdC GP, Viana Leite JP, dos Santos Costa Maldonado IR (2012). Effect of bark extract of Bathysa cuspidata on hepatic oxidative damage and blood glucose kinetics in rats exposed to paraquat. Toxicol Pathol 40(1):62–70. doi:10.1177/0192623311425059

[36] Peeters, M.-C., Defloor, I., Coosemans, J., Delcour, J. A., Ooms, L., Deliever, R., et al. (2001). Simple ion chromatographic method for the determination of chlormequat residues in pears. Journal of Chromatography A, 920(1-2), 255-259.

[37] Winnik, B., Barr, D. B., Thiruchelvam, M., Montesano, M. A., Richfield, E. K., & Buckley, B. (2009). Quantification of Paraquat, MPTP, and MPPþ in brain tissue using microwave-assisted solvent extraction (MASE) and high-performance liquid chromatography-mass spectrometry. Analytical and Bioanalytical Chem- istry, 395(1), 195-201.

[38] Robb, C. S., & Eitzer, B. D. (2011). The direct analysis of diquat and paraquat in lake water samples by per aqueous liquid chromatography. LC GC North America, 29(1), 54.

[39] Wang, Z., Wang, Z., & Xing, J. (2011). The quantitative analysis of paraquat in bio- logical samples by liquid chromatography-electrospray ionization-mass spectrometry. Journal of Analytical Toxicology, 35(1), 23-27.

[40] Merritt, T. J. S., Douglas, L., Rzezniczak, T. Z., & Watterson, J. H. (2011). Rapid and simple analysis of paraquat in tissue homogenate by ultra-high performance liquid chromatography. Analytical Methods, 3(6), 1428e1432.

[41] Winnik B,Barr DB, Thiruchelvam M,Montesano MA, Richfield EK, Buckley B (2009) Quantification of Paraquat, MPTP, and MPP+ in brain tissue using microwave-assisted solvent extraction (MASE) and high-performance liquid chromatography–mass spectrometry. Anal Bioanal Chem 395(1):195–201. doi:10.1007/s00216-009-2929-z

[42] Núñez O, Moyano E, Galceran MT (2002) Capillary electrophoresis–mass spectrometry for the analysis of quaternary ammonium herbicides. J Chromatogr A 974(1–2):243–255

[43] Núñez O, Moyano E, Puignou L, Galceran MT (2001) Sample stackingwithmatrixremovalfor thedetermination of paraquat, diquat and difenzoquat inwater by capillary electrophoresis. J ChromatogrA 912(2):353–361

[44] da Silva OB, Machado SAS (2012) Evaluation of the detection and quantification limits in electroanalysis using two popular methods: application in the case study of paraquat determination. Analytical Methods 4(8):2348–2354. doi:10.1039/c2ay25111f

[45] Braithwaite, R. A. Emergency Analysis of Paraquat in Biological Fluids. Hum. Toxicol. 1987, 6,83−86.

[46] Yao, F.; Liu, H.; Wang, G.; Du, L.; Yin, X.; Fu, Y. Determination of Paraquat in Water Samples Using a Sensitive Fluorescent Probe Titration Method. J. Environ. Sci. 2013, 25 (6), 1245−1251.

[47] Rai, M.; Das, J. V.; Gupta, V. K. A Sensitive Determination of Paraquat by Spectrophotometry. Talanta 1997, 45 (2), 343−348.

[48] Chuntib, P.; Jakmunee, J. Simple Flow Injection Colorimetric System for Determination of Para- Quat in Natural Water. Talanta 2015, 144, 432−438.

[49] Fang, H.; Zhang, X.; Jie, S.; Liu, L.; Mei, Y.; Jun, H. Chemical Ultrasensitive and Quantitative Detection of Paraquat on Fruits Skins via Surface-Enhanced Raman Spectroscopy. Sens. Actuators, B 2015, 213, 452−456.

[50] Bacigalupo, M. A., Meroni, G., Mirasoli, M., Parisi, D., & Longhi, R. (2004). Ultra- sensitive quantitative determination of paraquat: application to river, ground, and drinking water analysis in an agricultural area. Journal of Agricultural and Food Chemistry, 53(2), 216-219.

[51] Mallat, E., Barzen, C., Abuknesha, R., Gauglitz, G., & Barceló, D. (2001). Fast deter- mination of paraquat residues in water by an optical immunosensor and vali- dation using capillary electrophoresis-ultraviolet detection. Analytica Chimica Acta, 427(2), 165-171.

[52] Hanrahan G, Patil DG, Wang J (2004) Electrochemical sensors for environmental monitoring: design, development and applications. J Environ Monit 6(8):657–664

[53] Hart JP, Crew A, Crouch E, Honeychurch KC, Pemberton RM (2005) Some recent designs and developments of screen-printed carbon electrochemical sensors/biosensors for biomedical, environ- mental, and industrial analyses. Anal Lett 37(5):789–830

[54] Lojou É, Bianco P (2006) Application of the electrochemical con- cepts and techniques to amperometric biosensor devices. J Electroceram 16(1):79–91. doi:10.1007/s10832-006-2365-9

[55] Wang J (2006) Electrochemical biosensors: towards point-of-care cancer diagnostics. Biosens Bioelectron 21(10):1887–1892

[56] Tyszczuk-Rotko, K.; Bęczkowska, I.; Nosal-Wiercińska, A. Simple, Selective and Sensitive Voltammetric Method for the Determination of Herbicide (Paraquat) Using a Bare Boron-Doped Diamond Electrode. Diamond Relat. Mater. 2014, 50,86−90.

[57] Selva, T. M. G.; Reis de Araujo, W.; Cesar da Paixão, T. R. L. Non-Invasive Salivary Electrochemical Quantification of Paraquat Poisoning Using Boron Doped Diamond Electrode. Electroanalysis 2015, 27 (7), 1642−1648.

[58] De Souza, D.; Codognoto, L.; Machado, S. A. S.; Avaca, L. A. Electroanalytical Determination of the Herbicide Paraquat in Natural Water and Commercial Tea Samples with Gold Electrodes Obtained from Recordable Compact Disc. Anal. Lett. 2005, 38 (2), 331−341.

[59] De Souza, D.; Machado, S. A. S. Study of the Electrochemical Behavior and Sensitive Detection of Pesticides Using Microelectrodes Allied to Square-Wave Voltammetry. Electroanalysis 2006, 18 (9)

[60] Farahi, A.; Achak, M.; El Gaini, L.; El Mhammedi, M. A.; Bakasse, M. Electrochemical Determination of Paraquat in Citric Fruit Based on Electrodeposition of Silver Particles onto Carbon Paste Electrode. J. Food Drug Anal. 2015, 23 (3), 463−471.

[61] Gevaerd, A.; De Oliveira, P. R.; Mangrich, A. S.; Bergamini, M. F.; Marcolino-Junior, L. H. Evaluation of Antimony Microparticles Supported on Biochar for Application in the Voltammetric Determination of Paraquat. Mater. Sci. Eng., C 2016, 62, 123−129

8 MULTIPLEX SMARTPHONE DETECTION AND CONCLUSIONS

8.1 MULTIPLEX SMARTPHONE DETECTION

In order to study the multiplexation capabilities of the developed individual immunosensors, proof-of-concept experiments were carried out using a commercially available multiplexed carbon SPE (4W110) from DropSens (Oviedo, Spain). This electrode contains four working electrodes, thus enabling the simultaneous analysis of four different analytes/samples. The analytical data generated by the multipotentiostat can be transferred to a computer or a smartphone via Bluetooth. This data can then be transformed to a clear and consumer friendly “safe/not safe” message by a costumized application.

The proof-of-concept studies were performed with wheat flour and orange juice samples using the analytes chlorpyrifos and atrazine. A blank and a spiked sample was used in both cases. The 1st analyte on Figure 8.1 corresponds to the orange juice sample spiked with atrazine, the 2nd analyte was the wheat flour sample spiked with chlorpyrifos and the 3rd and 4th analyte were the blank orange juice and flour samples. The results of the measurements are first shown on the display of the smartphone in the form of voltammograms, which are then translated into easily interpretable signs telling the costumer whether or not the analyzed sample is safe to consume or not.

The outcome of these proof-of-concept experiments demonstrated the feasibility of the multiplex platform, since there were no interferences between the different immunoreagents and analytes and the results were also consistent with the ones previously obtained by the singleplex assays.

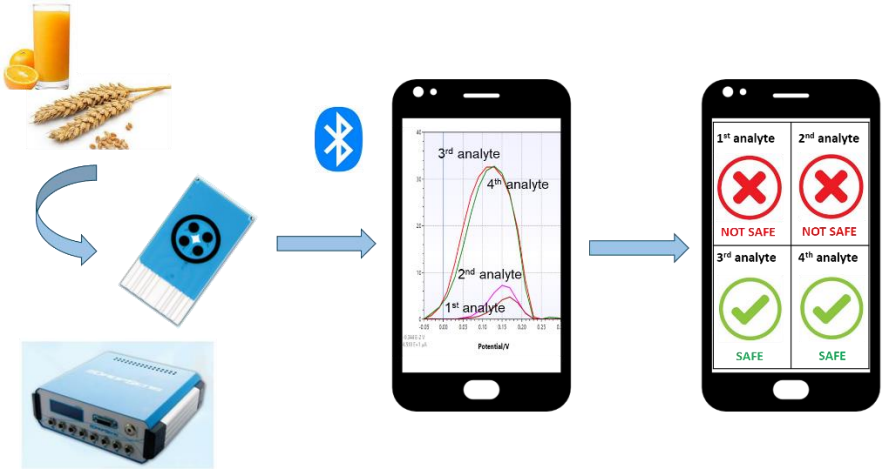

Figure 8.1. *Scheme of the multiplex smartphone detection sytem which involves the samples, a multiplex SPE, a multipotentiostat and a Bluetooth-connected smartphone with a custom designed App to analyse the results.*

8.2 CONCLUSIONS OF THIS THESIS

- All the necessary immunoreagents for the detection of the selected target pesticides were evaluated by ELISA experiments.
- Several different typologies of carbon-based screen printed electrodes were produced, modified and characterized. The modification of the electrodes was carried out with the nanomaterial carbon black, either during the printing process by directly mixing the particles in the ink or after the printing process by dropcasting these nanoparticles on the surface of the working electrode. The evaluation of these SPEs was based on the electrocatalytic effect of the electrode's surface on the redox couple $[Fe(CN)_6]^{3-/4-}$. The electrode with the best electrochemical properties was used as a platform for the development of different electrochemical immunosensors.
- The direct use of the SPE's surface, an ALP labelled secondary antibody and DPV as electrochemical detection technique was proven to be successful in the detection of the herbicide atrazine in PBST buffer and in orange juice, achieving LOD-s of 2.09 (0.45 μg L^{-1}) and 2.47 nM (0.53 μg L^{-1}) respectively, which are both well below the MRL established by the European Commission (0.05 mg kg^{-1}). Aside from having the desired sensitivity and specificity, the use of these parameters also provides an excellent applicability in terms of multiplexing and automatization.
- An electrochemical immunosensor was developed for the detection of the insecticide chlorpyrifos in wheat flour samples achieving LOD values around 5 μg kg^{-1}, well below the MRL of 0.5 mg kg^{-1} established by the European Commission. The feasibility of the developed sensor as a screening method for food safety monitoring was confirmed by the analysis of real samples and their validation by ELISA and a chromatographic reference method (GC-MS).
- Electrochemical immunosensors were developed in PBST buffer for the detection of the pesticides paraquat and bromopropylate, achieving LOD values (0.24 μg L^{-1} and 4.32 μg L^{-1} respectively) well below the European Commission's MRLs (0.02 mg L^{-1} and 0.01 mg L^{-1} respectively). In the case of bromopropylate, different juice (apple and peach) and jam (apricot and strawberry) samples were studied in the ELISA format achieving recovery values between 74 and 115 %.

- Finally, the multiplexation capabilities of the developed individual immunosensors were demonstrated with a proof-of-concept study of a smartphone-connected multiplexed sensor.
- The developed sensor has the potential to be integrated in an easy-to-use and affordable device, which could be used by farmers and inspectors (e.g. at borders) for at-line measurements in order to ensure food safety and quality in the coming years.

9 ANNEX: SEA-ON-A-CHIP PROJECT

9.1 SEA-ON-A-CHIP PROJECT

At the very beginning of my PhD I have participated in the European SEA-on-a-CHIP project (FP7, OCEAN 2013. 1-614168), which had the aim to develop a miniaturized, autonomous, remote and flexible immunosensor platform based on a fully integrated array of micro/nano-electrodes and a microfluidic system in a lab-on-a-chip configuration combined with electrochemical detection (impedimetric measurements) for real time analysis of marine waters in multi-stressor conditions. The final prototype was developed to use in aquaculture facilities for the rapid assessment of contaminants that could have an impact on aquaculture production.

My role in the project involved the development of a multiplexed amperometric immunosensor for the detection of four different marine pollutants (Irgarol 1051®, sulphonamide, chloramphenicol and 17β-estradiol) in seawater. A detailed description of the developed immunosensor can be found in the following publication:

J. Salvador, K. Kopper, A. Miti, A. Sanchis, M. Marco. Multiplexed Immunosensor Based on the Amperometric Transduction for Monitoring of Marine Pollutants in Sea Water. Sensors 2020, 20(19), 5532; https://doi.org/10.3390/s20195532

10 ACRONYMS AND ABBREVIATIONS

10.1 ACRONYMS AND ABBREVIATIONS

Ab	Antibody
Abs	Absorbance
AD	Aminodextran
Ag	Antigen
ALP	Alkaline Phosphatase
As	Antiserum
App	Application
BP	Bromopropylate
BSA	Bovine Serum Albumin
CB	Carbon black
ChA	Chronoamperometry
CSIC	Spanish Council for Scientific Research
CV	Cyclic Voltammetry
CE	Counter electrode
CPE	Constant phase element
DC	Direct current
dCB-SPEs	Screen printed electrodes dropcasted with carbon black
DMF	Dimethylformamide
DPV	Differential Pulse Voltammetry
EC	European Commission
EFSA	European Food Safety Authority
EIS	Electrochemical Impedance Spectroscopy
ELISA	Enzyme-Linked ImmunoSorbent Assay
EU	European Union
GC-MS	Gaschromatography coupled to Mass Spectrometry
HPLC	High Performance Liquid Chromatography
HQ	Hydroquinone
HRP	HorseRadish Peroxidise
iCB-SPEs	Screen printed electrodes with carbon black modified ink
IA	ImmunoAssay
IC_{20}	Concentration in which the signal is 80 % inhibited
IC_{50}	Concentration in which the signal is 50 % inhibited
IC_{80}	Concentration in which the signal is 20 % inhibited
IC_{90}	Concentration in which the signal is 10 % inhibited
IgG	Immunoglobulin G
IQAC	Institute of Advanced Chemistry of Catalonia

LOD	Limit Of Detection
LOQ	Limit Of Quantification
MAb	Monoclonal Antibody
MALDI-TOF-MS	Matrix Assisted Laser Desorption Ionization - Time of Flight Mass Spectrometry
MRL	Maximum Residue Limit
MW	Molecular Weight
Nb4D	Nanobiotechnology for Diagnostics Group
NADP	Nicotinamide Adenine Dinucleotide Phosphate
NADPH	Nicotinamide Adenine Dinucleotide Phosphate Hydrogen
NFC	Near-Field Communication
ON	Overnight
PAb	Polyclonal Antibody
PBS	Phosphate Buffered Saline solution
PBST	Phosphate Buffered Saline Tween-20 solution
PDMS	Polydimethylsiloxane
PMMA	Poly(methyl methacrylate)
POC	Point-Of-Care
PQ	Paraquat
QuEChERS	Quick, Easy, Cheap, Effective, Rugged and Safe
RE	Reference electrode
RT	Room Temperature
SD	Standard Deviation
SME	Subject-matter expert
SPE	Screen Printed Electrode
STC	Screening target concentration
TMB	3,3’,5,5’-TetraMethylBenzidine
WE	Working electrode
WHO	World Health Organization